University of Venda

Synthesis and properties of some electrolyte additives for lithium-ion batteries

By

AVHAPFANI WENDY BEBEDA

11565179

Submitted in fulfilment of the requirements for the Degree of

Master of Science (Chemistry)

in the Department of Chemistry

School of Mathematical and Natural Sciences

at the University of Venda

Supervisor: Prof. T. van Ree

Co-supervisor: Prof. I.D.I. Ramaite

Date submitted: February 2015

Declaration

I, Avhapfani Wendy Bebeda, hereby declare that the dissertation for the Master of Science (Chemistry) degree at the University of Venda, hereby submitted by me, has not been submitted previously for a degree at this or any other university, that it is my own, work in design and in execution, and that all reference material contained therein has been duly acknowledged.

Signature  Date 19.02.2015

Avhapfani Wendy Bebeda

Main supervisor 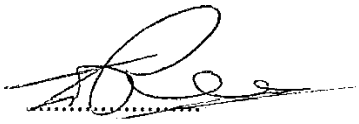 Date 19.02.2015

Prof. T. van Ree

Co-supervisor 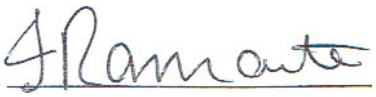 Date 19.02.2015

Prof. I. D. I. Ramaite

Plagiarism declaration

I, Avhapfani Wendy Bebeda (Student No: 11565179), hereby declare the following:

- I am aware and acknowledge that plagiarism is wrong. Plagiarism is the use of another person's ideas or published work and to pretend that it is one's own and it is a serious academic offence for which the university may impose severe penalties.
- I declare that this thesis is my own work and that I have correctly acknowledged the work of others. The work has not been previously submitted to the University of Venda or elsewhere for this degree.
- I have not allowed, and will not allow, anyone to copy my work with the intention of passing it off as their own work.

Signature:  Date: 19.02.2015

Abstract

As an alternative energy source, lithium ion batteries have become increasingly important with a wide range of applications in industry, and many international companies are investing in this big project. This study was aimed at the development of safer lithium-ion power sources by using new organic additives to overcome the possible safety problems.

In this study, the conformations and energies of several synthesized boronates were investigated through computational study using density functional theory (DFT) with the Becke's three-parameter hybrid method utilizing the Lee-Young-Parr correlation functional (B3LYP). After initial energy optimization using *Møller*-Plesset Perturbation theory (MP2), the conformational preferences and energetics *in vacuo* were investigated using DFT calculations and the 6-31G(d,p) basis set. Subsequently, cyclic voltammetry and electrochemical impedance spectroscopy were used to characterize the compounds in terms of their usefulness as electrolyte additives. At least two of these show excellent promise for use in lithium-ion batteries.

Keywords: *Boronate, Conformation, Electrochemistry, Electrolyte, Lithium-ion battery, LUMO energy, Organic additive.*

ACRONYMS AND ABBREVIATIONS

CMS	Carbon microsphere
COSY	Correlation spectroscopy
CV	Cyclic voltammetry
DEC	Diethyl carbonate
DEPT135	Distortionless enhancement by polarisation transfer using a 135° final proton pulse angle
DMC	Dimethyl carbonate
EC	Ethylene carbonate
EIS	Electrochemical impedance spectroscopy
EMC	Ethyl methyl carbonate
EO	Ethyleneoxy, $-(CH_2-CH_2-O)_n-$
EV	Electric vehicle
FTIR	Fourier transform infrared spectroscopy
HMBC	Heteronuclear multiple-bond correlation spectroscopy
HSQC	Heteronuclear single-quantum correlation spectroscopy
IR	Infrared spectroscopy
$LiAsF_6$	Lithium hexafluoroarsenate
LIB	Lithium-ion battery
$LiBF_4$	Lithium tetrafluoroborate
LiBOB	Lithium bis(oxalato)borate
$LiFePO_4$	Lithium iron(II) phosphate
$LiPF_6$	Lithium hexafluorophosphate

M	$mol.dm^{-3}$
MPBMDS	Methyl phenyl bis-methoxydiethoxysilane
NMR	Nuclear magnetic resonance spectroscopy
PC	Propylene carbonate
SEI	Solid electrolyte interphase
SEM	Scanning electron microscope
XPS	X-ray photoelectron spectroscopy
XRD	X-ray diffraction spectroscopy

ACKNOWLEDGEMENTS

1. Ms Yaqiong Yang of Fudan University, Shanghai, is thanked for recording the CV and EIS measurements.

2. The University of Venda and the National Research Foundation are thanked for generous financial support of this project, and SASOL Inzalo Foundation is thanked for a fellowship.

3. I would like to express my gratitude to my supervisor Prof Teuns van Ree for his continuous guidance and supervision throughout this project. I would like to thank him for his helpful suggestions and useful discussions that enabled me to complete my work successfully, and which made me enjoy my project.

4. Special thanks to my fellow chemistry colleagues for all the support and times we have spent together in the labs.

5. Special thanks to Mr Mutshaeni (chemistry lab technician) and Mr Pandelani (NMR operator) for all their support and encouragement.

6. I would like to express my very great appreciation to Mr Phaphana for his valuable, constructive suggestions and allowing me to use his office all the time when I needed the space to write my thesis.

7. I would like to express my deep gratitude to my uncle Norman for his care, love, and believing in me throughout my studies.

8. Finally I would like to express my deep gratitude to my husband, daughter (Evalian) and my son (Blessing) for their love, care, and support; it was not easy to spend most of the time away from them but their understanding made this work to be a success.

TABLE OF CONTENTS

Chapter 1

Introduction: Lithium-ion batteries

As the development of portable and latterly, wearable, electronic appliances and electrical vehicles continues, providing sustainable and clean energy has become a critical factor. The strategic importance of the search for novel energy storage materials has led to rapid development of the field.[1,2,3] Although electrical and kinetic energy are still produced mainly by burning of fossil fuels and nuclear power, solar radiation and wind generators are becoming increasingly important. However, production of electricity from renewable resources such as solar and wind power need reliable and safe high-capacity storage devices for their effective use. Therefore, energy storage devices such as batteries have an important role to play in the efficient use of renewable energy.

One of the most promising energy storage products is the commercial lithium-ion battery, which was introduced by Sony Corporation in the early 1990s. In a lithium-ion battery, the negative electrode is lithiated during the first charge. During discharge, lithium ions move through the electrolyte from the negative electrode (nowadays typically carbon) to the positive electrode (usually a lithium metal oxide); when charging, the lithium ions migrate through the electrolyte from the positive electrode to the negative electrode.[1]

Modern batteries are used for the safe storage and delivery of electricity at power densities up to 500 Wh/dm^3.[4] They can be made in all sizes and shapes and are useful in many different applications. However, at higher power densities, heat evolution starts to play a role. Batteries or cells are mainly of two types, primary and secondary.

1.1 Primary cells

Alessandro Volta invented the first practical electrochemical battery in 1799.[5] Although Volta got the credit for the invention, there have been assertions[6] that a similar design may date back to the ancient Persians some 1200-1800 years ago.

The main components of an electrochemical cell are:[7]

1. A negative electrode (or *anode*) providing electrons to an external circuit; it is oxidized during the electrochemical reaction.

2 A positive electrode (or *cathode*) that accepts electrons from an external circuit; it is reduced during the electrochemical reaction.

3 The medium that transports a charge, as ions, inside the cell between the negative electrode and the positive electrode, called the *electrolyte*. The first electrolytes were liquid solutions, such as salt water, but solid and gel electrolytes are becoming more common.

During storage, primary cells are discharged (called *self-discharge*) at a very low rate. Modern primary cells require little maintenance and can provide high energies when discharged slowly. However, the cell reactions are not easily reversed; therefore, primary cells (and thus, primary batteries) are not recharged and are discarded or recycled if possible, after full discharge.

With the development of high-voltage and low weight lithium batteries in the 1970's the traditionally used alkaline−MnO_2 primary batteries[8,9] were gradually replaced.

1.2 Secondary cells

Secondary batteries can be recharged electrically after being discharged. Charging is done by passing a current through the battery in the direction opposite to the discharge, reversing the movement of ions and the chemical reduction and oxidation processes. Traditionally, lead-based batteries dominated the market in rechargeable cells but they are gradually being replaced by lithium-based cells.[4]

Unfortunately, the first generations lithium batteries used to behave self-destructively in abuse situations, such as short circuiting or overcharging. Overcharge may cause a condition known as *thermal runaway* in the original lithium negative electrode, usually resulting in explosion and combustion of the inflammable electrolyte. It was therefore necessary to find materials that could replace the lithium metal negative electrode but still can intercalate and de-intercalate lithium at a high rate. In 1991, a negative electrode of carbon and a positive electrode of layered lithium cobalt oxide were introduced by Sony,[8] laying the foundation of the modern lithium-ion battery. However, now that modern lithium batteries are quite safe thanks to further developments of the electrode materials, they still need to be handled carefully to avoid another unwanted effect, called *capacity fade*. This is where the amount of charge a battery can deliver at the rated voltage

decreases with use,[10,11] and is expressed as a percentage of initial capacity after a specified number of cycles.

A battery combined with protection and monitoring electronics (such as those found in all modern Sony camera's) is often referred to as a 'smart' battery. With the development of more and more wireless and 'wearable' devices, the need for very light and smart LIBs continues to increase. On the opposite end of the scale, with the development of electric vehicles (EVs), much effort is being expended on the development of smart, safe, high-power LIBs that are also environmentally friendly. Such scaled-up lithium-ion batteries still raise safety concerns, especially when they are overcharged.[12-18] Therefore, efforts continue to improve the thermal stability of positive electrodes, negative electrodes, separators, and electrolytes within the battery to counter thermal runaway. Thermal runaway is still a potential threat because of the high flammability of the liquid electrolytes in use.[19] Addition of protection and monitoring electronics add to the battery cost and cause a lower energy density. Therefore, development of solid, gel and water-based electrolytes and electrolyte additives that would protect these batteries but simultaneously maintain their efficiency has become crucial.

1.3 Safety issues with lithium-ion batteries

Short-circuiting and overcharging can easily damage lithium-ion batteries. The conventional lead-acid, Ni-MH and Ni-Cd batteries perform safely under strenuous short-circuiting and overcharging conditions, because they have low energy capacities and use non-flammable electrolytes. But when a lithium-ion battery short-circuits, a high electricity flow can result, and the temperature of the battery can increase to several hundred degrees within seconds; neighbouring cells then also heat up and the entire battery ignites.[20] When lithium-ion batteries are overcharged, the chemical structures of the negative electrode and the positive electrode are destroyed, with some of the reduced lithium crystallizing into snowflake-shaped deposits called *dendrites*. These dendrites are electrically conducting and can cause the battery to short-circuit, or even explode and catch fire. If the lithium metal is not sufficiently pure, the battery materials are poisoned, which can cause dendrite formation, potentially causing short-circuits and explosions.[21] Lithium-ion batteries are sold as battery packs with precise voltage control systems designed to prevent overcharging. Lithium-ion cells cannot simply be installed into a given electronic

application, and even though lithium batteries have a number of safety features, further safety measures need to be developed for EV use.

Modern applications require high-performance secondary batteries, and current lithium-ion battery technology is considered environmentally friendly. Relatively few toxic metals are used to manufacture LIBs. Like most rechargeable batteries they are recyclable, provided the consumer deposits them at a suitable recycling centre.

Having briefly introduced primary and secondary electrochemical cells based on lithium, and several safety issues of such batteries, relevant aspects of lithium-ion batteries will now be discussed in more detail.

A battery is composed of several interconnecting electrochemical cells, with each cell constructed of at least four different components: positive electrode, negative electrode, electrolyte, and separator.[7] The particular role and characteristics of the electrolyte, and ways to improve performance, will be discussed in the following paragraphs.

1.4 Electrolytes

In lithium-ion cells, as in all electrochemical cells, the electrolyte provides the transport medium for the transfer of lithium ions between the negative electrode and the positive electrode during cell charge-discharge cycles (Fig. 1.1). The lithium ion source is usually an aprotic lithium salt such as lithium hexafluorophosphate ($LiPF_6$).[22] In modern cells, the lithium salt is usually dissolved in a mixture of organic solvents, usually containing at least one of these organic carbonates: ethylene carbonate (EC), propylene carbonate (PC), dimethyl carbonate (DMC), diethyl carbonate (DEC), and ethyl methyl carbonate (EMC).[23]

The performance (*i.e.* capacity, cycling, and safety aspects) of lithium-ion batteries is highly dependent on the electrolyte solvent. Modern commercial lithium-ion batteries are based mainly on ethylene carbonate (EC)-based electrolytes, but propylene carbonate (PC) also has useful properties as a safe, nonaqueous electrolyte solvent in lithium-ion batteries for use at low temperatures.[24,25] However, PC has a strong tendency, after solvating lithium cations, to co-intercalate into the crystal structure of a graphite electrode, causing its destruction.[25,26,27] Moreover, organic carbonate solvents can react vigorously with lithiated graphite negative electrodes and delithiated metal oxide positive electrodes such as

Li_xCoO_2 ($x < 0.5$) at high temperatures.[28] A delithiated positive electrode is highly oxidizing and reacts exothermically with organic carbonate solvents. In addition, with a graphite negative electrode the SEI is also destroyed, resulting in rapid and violent reaction of the solvent with the lithiated graphite underneath. Therefore, several complex salts have been proposed[29] as alternatives to replace $LiPF_6$ as electrolyte, such as LiBOB (lithium bis(oxalato)borate)[30] and lithium fluoroalkylphosphates (*e.g.* $Li[PF_3(C_2F_5)_3]$).

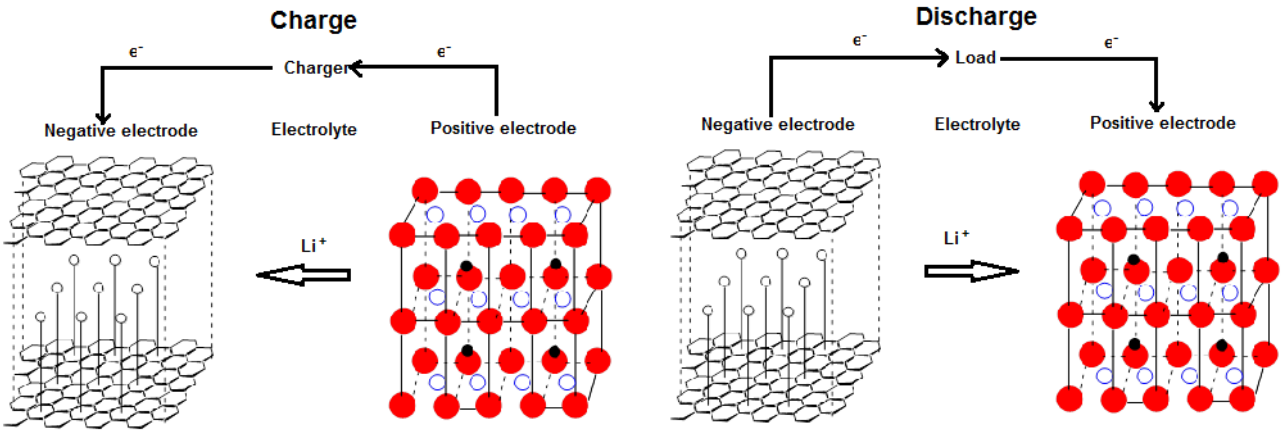

Figure 1.1 Schematic representation of the charge-transport mechanism in lithium-ion batteries when charging and discharging. In the positive electrode, ●: Oxygen, O: Co (or other transitional metal), •: lithium. Adapted from[7] with permission.

Additives that can improve the safety and performance of electrode materials over a wide temperature range by forming a protective film on the electrode surface are continually being developed. At most, about 5% additive is used because additives may lower the conductivity of the SEI. However, appropriate additives can improve the cyclability and cycle life of LIBs significantly.[19] Most probably, the additives electropolymerize on the electrode surfaces.[31-39] Many additives also lower the electrolyte flammability, a crucial factor when the cell vents solvent. Redox couples that shuttle between oxidized and reduced forms, and additives producing a gas when overcharging are also attracting interest. In the latter case, the formed gas is used to activate a current interrupter.

When developing solvents and additives for use in lithium-ion batteries, a balance between battery performance and safety must usually be found. For example, to ensure good performance, additives should be sufficiently reactive to participate in SEI-building

reactions on electrode surfaces. Secondly, additives should not adversely affect the electrolyte's desirable properties, such as good ion conductivity, low viscosity, and high wettability. Thirdly, to improve battery safety, an additive that decreases the flammability of the organic solvents and protects the battery against overcharging would be beneficial.

1.5 Negative electrode materials

Carbon-based materials and alloys of lithium are the most widely used negative electrode materials. These materials reduce the lithium reactivity with the electrolyte and solvents and therefore improve battery safety, but unfortunately also cause a drop in the cell voltage. The electrochemical potential of lithium metal lies above the LUMO energy of all electrolytes so that a passivation layer is formed by reaction of lithium with electrolyte. On discharge, Li^+ ions pass through this layer, but during charging the redeposited lithium tends to form dendrites (flaky crystals). These can travel through the electrolyte and separator, resulting in electronic pathways that short-circuit the cell. Negative electrode alloy materials that are currently under development for use in commercial batteries are nanocomposites such as titania-C,[40] silicon-C,[41] silicon-silica,[42] SnO_2-CNT,[43] and MoO_2;[44] however, graphite is still the negative electrode material of choice. Unfortunately, with prolonged battery use at high charging rates and temperatures,[45] the graphite undergoes extensive disordering of the surface structure,[46] resulting in failure.

Adding certain substances to propylene carbonate-based electrolytes,[47,48] results in enhanced SEI film formation during the first charge cycle before decomposition of the PC. Consequently, Li^+ ions can intercalate and de-intercalate reversibly into and out of graphite electrodes.[49-53] For example, substances such as allyl ethyl carbonate,[54] acrylonitrile,[55] tetrachloroethylene,[56] ethylene and propylene sulphites,[57,58] vinylene carbonate (VC),[59] chloroethylene carbonate,[60] silanes,[47,61] triethyl orthoformate,[38] 2-phenylimidazole (PID),[62] and *N*-phenylmaleimide (NPM)[63] have been used.

Some silanes and ethyleneoxy (EO) compounds tend to behave like crown ethers and cryptands by forming guest-host complexes with metal cations.[64-66] **Danil de Namor *et al*.[67] calculated** stability constants (log pKs) and enthalpies of complexation of lithium ion complexes with crown ethers such as 12-crown-4 and 1-benzyl-1-aza-12-crown-4 in the widely used electrolyte solvent propylene carbonate (PC); they showed an increase in ionic

conductivity with increasing stability of the complexes**. On the other hand,** Sporzyński *et al.*[68] confirmed by means of NMR, ESI and MS studies that certain ethyleneoxy boronates form 1:1 complexes with Li^+ and Na^+ cations. The stabilities of these pseudo-crown structures increased with increasing number of O atoms in the EO chains. **The lithium coronands also showed higher molar ionic conductivities than the bare electrolyte.**

The electropolymerization of polyoxasilanes results in a protective polymer network covering the surface of a graphite electrode, but which still permits lithium ion transfer between the electrode and the electrolyte. For example, a compound such as phenyl tris-2-methoxydiethoxysilane (PTMS) forms such a cross-polymerized network consisting of Si-O-Si bonds on the graphite surface; this seems to prevent propylene carbonate and lithium ions from co-intercalating into graphite electrodes.[47] These polyoxasilanes, like the boronates, show some fire-retardant activity, thereby improving the safety of lithium-ion batteries in their applications. During final revision of this report, a paper appeared showing that the 12-crown-4 complex with Li^+ ions lowered the cation-anion interaction in electrolyte solid solution, increasing the ionic conductivity of a solid electrolyte to 39.3 and 153 μS cm^{-1} at 25 and 80 °C, respectively.[69]

1.6 Positive electrode materials

Because lithium negative electrodes do not have reliable reversibility, high-potential oxide positive electrodes were developed. Widely used positive electrode materials, such as the mixed oxides of lithium with transition metals, are oxidized to higher valencies upon delithiation.[70] In such mixed oxides, the transition metal is oxidized to maintain charge neutrality, but such oxidation in turn usually leads to unwanted phase changes that could influence battery performance. For good battery performance a stable crystal structure must be produced.[71] The most successful and commonly used positive electrode material is $LiCoO_2$,[72] but less expensive and more stable alternatives are needed for large-scale application in EVs. Cobalt is not only costlier than other transition metals, such as manganese, nickel, and iron, but $LiCoO_2$ is also less stable than other electrode materials. When overcharged, $LiCoO_2$ positive electrodes can fail and undergo degradation.[73]

The $LiCoO_2$ positive electrodes were preferred to $LiNiO_2$ because they are more stable. However, nickel is less expensive than cobalt and its use in electrodes would contribute to

lowering battery costs. Replacing most of the cobalt with nickel, such as in $LiNi_{1-x}Co_xO_2$, which typically contains mostly nickel ($x\sim 0.2$), results in formation of a new low-cost material that benefits from the higher charge-discharge capacity of nickel relative to cobalt.[74] Similarly, a high capacity and good rate capability are obtained when nickel, or nickel and cobalt, are added to monoclinic $LiMnO_2$ to form a compound like $Li(Ni_{1/3}Mn_{1/3}Co_{1/3})O_2$.[75] $LiMn_2O_4$ forms a spinel structure with manganese occupying the octahedral sites in the crystal lattice and lithium mostly occupying the tetrahedral sites.[76] $LiMn_2O_4$ is less expensive than $LiCoO_2$, but has a lower charge-discharge capacity than other positive electrode materials; addition of some cobalt might improve its capacity. Vanadium can have several valencies and layered vanadium oxides such as orthorhombic V_2O_5 and monoclinic LiV_3O_8 can be used as electrode materials. Although these materials have high capacities, they produce lower voltages than the other materials.[77]

1.7 Solid electrolyte interphase (SEI) formation

The solid electrolyte interphase is generally understood to be a thin layer about 30 to 50 nm thick, consisting of inorganic and organic products that are formed on the electrode surface during cycling. During a succession of charge and discharge cycles, the electrolyte and solvent(s) are reduced to some extent at the negative electrode. The formation of a stable, continuous and permeable SEI layer on the negative electrode is a crucial aspect of the first charge event, because such a passivation layer[78] protects the electrode against exfoliation and permits the ion conduction needed for lithium ion insertion and extraction.[3]

With cyclic carbonate solvents such as ethylene carbonate or propylene carbonate, SEI film formation typically starts with a ring-opening reaction in the presence of the electrolyte. The ability of the SEI membrane to enhance cell performance and even improve its safety must be developed further and an understanding of the processes involved is crucial for future electric vehicle (EV) development.[79]

Thus, the SEI consists mainly of the decomposition products of electrolyte solvents and salts. These typically are Li_2CO_3, lithium alkyl carbonate, and lithium alkoxide, but other lithium salts such as LiF can also be formed. Two competing mechanisms are generally accepted[19] for the reduction of carbonate-based solvents such as PC and EC in a cell (Scheme 1.1).

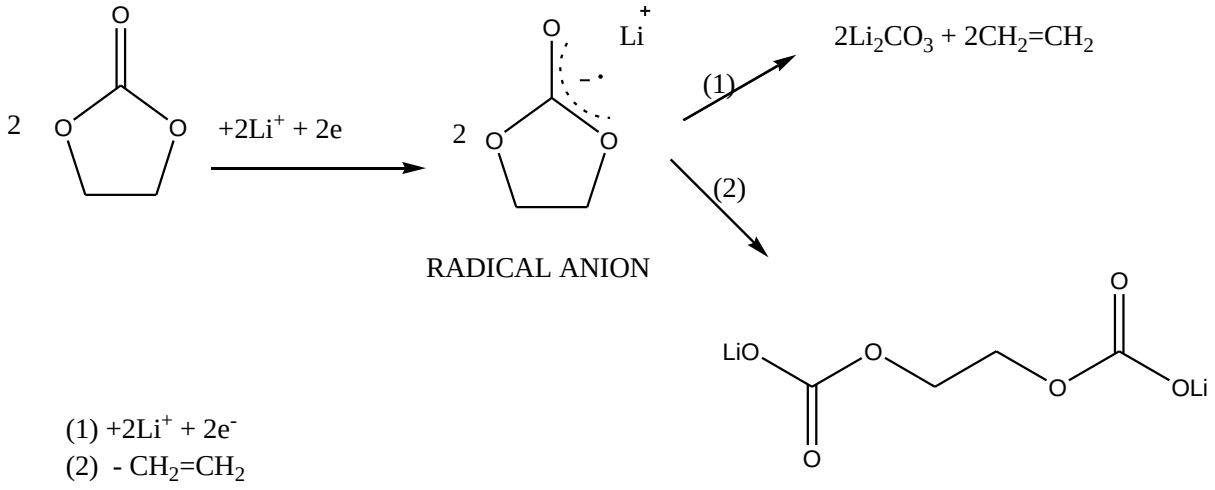

Scheme 1.1 The two competing two-electron mechanisms for SEI formation.[19]

In mechanism 1, the solvents are reduced to form gaseous products, forming an unstable SEI containing mostly Li_2CO_3, whereas mechanism 2 leads to formation of less gas and insoluble products, resulting in a more stable and compact SEI. Modification of the surface of a graphite electrode by mild chemical oxidation[80] or by coating the electrode surface with a permeable polymer film can assist in SEI formation during the first cycle and also reduces gas generation.

The SEI forms over two voltage ranges. In the first phase a highly resistant SEI with a porous and dimensionally unstable structure is formed; it is generated during the first charge, before the first intercalation of lithium ions into the electrode. In the second phase, which happens during intercalation of lithium ions, a very compact and conductive SEI is produced. Whereas the SEI formed in the first phase consists mostly of inorganic components, the SEI developed during the second phase is enriched in organic compounds. Presumably the formation of a network of organic compounds coordinated with lithium ions and organic carbonate ions (Figure 1.2) increases the stability of the SEI formed during the second phase.[81]

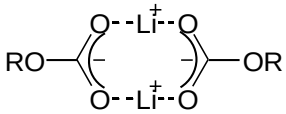

Figure 1.2 Coordination of lithium ions with organic carbonate ions.

The ion conduction in the SEI presumably is the result of the migration of solvated lithium ions through microchannels in the SEI. Additives that support this characteristic would

therefore be very useful. For example, when an organic film is coated chemically or electrochemically onto the surface of an electrode, SEI formation can be induced if the additive has a higher reduction potential than the electrolyte solvent. This results in the preferential reduction and possible polymerization of the additive before the electrolyte solvent is reduced; the surface of the electrode is then covered by an insoluble solid product. Such a film would inactivate the catalytic activity of the electrode surface and prevent the reaction of the solvent. Most successful additives therefore have one or more C=C double bonds or other features that could participate in electropolymerization (Figure 1.3).

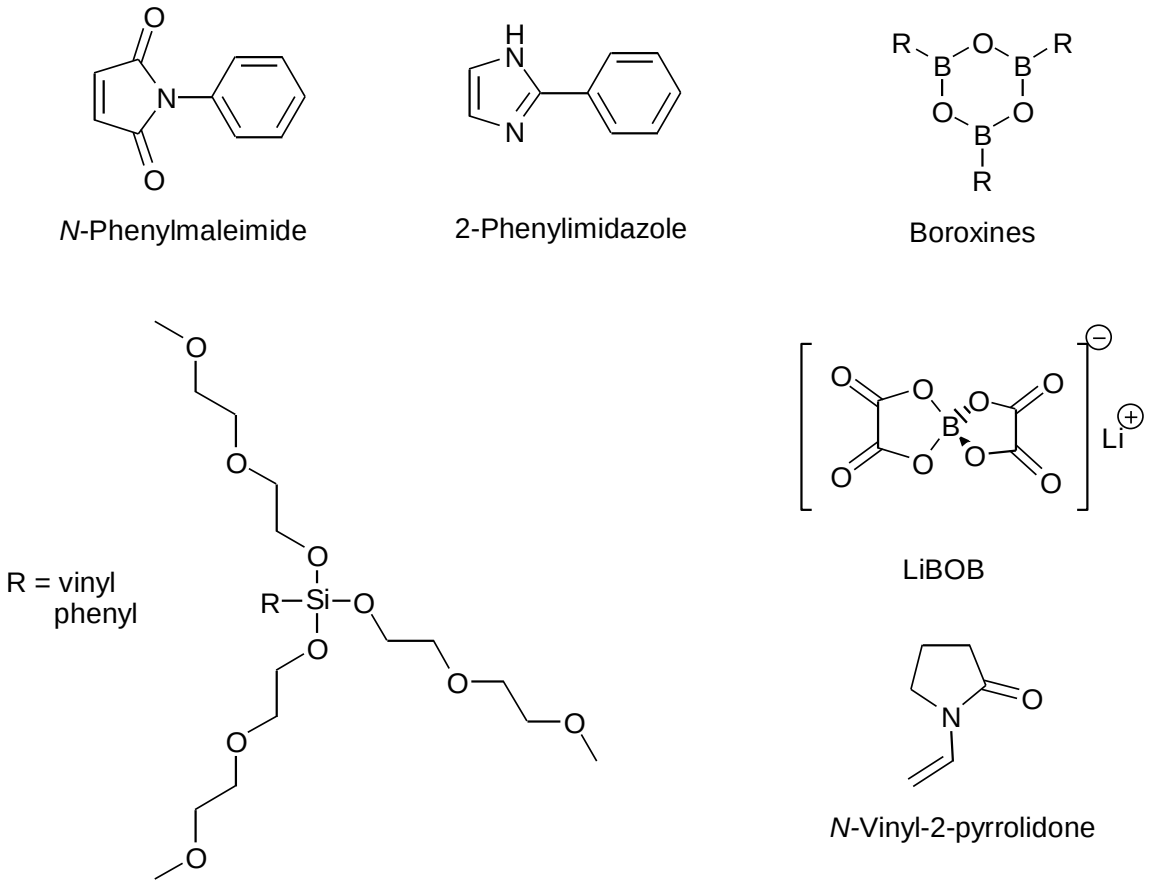

Figure 1.3 Electropolymerizable additives.

The product of this decomposition develops a solid layer on the surface of the electrode material. Continued SEI formation over the lifetime of the battery would soon render LIBs unusable due to the continued loss of lithium.[82] Lithium-ion batteries can continue to operate because the SEI does not conduct electrons and is almost impenetrable to electrolyte molecules, while the intercalation of lithium ions can continue, which is the desired electrochemical reaction. After formation of the SEI layer, the electrolyte and

solvent molecules cannot be transported through the SEI. As a result, further SEI growth is inhibited because the electrolyte does not reach the electrode surface and cannot react with the active materials. Lithium intercalation is not suppressed because the lithium ions pass through the SEI by ion exchange between the electrolyte, SEI components, and lithium in the electrode material. Now the battery can undergo several thousand charge-discharge cycles.[83] Figure 1.4 provides a schematic diagram of the composition of the SEI on a graphite electrode.[82]

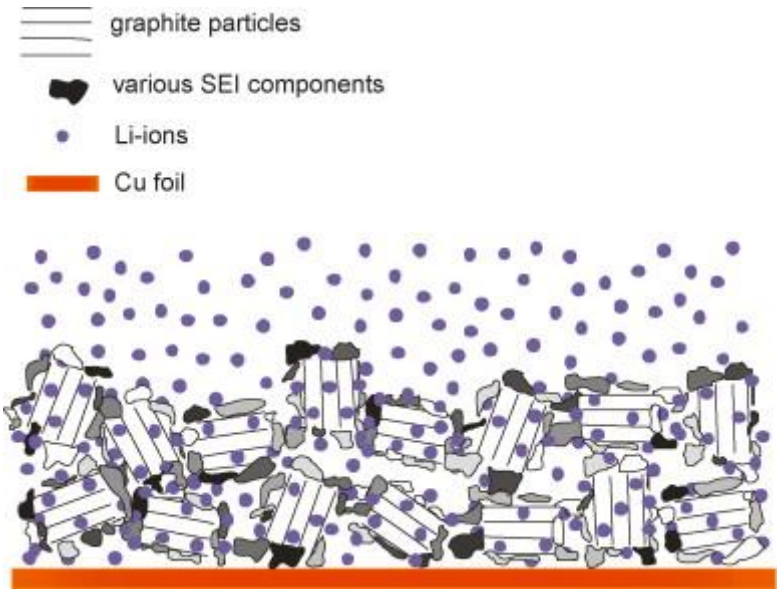

Figure 1.4 A lithiated composite graphite electrode covered by organic and inorganic SEI components (reproduced from[82] with permission of the publisher).

1.8 Overcharge protection

Overcharging a lithium-ion battery can be risky. Overcharge can take place when a cell is already fully charged but current continues to flow through it. The charge is above the charge-storage capability of the cell, which can lead to a range of reactions of the battery components. The result is usually a rapid temperature increase, self-accelerating reactions and explosion.[1,84] Overcharge protection additives may be classified as redox shuttles, which reversibly protect the cell from overcharging, or shutdown additives, which permanently terminate cell operation.

Because battery shutdown is undesirable, overcharge protection by means of redox shuttle additives that enable continued operation of lithium-ion batteries, has been investigated

widely. A redox shuttle should be oxidized reversibly at a potential just above the end-of-charge potential of the positive electrode, or reduced reversibly at a potential just below the end-of-charge potential of the positive electrode. This mechanism protects the battery against overcharging because the potential of the positive electrode does not exceed the oxidation potential of the redox shuttle. As can be deduced from the above arguments, two kinds of shuttles can be distinguished. With the 'p-type' shuttle, *during charging* the shuttle molecules must be oxidized reversibly at slightly higher potentials than the standard end-of-charge potential of the positive electrode, and reduced reversibly at the negative electrode (Figure 1.5(a)). When the overcharged state is reached after full delithiation of the positive electrode, the shuttle molecules will be oxidized at the positive electrode and the oxidized shuttle molecules migrate to the negative electrode; here the shuttle is reduced to the original state. On the other hand, 'n-type' shuttle molecules are designed to be reduced reversibly during charging at potentials below the normal end-of-charge potential of the negative electrode, and oxidized at the positive electrode (Figure 1.5(b)). In this case, the potential of the fully lithiated negative electrode material decreases to a value where the reduction of the shuttle molecule kicks in. The reduced shuttle then diffuses to the positive electrode where the oxidized form is regenerated. The detailed mechanism as described by Wang *et al*.[85] is shown in Fig. 1.5.

From the above description, it can be seen that a highly reversible shuttle reaction at an oxidation potential just above the normal end-of-charge potential of the positive electrode, but lower than the decomposing potential of the electrolyte solvents, is desired. Of course, both the oxidized and reduced forms must be soluble in the electrolyte solvent.

The described shuttle action results in the permanent locking of the positive electrode potential at the oxidizing potential of the shuttle molecule, and the current supplied during overcharging is converted to heat.

Quantum-chemical calculations nowadays assist in the search for redox shuttles.[86] The shuttle mechanism as extensively investigated for the anisole family[19] is represented schematically in Scheme 1.2.

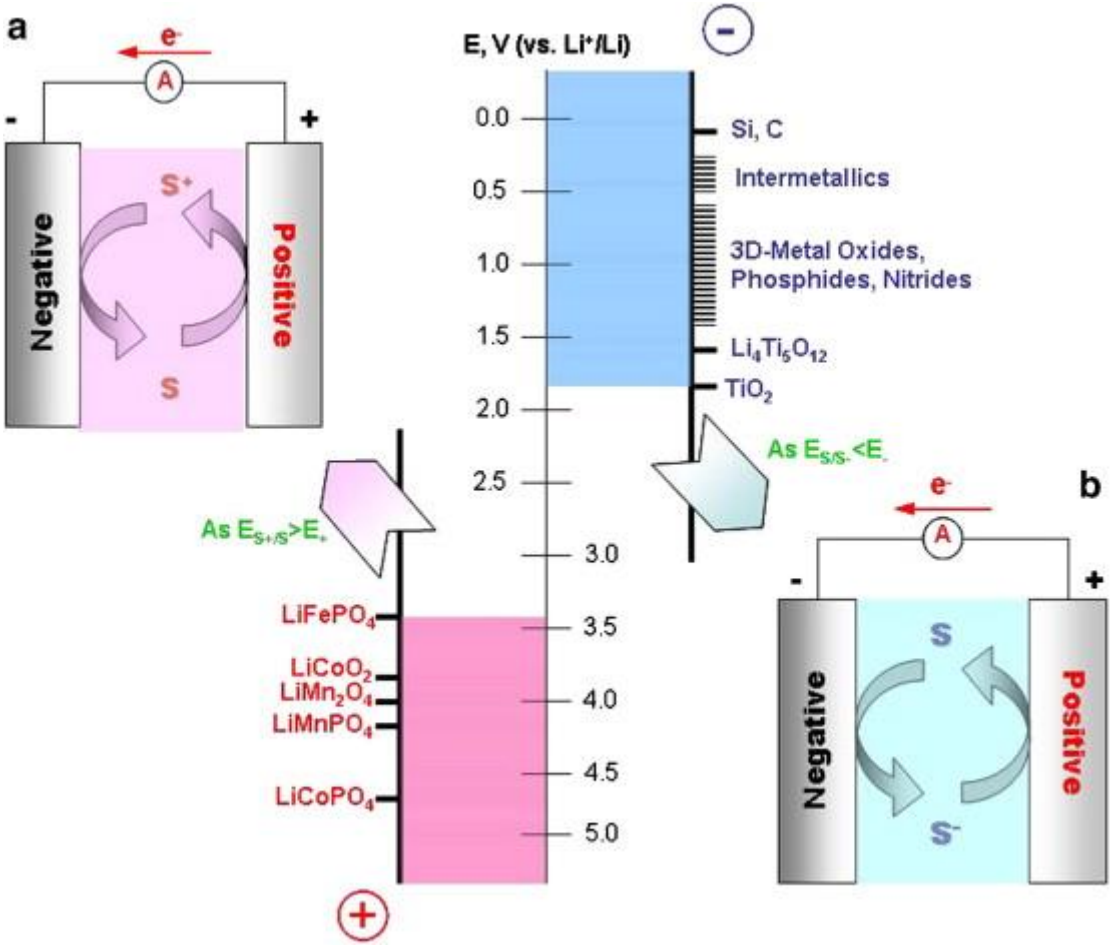

Figure 1.5 Overcharge protection by a redox shuttle **S** (reproduced from[85], with permission): (a) p-type shuttle action; (b) n-type shuttle action.

The redox potential, the reversibility and efficiency of shuttle molecules based on anisole derivatives are all determined by the types and positions of the alkoxy groups and other substituents attached to the aromatic ring.[23,78]

1.9 Properties of vinyl tris-(methoxydiethoxy)silane (VTMS), a flame-retardant electrolyte additive

This part of the work was undertaken previously in collaboration with Ms KA Thavhiwa (Univen) and the Fudan University group in Shanghai, China. An excerpt of our own previously published work [47,84,87] follows as a practical illustration of the desired effects of additives on electrolyte safety, electrode integrity and the SEI.

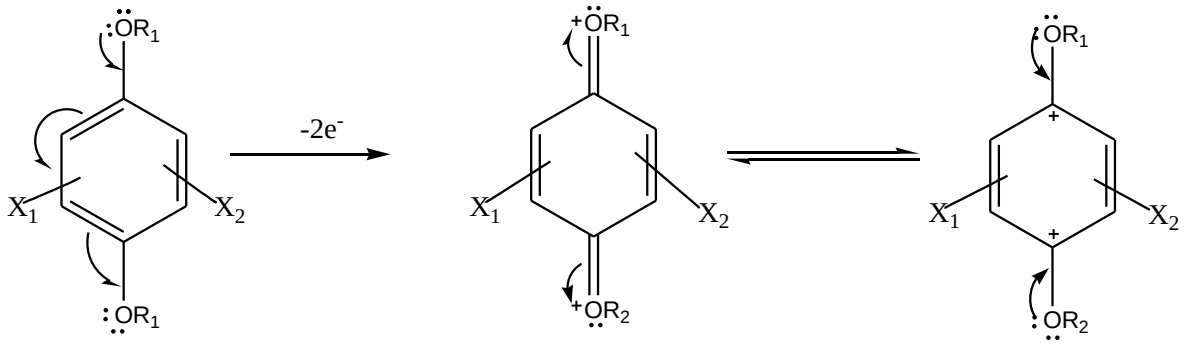

Scheme 1.2 Redox shuttle mechanism for anisole derivatives, where R_1 and R_2 are different alkyl groups, and X_1 and X_2 are H, halogen, or alkyl groups.[19]

Vinyl tris-(methoxydiethoxy)silane (VTMS) is commercially available, but also readily prepared by reaction of vinyl trichlorosilane with anhydrous diethylene glycol monomethyl ether (Scheme 1.3). VTMS has a high thermal stability, which explains its fire retardancy. It is closely related to other ethyleneoxy additives such as methyl phenyl bis-(methoxydiethoxy)silane,[84] which prevents the decomposition and co-intercalation of PC and also acts as a flame retardant. Similarly, phenyl tris-(2-methoxydiethoxy)silane (PTMS)[47] also prevents the decomposition and co-intercalation of PC by forming a SEI. VTMS can be considered a bi-functional additive: acting as a flame retardant (as demonstrated in Fig. 1.6) and SEI component preventing the exfoliation of graphite for ethylene carbonate (EC) -based electrolytes (as shown by the CV in Fig. 1.7 and EIS in Fig. 1.8). Addition of these substances to electrolyte resulted in C-Si-O and Si-O-Si bond formation on the surface of the graphite anode, as evidenced by X-ray photoelectron spectroscopy (XPS) and FTIR spectroscopy.

The flame propagation and burning-up times of EC-based electrolyte with different amounts of VTMS are shown in Fig. 1.6. The bare electrolyte is highly flammable; its flame propagation and burning-up times are quite short, respectively at 4.8 and 47.5 seconds. As the amount VTMS added increases, there is a decrease in the flame propagation rate, and an increase in the burning-up time. At 10 vol.%, VTMS the flame propagation time of the electrolyte is 10 s, more than double that of the bare electrolyte. The burning-up time is also higher as the VTMS content rises.

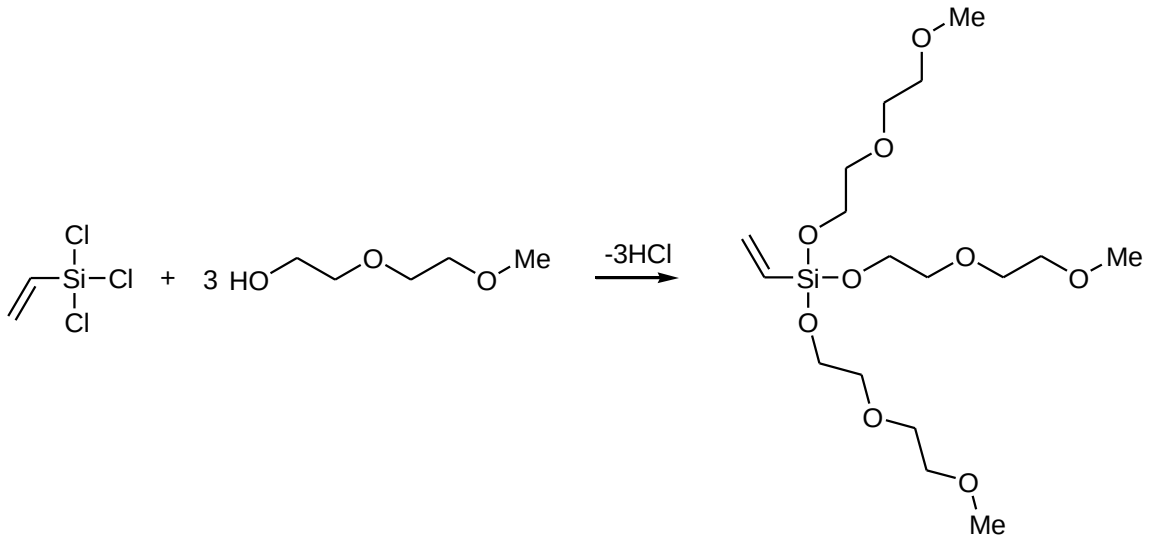

VTMS

Scheme 1.3 Synthesis of vinyl tris-(methoxydiethoxy)silane (VTMS).

The CV curves of a $LiCoO_2$ positive electrode in electrolyte before and after adding 5 vol.% VTMS are shown in Fig. 1.7. In addition to the lithium de-intercalation and intercalation peaks between 3.5 and 5.0 V, the electrolyte with VTMS added displays an additional peak at 5.35 V, corresponding to the oxidation of VTMS. This shows that VTMS remains stable in the normal voltage range of lithium-ion batteries; it should therefore be a feasible additive to the electrolyte.

Electrochemical impedance spectroscopy (EIS) was used for further study of the additive behaviour. EIS studies can assist in determining the resistances involved in the overall lithium ion storage process, as well as the insertion-extraction process occurring during the cycling of the battery.[88] In EIS, an AC potential is applied to an electrochemical cell and the changing current through the cell is measured. When such an AC potential is applied, the response to this potential is also an alternating current. Analysing this response by Fourier transform as a sum of sinusoidal functions leads to the electrochemical impedance, which is expressed as a complex number,

$$Z(\omega) = {}^{E}/_{I} = Z_0\exp(j\phi) = Z_0(\cos\phi + j\sin\phi)$$

$Z(\omega)$ consists of a real and an imaginary part. A graph of the imaginary part *versus* the real part is called a 'Nyquist Plot.' The Nyquist Plot is therefore a graph of the impedance versus frequency.

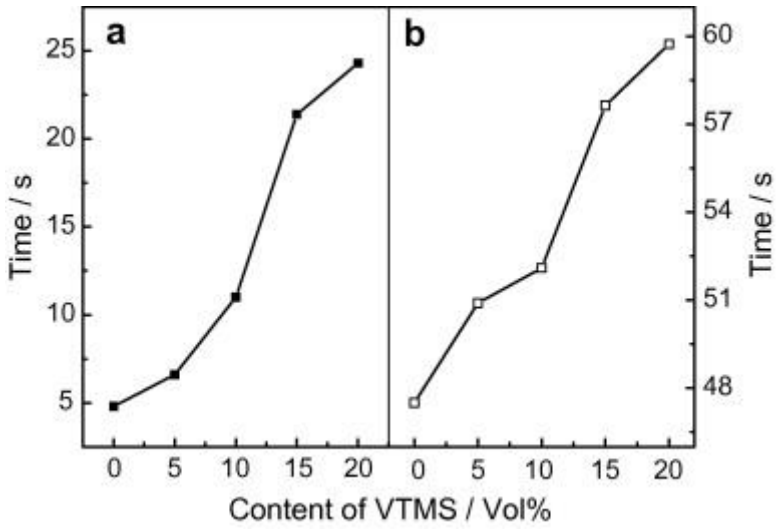

Figure 1.6 (a) Flame propagation and (b) burning-up times of 1.0 M $LiPF_6$ in EC/EMC/DMC (1:1:1 v/v/v) with different amounts of VTMS added (reproduced from[87] with permission).

The Nyquist plots at the 20th charge-recharge cycle of a $LiCoO_2$ positive electrode in bare electrolyte and in electrolyte containing different amounts of VTMS, are shown in Fig. 1.8. The high-frequency semicircle region is usually attributed to SEI film and the Li^+ charge-transfer impedance on the electrode/electrolyte interface. The semicircles are similar in radius, showing the relatively small effect of VTMS on the impedance of the surface film. The radii of the semicircles at medium frequencies are related to the charge transfer resistance (R_{ct}) of the positive electrode. In electrolyte with 5 vol.% VTMS, the R_{ct} increases very little. With more than 5 vol.% VTMS added, the R_{ct} increases and the electrochemical performance becomes poor.

Figure 1.9 illustrates the effect of a suitable additive, this time methyl phenyl bis-methoxydiethoxysilane,[84] on the surface morphology of a carbon microsphere (CMS) electrode before and after several charge-discharge cycles in a propylene carbonate (PC) – based electrolyte. Figure 1.9(a) clearly shows the smooth spherical surface of the original CMS. After a number of charge-discharge cycles in an electrolyte containing the additive, a uniform layer of surface film covering the CMS spheres could be observed (Fig. 1.9(b)). However, when the CMS was cycled in bare PC-based electrolyte the graphite layers were badly exfoliated by co-intercalation of solvent,[18,24,89] as shown in Fig. 1.9(c).

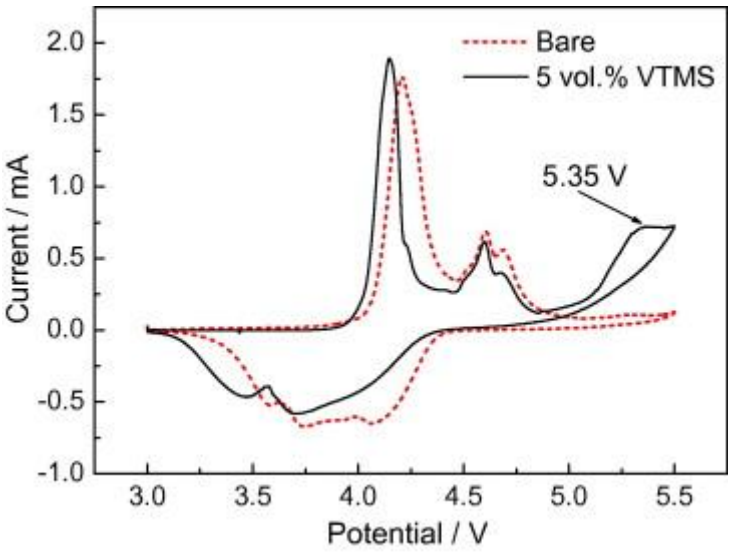

Figure 1.7 CV curves of a $LiCoO_2$ electrode with 1.0 M $LiPF_6$ in EC/EMC/DMC (1:1:1 v/v/v) as electrolyte, before and after addition of 5 vol.% VTMS (reproduced from[87] with permission).

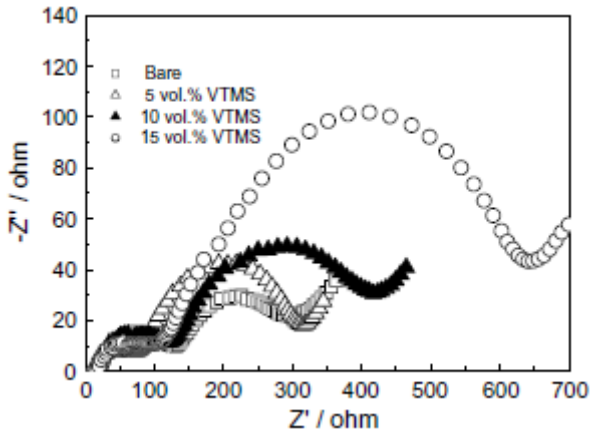

Figure 1.8 Nyquist plots (after 20 cycles) of a $LiCoO_2$ electrode with 1.0 M $LiPF_6$ in EC/EMC/DMC (1:1:1 v/v/v) as electrolyte, containing various amounts of VTMS (reproduced from[87] with permission).

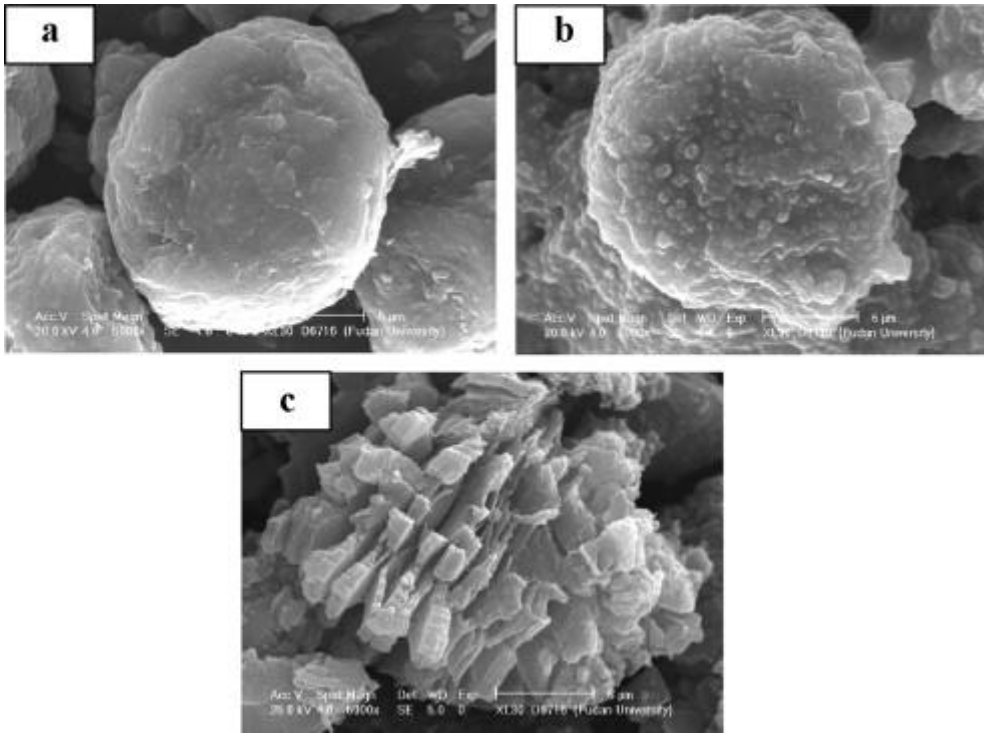

Figure 1.9 SEM images of CMS electrode in 1 M $LiPF_6$ electrolyte in PC/DMC 1:1 (v/v): (a) before cycling, (b) after 5 cycles in electrolyte with 4% (w/w) methyl phenyl bis-methoxydiethoxysilane additive, and (c) after 5 cycles in electrolyte without additive (reproduced from[84], with permission).

1.10 Problem statement, aims and objectives

The development of lithium-ion batteries has been very rapid since their appearance in the early 1990s, due to their advantages over traditional rechargeable batteries, such as high output voltage, high energy density, freedom of memory effects and long cycling life. However, in high-power applications the safety issue becomes serious. At high current densities, the liquid electrolyte can react with the positive electrode material, leading to the release of heat and thermal run-away. It is therefore crucial to find new kinds of additives and electrolytes to reduce this thermal production.

Compound **7** (3,5-bis(trifluoromethyl)phenylboronic acid, Figure 1.10) was recently shown to be reduced at a higher potential than that of Li^+ ions in PC-based solvent because it has a lower LUMO energy than PC.[48] This additive actively suppresses the decomposition of carbonate-based solvents that leads to exfoliation of graphite electrodes; in this way, the additive allows the reversible intercalation and deintercalation of lithium. This compound

also has fire-retardant activity as a bonus function. As described above, ethylene glycol oligomers have found wide application in lithium-ion battery electrolytes as film-forming additives preventing the decomposition and the co-intercalation of PC, and boronates are known as redox shuttles, as noted before.

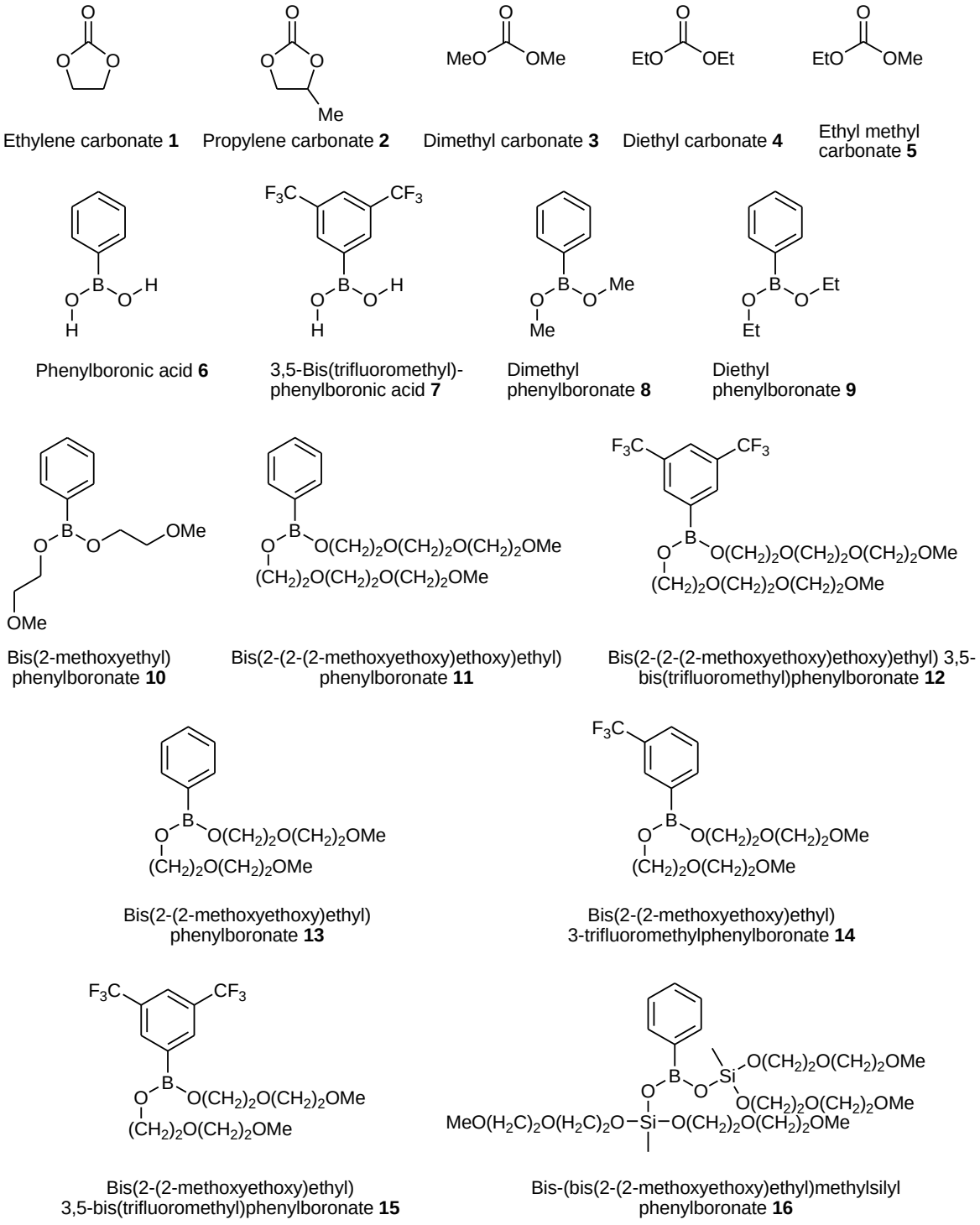

Figure 1.10 Structures of Compounds **1** to **16**, described in this dissertation.

Lithium ion coordination to crown ethers and cryptands similar to the envisaged boronates is a well-known phenomenon,[68,90] also in lithium ion batteries;[67,69] duplicating the investigation of the lithium ion – boronate complexes would diffuse the focus of this study and was therefore not included in the scope of this project. Lithium salts form stable complexes with 12-crown-4 and its derivatives.[67] Calculation of standard Gibbs energies and standard entropies of these complexes in propylene carbonate (PC), a commonly used electrolyte solvent, showed a correlation between the stability of the lithium-ion – crown complex and also an increase in the conductivity of the complexed relative to the free cation; the lithium coronands were shown to have a higher ion conductivity than the bare electrolyte.[67]

It is also well known that ethyleneoxy boronates form 1:1 complexes with Li^+ and Na^+ ions in a pseudo-crown structure.[68,69] The stabilities of the complexes increase with increasing length of the EO chain; however, as shown very recently during revision of this dissertation, there is an optimum size for use in lithium-ion batteries.[69] Addition of the Li^+ - 12-crown-4 complex (Figure 1.11) to a solid state electrolyte decreased the lithium cation – anion interaction, resulting in improved electrochemical properties of the electrolyte. This was explained by inhibition of crystal growth, which ensures more amorphous and smoother areas in the electrolyte, which becomes better conducting by the movements of the crown segments.[69]

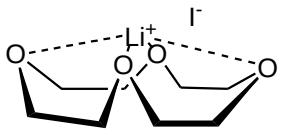

Figure 1.11 The Li^+ - 12-crown-4 complex, with iodide as counter-ion.

With these observations in mind, it was hypothesised that combining these two functions in one molecule would significantly enhance the performance of such an additive. Theoretical (molecular modelling) studies of the HOMO and LUMO energies of novel EO-boronate derivatives were envisaged, which would enable comparison of expected electrochemical properties to those of the commonly used electrolyte solvents.

1.10.1 Aims

This study is aimed at developing safer lithium-ion power sources by introduction of new additives to overcome the possible safety problems. The overcharged states of batteries cause serious safety problems because overcharging results in highly oxidized positive electrodes in which highly exothermic reactions can take place, which could lead to thermal runaway. To protect batteries from overcharging, electropolymerizable monomers, redox shuttles and many other kinds of electrolyte additives have been developed. Several organic materials, such as boronate esters and oligoethylene glycols, have also been suggested to overcome these safety problems.

1.10.2 Objectives of the study

The main aim of this project was to find new organic additives to try to improve the safety behaviour of lithium-ion power sources, and so pave the way for the commercial production of electric vehicles. Consequently, the following objectives were pursued in this study:

- Synthesis of novel boronate and ethyleneoxy (EO) derivatives from substituted boronic acids and other precursors.
- Theoretical (molecular modelling) studies of these derivatives with respect to their expected electrochemical properties.
- Electrochemical studies of the derivatives.

Chapter 2
Results and discussion

Molecular orbital modelling and calculations are very useful tools to screen electrolyte additives. It is widely accepted that the structural characteristics of a molecule determine its physical and electrochemical properties. In this study, the conformations and electrochemical properties of various boronates (*see* Fig. 1.10) were investigated. The computational study used density functional theory (DFT) applying the Becke's three-parameter hybrid method with the Lee-Young-Parr correlation functional (B3LYP). Initial energy optimization with *Møller*-Plesset Perturbation theory (MP2) was followed by an investigation of the conformational preferences and energetics using DFT calculations and the 6-31G(d,p) basis set *in vacuo*. Typical output is shown in Appendix A.

Apart from the computational studies, several of the compounds studied theoretically were also synthesised and characterized, and investigated by cyclic voltammetry (CV) and electrochemical impedance spectroscopy (EIS). The results obtained are discussed in the following sections.

2.1 Theoretical models used in Computational Chemistry

Molecular mechanics (MM) simulations use the laws of classical physics to predict structures and properties of molecules, while electronic structure methods use the laws of *quantum mechanics* (QM) as the basis for computation.

The different MM methods that are available are each characterized by their force field.[91] Such a force field consists of

- A set of equations describing the variation of the molecule's potential energy with the positions of its atoms;
- A series of atom types describing the behaviour of an element depending on its hybridization, charge, and environmental factors;
- Parameter sets consisting of force constants, bond lengths and angles that fit the equations and atom types to experimental data.

Single point energy calculations are done to predict the total energy and other properties of a specific molecular geometry, and their validity depends on defining a reasonable structure for the molecule. These calculations can be done at different levels of theory and with small or large basis sets, depending on the objectives and computer resources. MM computations are computationally inexpensive and can be used for very large systems, but have several limitations; for example:

- Each force field is suitable only for a limited class of molecules, depending on the parameter sets;
- Electrons are neglected, so that bond formation and breaking and other properties depending on electronic effects cannot be modelled.

On the other hand, electronic structure methods or *quantum mechanics* (QM) depend on solving the Schrödinger equation, which becomes computationally intractable for real systems. Therefore, various mathematical approximations have been developed for solution, such as semi-empirical methods,[92] *ab initio* methods,[93] and density functional theory (DFT) methods.[94]

Semi-empirical methods, such as AM1,[95] MINDO/3,[96] and PM3,[97] implement experimental data to simplify calculations in solving an approximate form of the Schrödinger equation. The different methods are characterized by their different parameter sets. Semi-empirical methods are computationally inexpensive at the cost of accuracy, and can be used

- For very large systems;
- As a first step for large systems, for example starting with a semi-empirical optimization to obtain a starting structure for a subsequent HF or DFT optimization. *This approach was followed in the current study*.
- For ground-state systems that are well-parametrized and well-calibrated, such as simple organic molecules;
- To generate qualitative information about molecular orbitals, atomic charges, or vibrational normal modes.

However, semi-empirical methods should only be used for systems with well-developed parameters for all atoms, and they do not perform well when hydrogen bonding, transition structures and atoms for which they are poorly parametrized are involved.

Ab initio methods are based solely on the laws of quantum mechanics and on the values of known physical constants such as the speed of light, masses and charges of electrons and nuclei, and Planck's constant. A series of rigorous mathematical approximations is used to solve the Schrödinger equation. High quality quantitative predictions can be made for a broad range of systems, at the cost of more computational resources (memory and time). Hartree-Fock (HF) theory is mostly used. However, electron correlation is not treated fully, and bond lengths and lower IR frequencies are predicted poorly.

Post-SCF methods, such as DFT, are attractive because they include the effects of electron correlation in their models - electrons in a molecule react to neighbouring electrons' motions and attempt to avoid each other. In HF calculations this effect is considered only in an average sense, while DFT accounts for the instantaneous interactions of pairs of electrons with opposite spin. DFT methods are similar to *ab initio* methods and DFT can therefore provide the benefits of more expensive *ab initio* methods at the cost of HF-level calculations. Electron correlation is computed using general *functionals* (functions of functions) of the electron density. Many such functionals have been defined, depending on how they treat the exchange and correlation components of the electron-electron interaction energies:

- *Local* exchange and correlation functionals use the values of the electron spin densities only;
- *Gradient-corrected* functionals involve both electron spin densities and their gradients. Most popular amongst these is the functional proposed by Becke,[98] used together with the Lee-Yang-Parr (LYP)[99] functional in the BLYP method. This method has been modified by Becke to use a linear combination of HF, local and gradient-corrected exchange terms, and combining this with a local and/or gradient-corrected correlation functional. This is the widely-used B3LYP method,[100] *used in this study*, which has been proved to be superior to the preceding functionals.

The *basis set* represents a molecule's molecular orbitals (MOs) mathematically and restricts each electron to a particular region of space. The larger the basis set, the fewer the constraints on the electrons and the more accurate the calculated MOs. *Minimal basis sets* contain the minimal number of basis functions needed for each atom. For example, carbon has five basis functions: 1*s*, 2*s*, 2p_x, 2p_y, and 2p_z. The STO-3G basis set uses three gaussian

primitives (hence '3G') per basis function. 'STO' means 'Slater-type orbitals', which are more accurate than gaussians but less convenient to use.[101]

Polarized basis sets allow orbitals to change size and shape by adding orbitals with angular momentum beyond what is required for the ground state. The basis set 6-31G(d,p), *used in this study*, has become common for calculations of medium- to large-sized systems. It adds *d* functions to heavy atoms and *p* functions to hydrogen atoms.

2.2 Predicting IR spectra

Energy calculations use an idealized, static view of nuclear positions, but in reality the nuclei are constantly in motion. These vibrations are regular and predictable and are used to identify molecules by means of their IR and Raman spectra. The vibrational frequencies are calculated from the second derivative of the energy with respect to the nuclear positions and are available mainly for the HF, MP2 and DFT (B3LYP) procedures. These calculations are valid *only* at stationary points on the potential energy surface and must therefore be performed on structures optimized at the same level of theory, using at least the 6-31G(d) basis set (6-31G(d,p) *was used in this study*). Obtaining a negative (or imaginary) frequency indicates that a saddle point was reached, not an energy minimum.

2.3 Calculations of LUMO energies of selected compounds

To be of practical use for the electrolyte solution of lithium-ion batteries, the solvent must be electrochemically stable, which is determined by the energies of the frontier orbitals (*i.e.*, the HOMO, LUMO, and some adjacent orbitals). The reduction potentials of solvents and any additives are related to their LUMO energies;[102] therefore, molecular orbital modelling is widely used to screen electrolyte additives.[86,103]

The approach followed here was to start with an approximation of the structures of a range of organic solvents and additives (Figure 1.10), using the Parameterized Model 3 (PM3). This was followed by optimization using density functional theory (DFT) in Gaussian 03.[104] The basis set used was 6–31G(d,p), which provides reasonably accurate results in manageable timeframes. In Table 2.1, the results of extensive optimization calculations are shown. IR frequency calculations confirmed that energy minima were reached. In the case

of the boronate ester/acid part of the molecules, three limiting relative conformations were considered, with the example of phenylboronic acid presented in Figure 2.1. For convenience they are named 'in-in' (where the HO or ester groups are both directed towards the aromatic ring), 'in-out' (where only one HO or ester group is oriented towards the aromatic ring), and 'out-out' (both groups pointing away from the aromatic ring). In each case two energy optimizations were done, with the starting dihedral angle between the boronate group and the aromatic ring 0° (coplanar) and 90° (perpendicular). These conformations are shown for phenylboronic acid (**6**) in Figure 2.2.

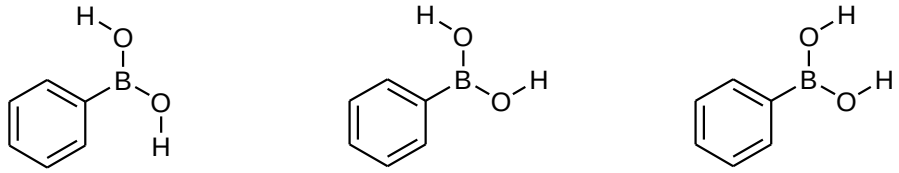

Figure 2.1 Phenylboronic acid (**6**) geometries.

(a) 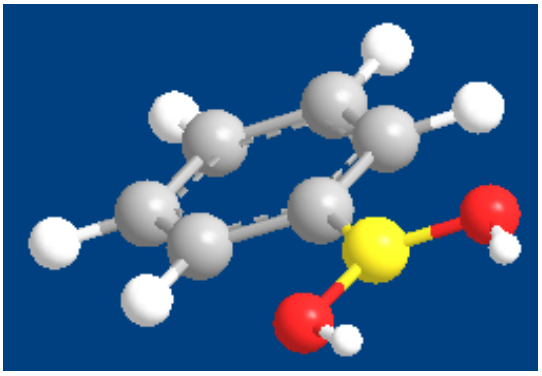 (b) 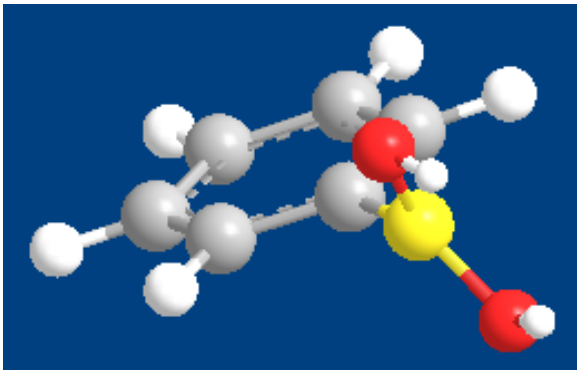

Figure 2.2 Phenylboronic acid (**6** 'Out-Out') dihedral angles: (a) 0°, and (b) 90°.

The conformational preferences (lowest-energy conformers) of the boronates studied by DFT calculations (**6**, **7**, **8**, **9**, **10, 11, 12, 13, 14, 15**) were always 'in-out', with dihedral angles between the aromatic ring and boronate group varying between 11° and 14° for the boronic acids, and 32° to 35° for the esters (Table 2.1). Clearly, on *electronic* grounds coplanarity would be preferred, because of hyperconjugation and backbonding of the aromatic ring with the empty boron 2*p* orbital. Arylboronic acids have been shown to exist as hydrogen-bonded dimers in solution,[105] and weak hydrogen bonding between the *ortho*-hydogens and boronate oxygens might also play a role. These effects are borne out by the

smaller dihedral angles of the boronic acids. These stabilizing effects are countered by the *steric* effect of the EO ester chains, resulting in increased dihedral angles. In turn, the non-coplanarity would have an effect on the solvent accessibility and redox activity of the boron atom. Dihedral energy scans at the RHF level of Compound **6** (phenylboronic acid) are shown as an example in Figure 2.3, and show a relatively low torsional energy barrier of 3 to 6 kcal/mol. Interestingly, the 'In-In' conformation exhibited energy maxima at 90° and 180° (Fig. 2.3c), possibly due to steric interaction between H atoms in the coplanar case, and electronic interaction between the H atoms and the π electron cloud in the perpendicular case. This phenomenon deserves further study. On the other hand, the planar 'Out-Out' geometry (Fig. 2.3a) turned out to be lowest energy conformation, a result that could not be confirmed by the DFT calculations. This might be explained by the combined effect of boron back-bonding and intramolecular hydrogen bonding with carbonate solvent (Fig. 2.4). The frontier orbitals of these three geometries of phenylboronic acid **6** show that, while there is still some skewing of the LUMO of the In-In and In-Out geometries, the Out-Out geometry is fully planar (Fig. 2.5).

Using both the perpendicular and the coplanar conformations as starting points for the energy optimizations led to the same conformer in every case. Calculations for compound **16** proved too expensive in terms of time and memory requirements, but this series of calculations suggests it would tend towards a similar conformation and energies.

It is known that, depending on the substituents on the aromatic ring, phenylboronic acids can form dimers in solution by means of hydrogen bonding.[105] However, it seems unlikely that dimerization will take place in vacuum or at low concentrations in a polar aprotic solvent such as EC or PC. Although the possibility of intermolecular hydrogen bonding with solvent molecules (Figure 2.4) cannot be discounted, there is little or no difference between the geometries in vacuum and in solution (results of ongoing research, 2016), which seems to support the probability of intramolecular hydrogen bonding of the boronic acid oxygens and the *ortho* hydrogens. However, the calculated C-H bond lengths of the aromatic ring differ by less than 0.01 Å; this phenomenon therefore deserves further study.

(a)

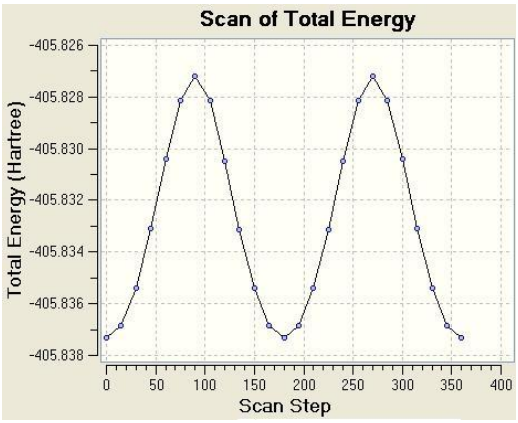

(b)

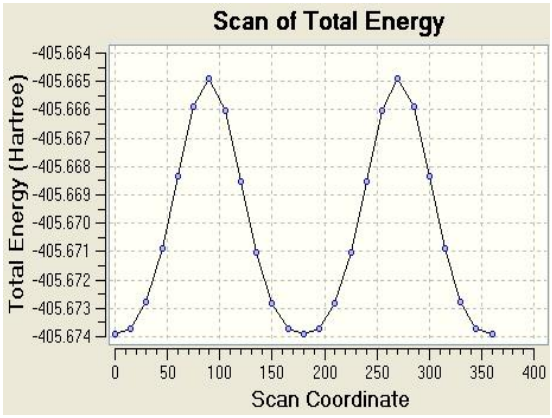

(c)

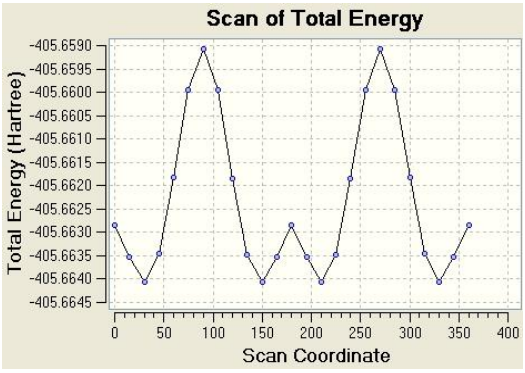

Figure 2.3 Dihedral angle *v*. total energy plots for Compound **6**: (a) 'out-out', (b) 'in-out', and (c) 'in-in' conformations.

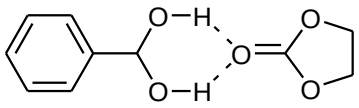

Figure 2.4 Phenylboronic acid hydrogen bonding with ethylene carbonate (EC).

Table 2.1 Dihedral angles and preferred conformations of Compounds **6-15**.

Compd	ϕ/°	Structure
6	**11.8**	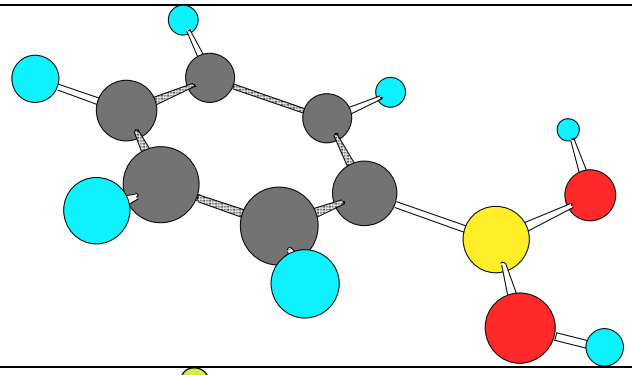
BA (7)	**13.5**	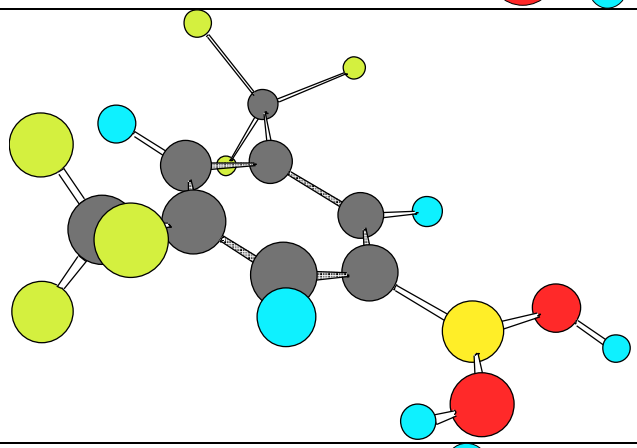
8	**34.9**	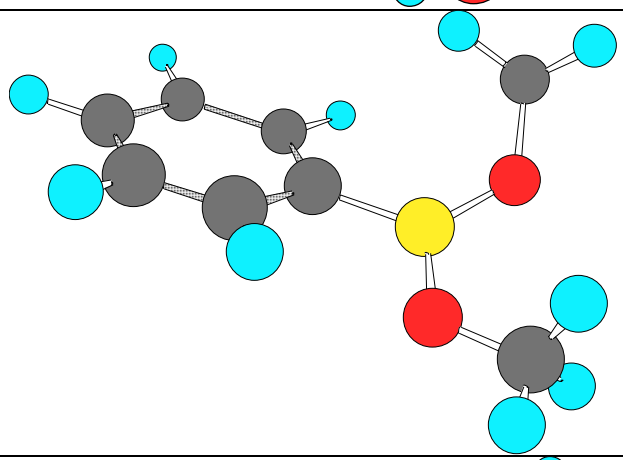
9	**34.5**	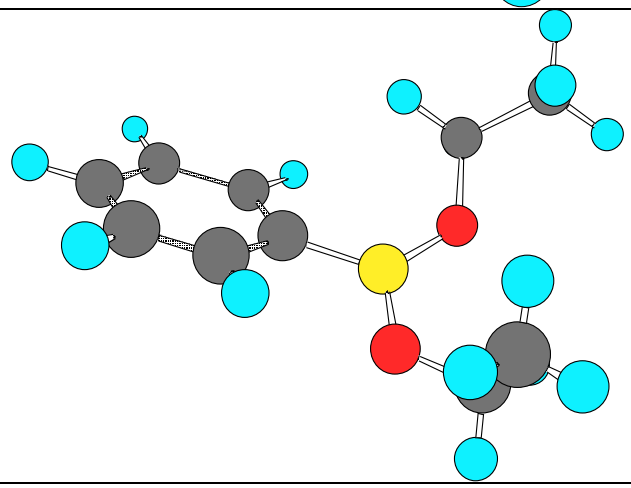

10	**32.0**	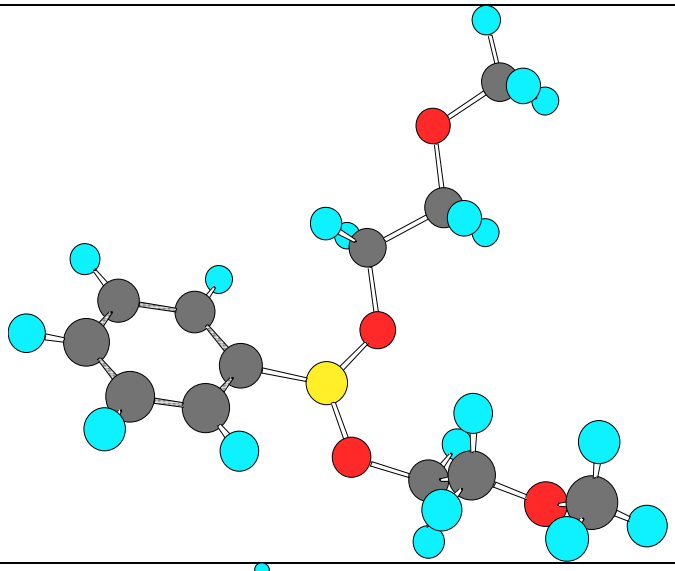
11	**33.6**	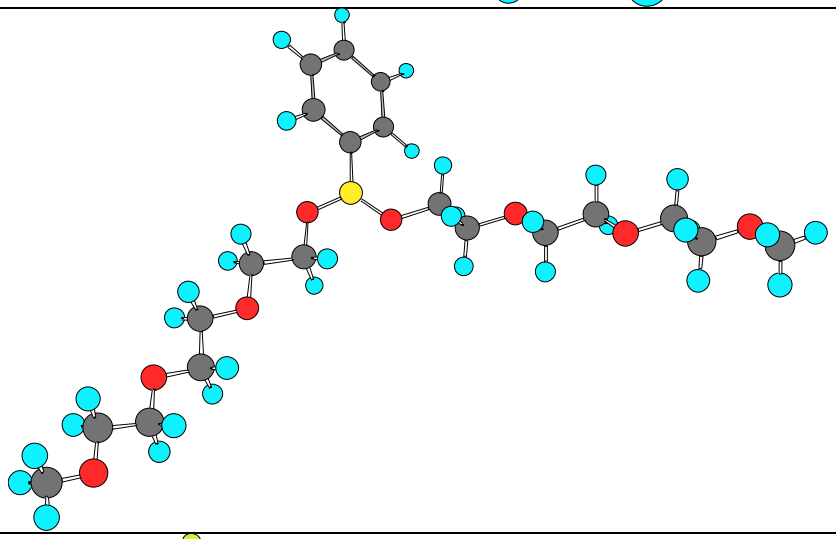
12	**29.5**	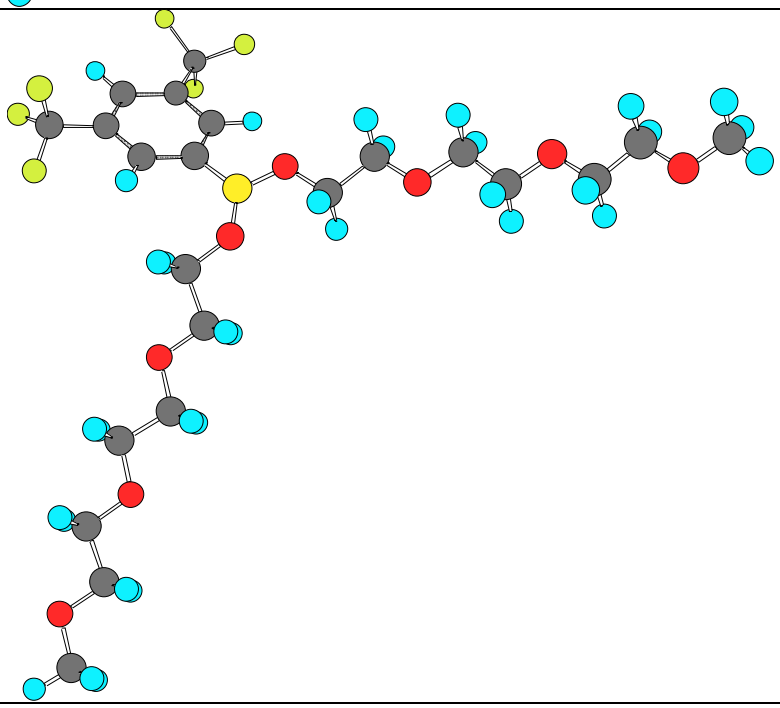

13	**32.4**	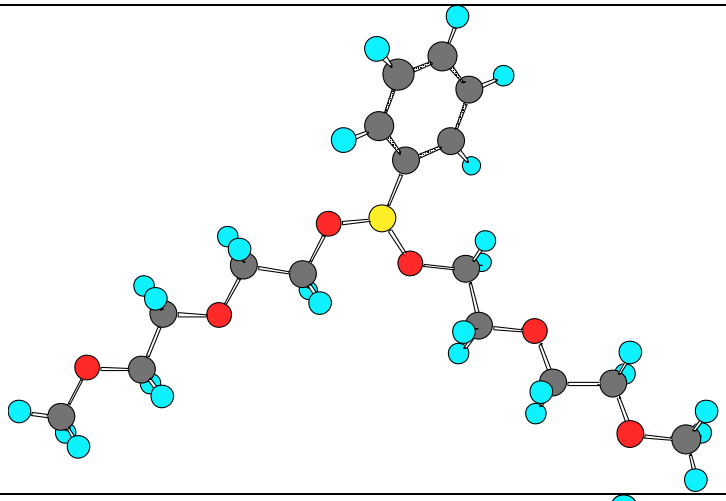
14	**32.3**	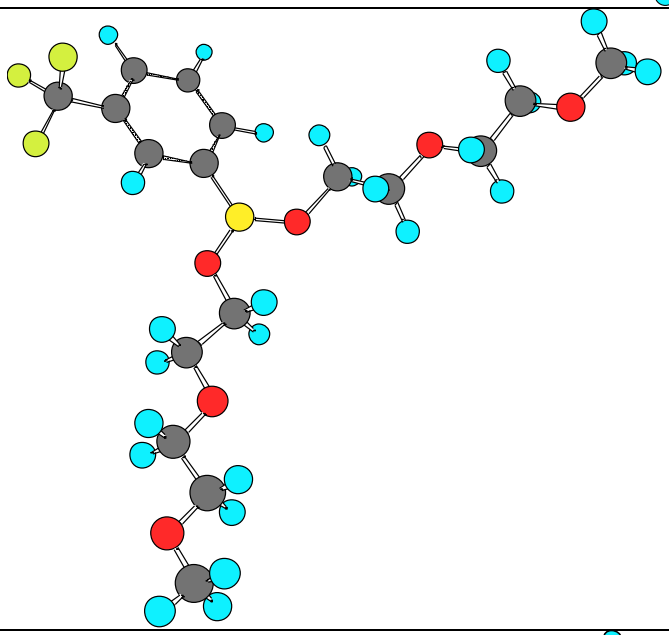
15	**32.2**	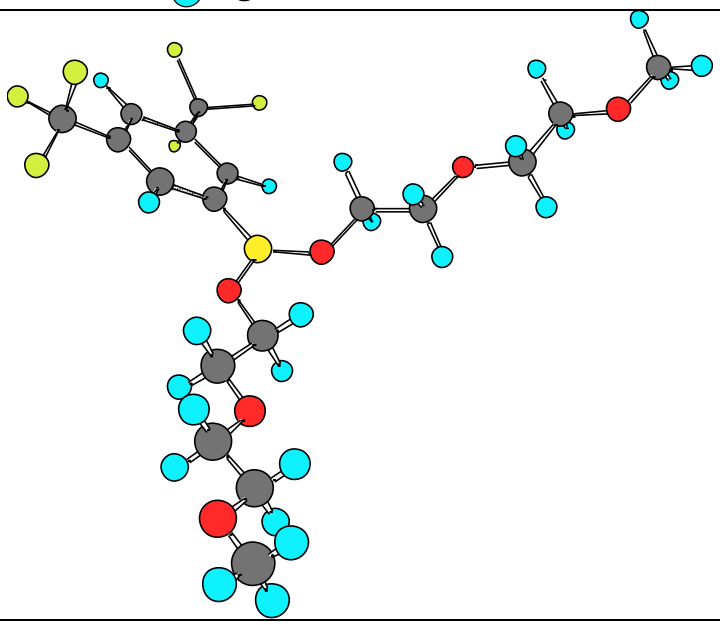

a)

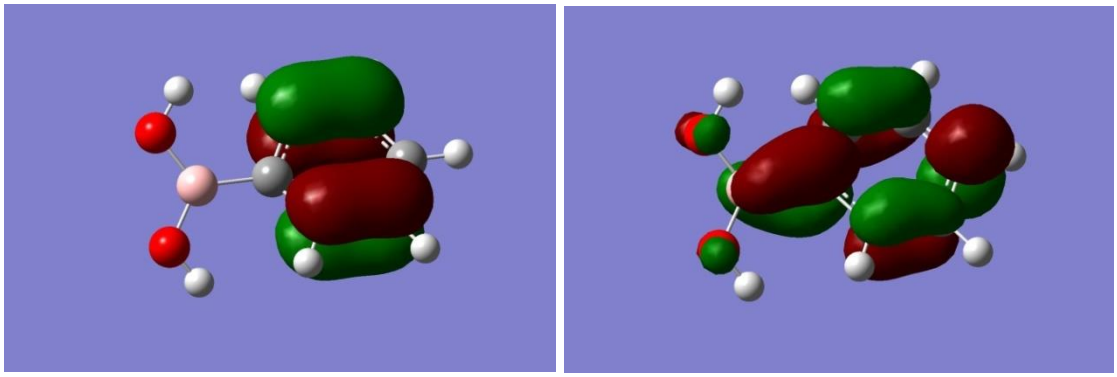

(i) (ii)

b)

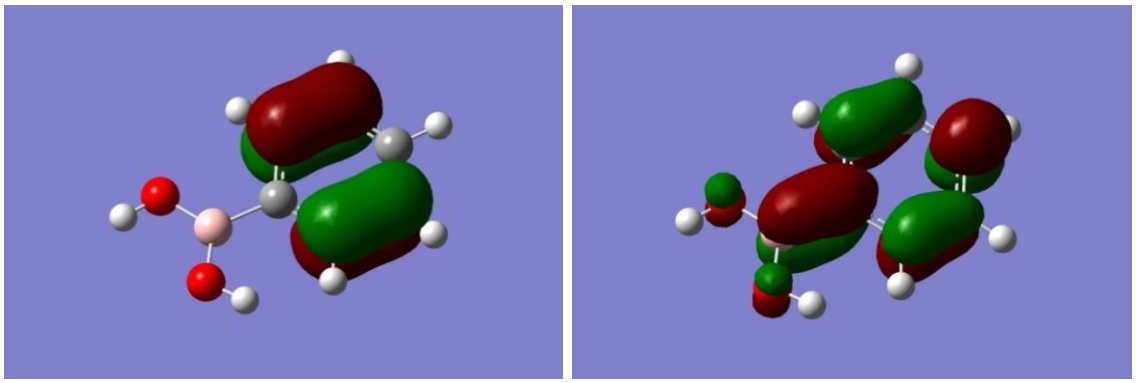

(i) (ii)

c)

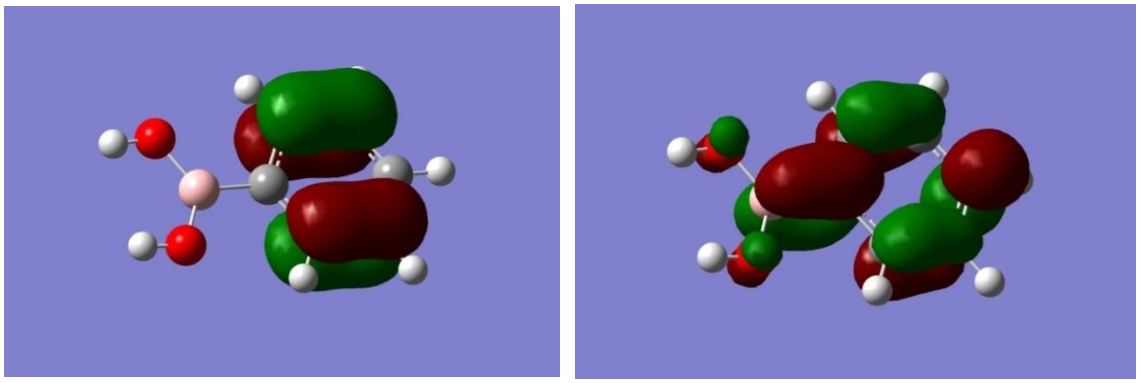

(i) (ii)

Figure 2.5 Frontier orbitals of phenylboronic acid:

(a) In-In geometry: (i) HOMO; (ii) LUMO.

(a) In-Out geometry: (i) HOMO; (ii) LUMO.

(a) Out-Out geometry: (i) HOMO; (ii) LUMO.

The calculated HOMO and LUMO topologies and energies for the lowest energy conformers of these compounds are shown in Table 2.2. The two frontier orbitals (HOMO and LUMO) of selected molecules are discussed in the following paragraphs.

Table 2.2 HOMO and LUMO topologies and calculated energies of Compounds **1-15**. The *anti* staggered ('linear') conformations of ester chains are the lowest-energy conformers in every case.

Compd	SCF Energy, hartrees	HOMO	LUMO	E_{HOMO} / kcal/mol	E_{LUMO} / kcal/mol	ΔE/ kcal/mol
1 (EC)	-342.40315	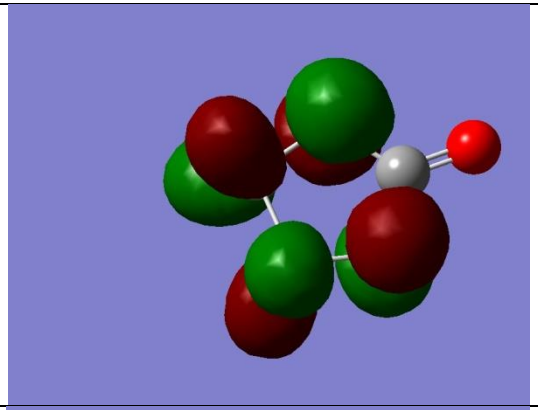	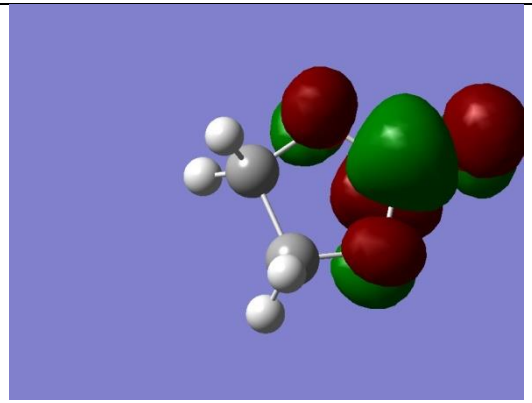	-185.002	24.561	209.563
2 (PC)	-381.72808	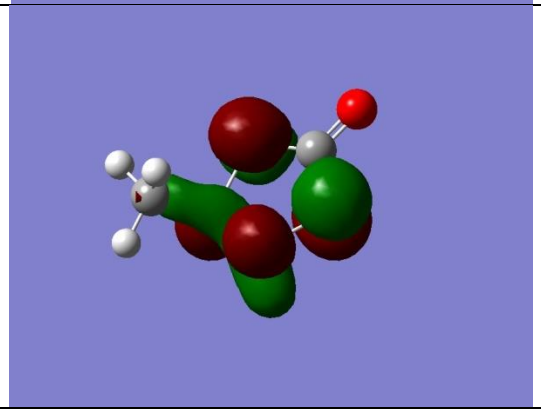	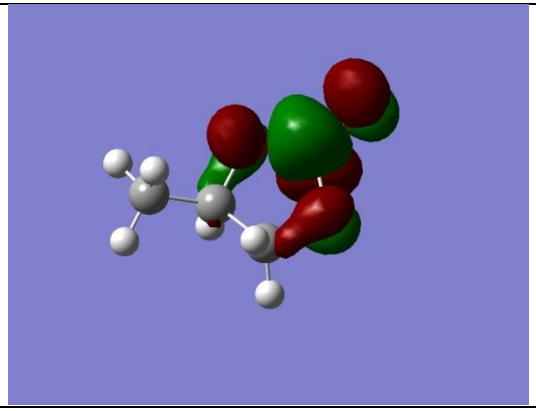	-182.298	23.055	205.353

3 (DMC) 'linear'	**-343.61573**	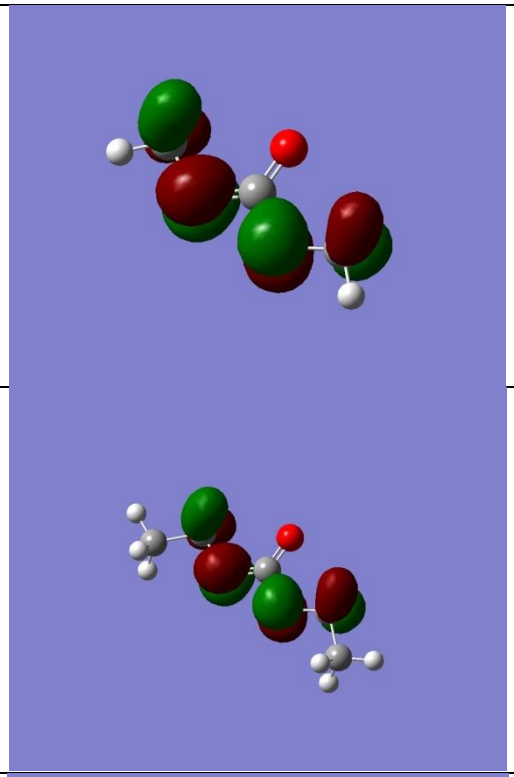	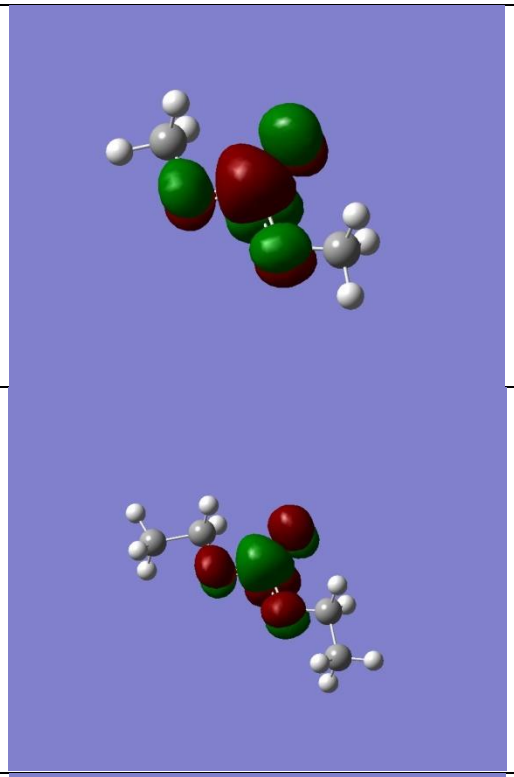	**-178.640**	**26.148**	**204.788**
4 (DEC) 'linear'	**-422.25996**			**-175.433**	**28.966**	**204.399**
5 (EMC) 'linear'	**-382.93788**	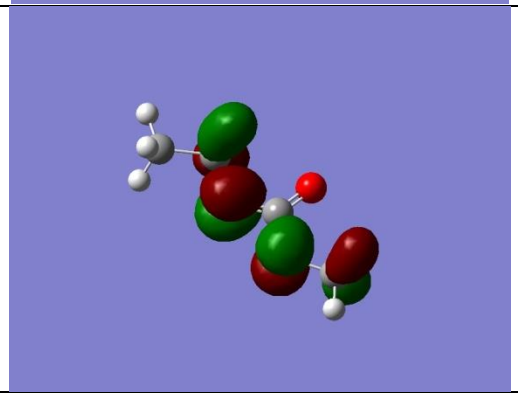	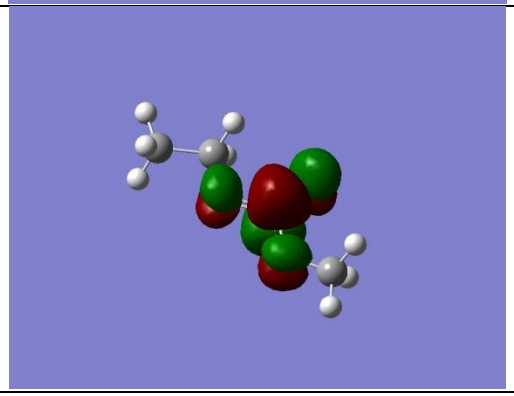	**-177.014**	**27.585**	**204.600**

6 (Phenyl-boronic acid)	-408.28240	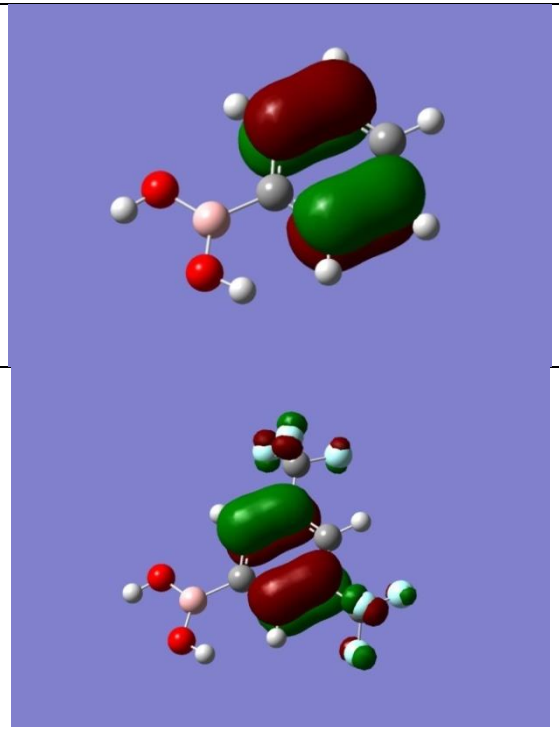	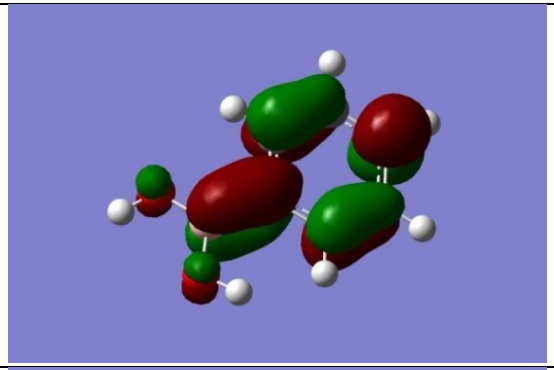	-155.635	-14.025	141.610
7 (BA)	-1082.3529		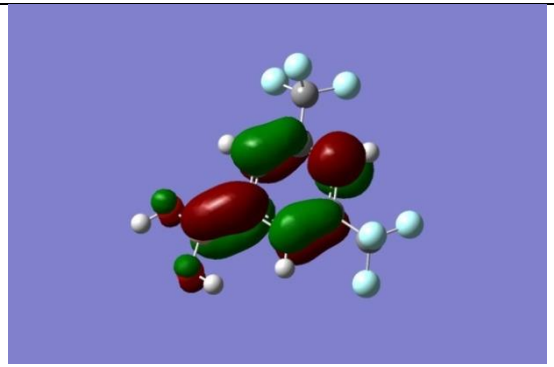	-177.736	-34.808	142.928
8	-486.88275	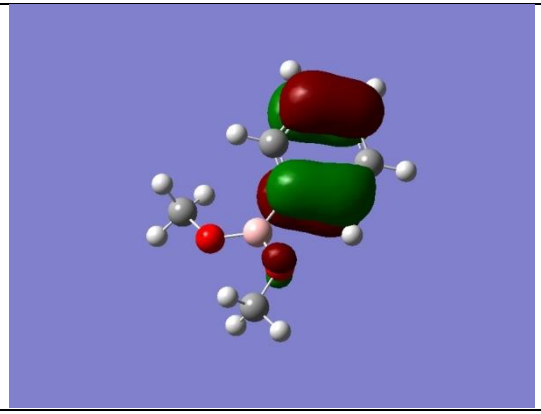	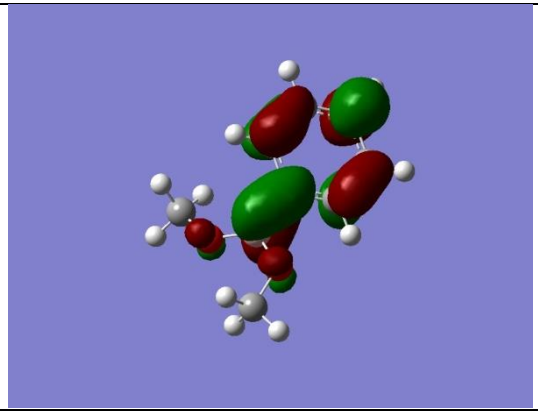	-152.278	-9.463	142.815

9	**-565.52710**	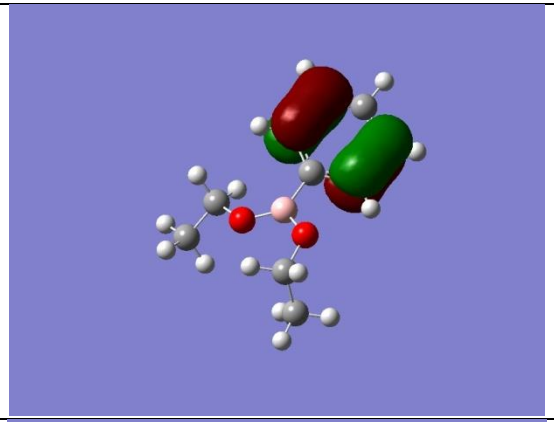	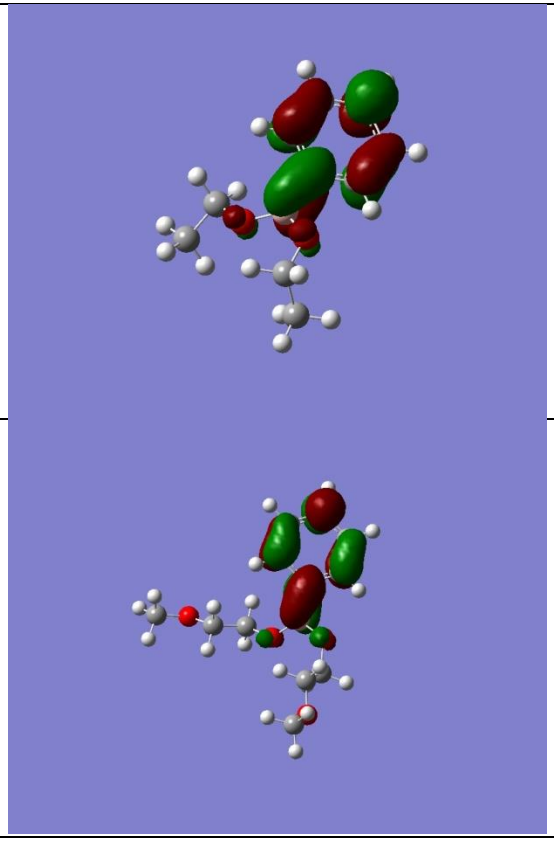	**-151.562**	**-8.710**	**142.853**
10	**-794.55569**	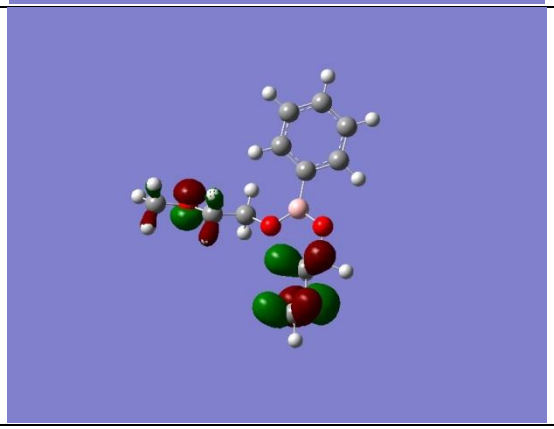		**-153.006**	**-11.063**	**141.943**

11	**-1409.9003**	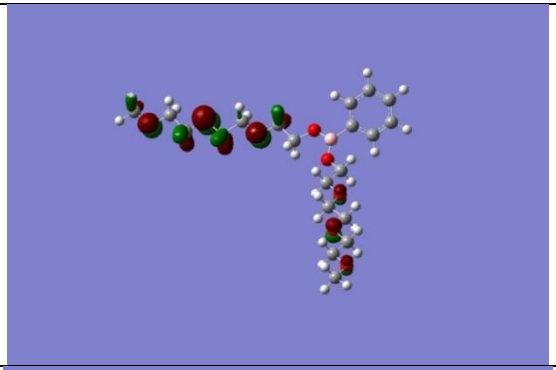	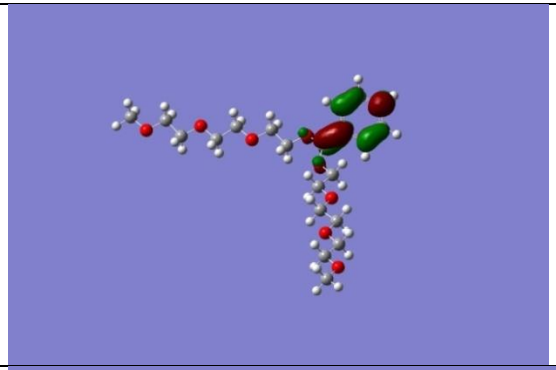	**-153.759**	**-11.678**	**142.081**
12	**-2083.9713**	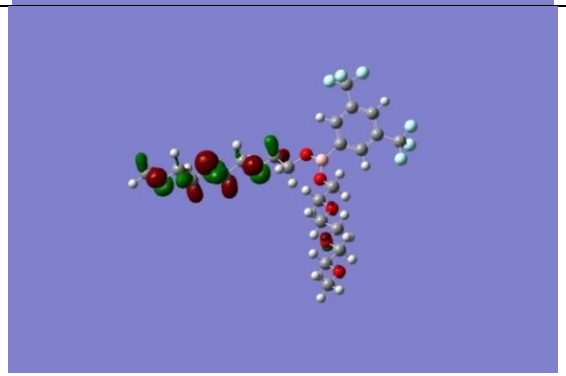	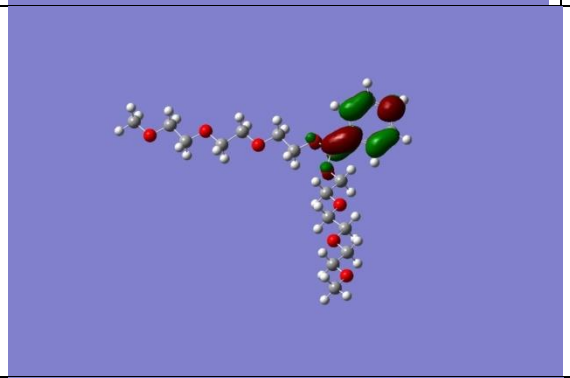	**-159.965**	**-31.595**	**127.944**
13	**-1102.2282**	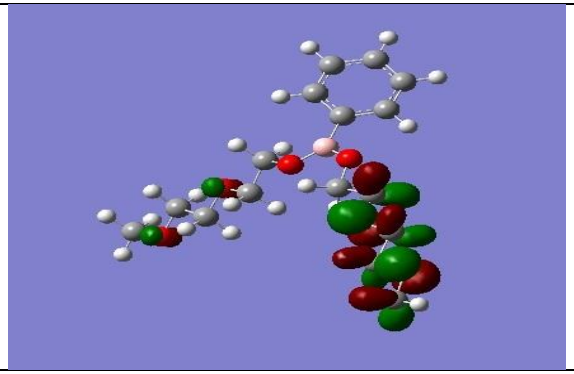	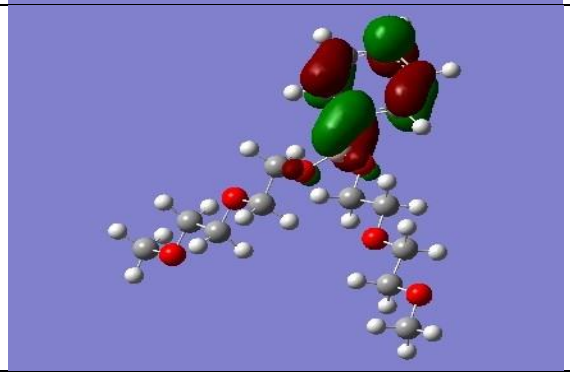	**-153.539**	**-11.659**	**141.880**

14	**-1439.2646**	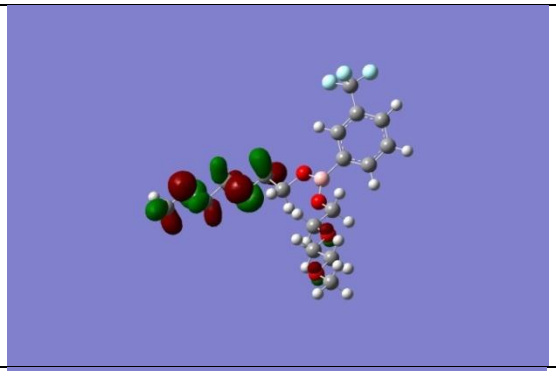	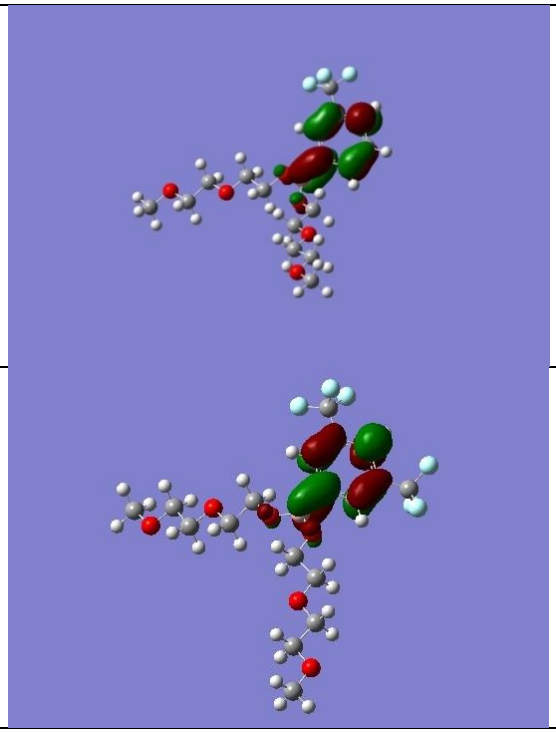	**-156.419**	**-33.296**	**123.123**
15	**-1776.2992**	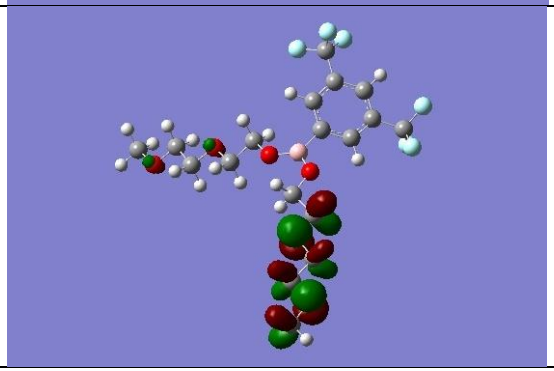		**-158.126**	**-42.746**	**115.380**

In the phenylboronic acids and short-chain esters (**6** – **9**) the HOMO is delocalized with a contribution only from the phenyl ring. There are nodal planes coincidental with and perpendicular to the ring. The LUMO is similar to the HOMO but now also with participation by the boronate, an indication of the possibility of back-bonding. This is a familiar occurrence with boron. The boron *p* orbital figures prominently at the centre of the orbital.

In the esters (**10** – **15**) the HOMOs always involve one of the ethyleneoxy chains and the LUMOs are similar to those of the boronic acids.

The LUMO energies of the boronic acids and boronates were significantly lower than the LUMO energies of the commonly used electrolyte solvents EC, DMC and PC. Assuming the decomposition of these compounds on the negative electrode according to the proposed decomposition pathways, compounds with LUMO energy below that of the carbonate solvent would decompose before the solvent decomposes, because they are better electron acceptors than the solvent. This shows that the boronic acids and boronates would be reduced easily before the carbonate solvent and would be effective redox shuttles. They would also be expected to contribute to the formation of SEI membrane on the graphite electrode.

The HOMO-LUMO energy differences also give an indication that the boronates are more reactive than the solvents, which would be expected to contribute further to effective SEI formation. These calculations suggest that these boronates would be effective electrolyte additives to a PC-based electrolyte.

While these figures may be useful for the qualitative understanding of these molecules, one should remember that they are the result of mathematical functions that are not related to physical reality.

2.4 The Infra-Red spectra

After calculating the energies of the optimized input structures, the IR frequencies of each compound were calculated, with their relative intensities. GaussView enabled visualization and identification of the normal modes for each vibration; although complex, the spectra are characterized by the rocking and wagging motions of the ethyleneoxy chains at around

566/568 and 844/887 cm^{-1}, respectively, the aromatic C-H bending patterns (around 648-967 cm^{-1}), the symmetric B-O stretch at 1065-1124 cm^{-1} and the two asymmetric B-O stretching bands at about 1440-1456 and 1341-1354 cm^{-1}, and the aromatic C=C stretch (1573-1593 cm^{-1}) and aromatic (3030-3054 cm^{-1}) and aliphatic (2877-2878 cm^{-1}) C-H stretching vibrations.[107] These characteristics are illustrated by the measured and calculated spectra of compound **12** (Fig. 2.6). Other calculated and measured spectra are shown in Appendix B.

a)

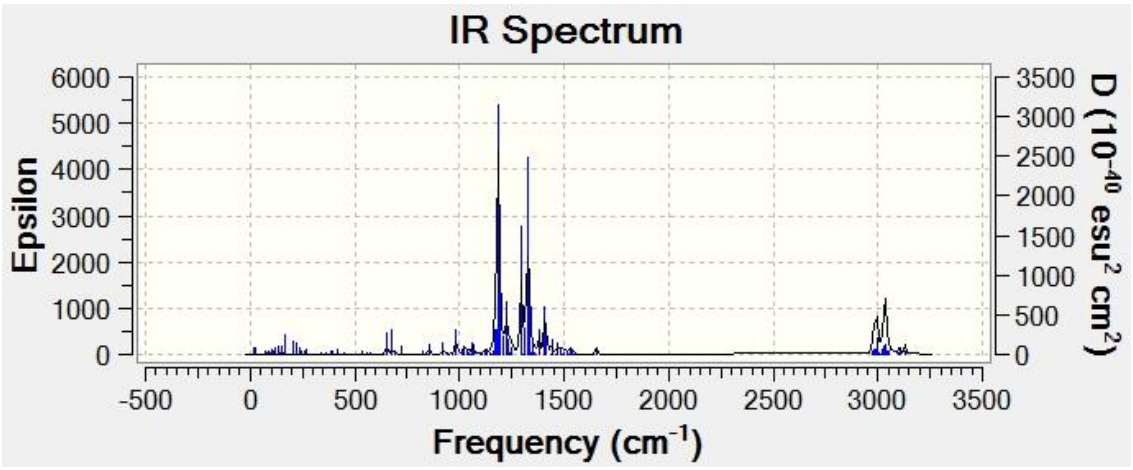

b)

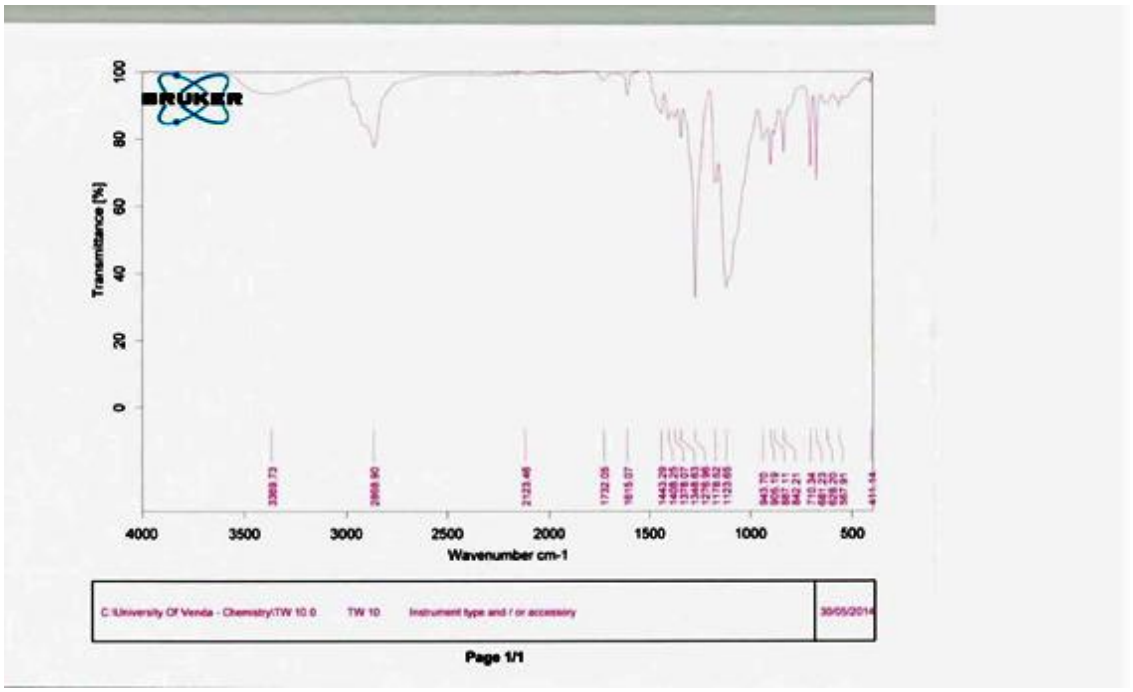

Figure 2.6 Compound **12** (a) Simulated and (b) Experimental IR spectrum.

2.5 Synthesis of substituted boronates

Aromatic boron derivatives are currently enjoying prominence in the continuing development and improvement of commercial lithium-ion battery technology. As Lewis acids, these molecules can function as anion receptors assisting in the dissolution of LiF formed during the operation of lithium-ion batteries.[106] Previously,[48] boronic acid derivatives such as 3,5-bis(trifluoromethyl)benzeneboronic acid (**7**) were found to enhance electrochemical performance and overcharge safety in propylene carbonate-based electrolytes. A range of boronates was modelled (discussed in the previous section) in attempts to determine structure-activity relationships (Figure 1.10).

The EO-boronate esters **11-15** were synthesized in nearly quantitative yields by condensation of suitable arylboronic acids and diethylene or triethylene glycol monomethyl ether following literature methods[13,106] (Scheme 2.1, Table 2.3). The arylboronic acid was dissolved in anhydrous benzene, and a Dean-Stark trap was used to remove benzene-water azeotrope from the system to ensure anhydrous conditions. The solution was cooled down to about 70 ºC and diethylene or triethylene glycol monomethyl ether (EO) was added. The solution was heated under reflux, and excess diethylene or triethylene glycol monomethyl ether was removed by vacuum distillation to yield a colourless oil quantitatively. In the case of compound **16**, phenylboronic acid was first reacted with two equivalents methyl trichlorosilane, followed by four equivalents diethylene glycol monomethylether. Spectroscopic properties of the boronates are discussed in the following paragraphs.

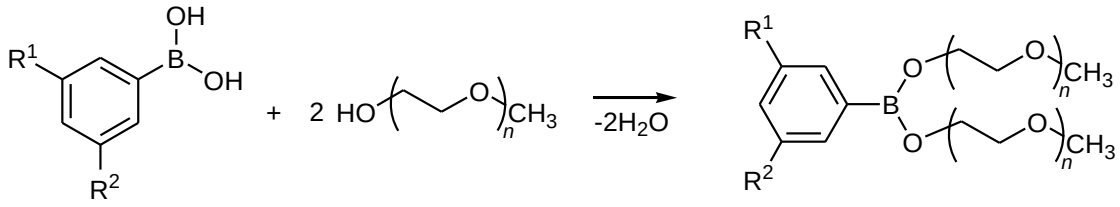

Scheme 2.1 Synthesis of boronates **11 -15**.

Table 2.3 Synthesis of Compounds **11 – 16** (Scheme 2.1).

Compound	R^1	R^2	*n*	% Yield
11	H	H	3	99
12	CF_3	CF_3	3	96
13	H	H	2	94
14	CF_3	H	2	75
15	CF_3	CF_3	2	89
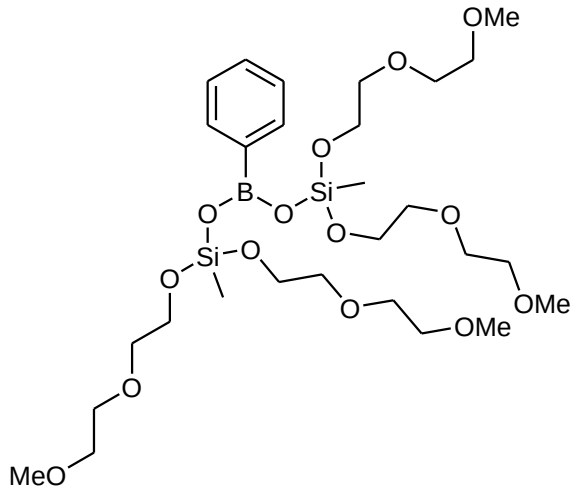 **16**				101

Compounds **11**, **12**, and **13**, which are new compounds, were characterised using ^{1}H-NMR, ^{13}C-NMR and IR spectroscopic techniques. The results were in agreement with the little data available for compounds **11** and **13**.[68] No MS data have been published for these compounds, probably because they are non-volatile and decompose easily under the GC-MS or MS conditions to boroxines.[118,119] For example, compound **13** displays a molecular ion signal, with the typical boron isotope satellites, at *m/z* = 312.13 (Appendix C) for 2,4,6-triphenylboroxine.

In the ^{1}H-NMR spectrum of bis(2-(2-(2-methoxyethoxy)ethoxy)ethyl) 3,5-bis-(trifluoromethyl)phenylboronate (**12**), a new compound, we observe the characteristic singlet at δ 3.24 ppm corresponding to the methoxy groups (2x -OCH_3), multiplets at δ 3.3-3.5 ppm and 3.94 ppm corresponding to methylene groups (24x CH_2), and singlets at δ 7.62 (2H) and 8.07 (1H) ppm. The ^{13}C-NMR spectrum of compound **12** showed signals at δ 61.0 ppm (2x -OCH_3) for the methoxy groups, signals at δ 66.2, 69.3, and 70.1 ppm of the methylene groups (12x CH_2), and aromatic signals at δ 123.2 (–*C*H– arom.), 127.6 (–*C*H– arom.). The CF_3 groups appeared as a 130 Hz quartet at δ 130.1 ppm, with two more aromatic carbons coupled to the F at δ 134.0 and 137.0 ppm. In the IR spectrum, the

aliphatic C-H stretch (ν_{max} 2878 cm^{-1}), aromatic C-H bending pattern (ν_{max} 710 and 681 cm^{-1}), and the symmetric B-O stretch at ν_{max} 1124 cm^{-1} were prominent.

The ^{1}H-NMR spectrum of bis-(2-(2-methoxyethoxy)ethyl) 3-trifluoromethylphenyl boronate **14**, on the other hand, is characterized by a singlet at δ 3.24 ppm corresponding to hydrogens of the methoxy groups (2x OCH_3), multiplets at δ 3.52 ppm and 3.59 ppm corresponding to the hydrogens of methylene groups (6x CH_2), a multiplet at δ 4.07 ppm corresponding to hydrogens of methylene groups (2x CH_2) adjacent to B-O bonds, and multiplets at δ 7.43 ppm (3H) and 7.80 ppm (1H) for the aromatic protons. The ^{13}C-NMR spectrum of compound **14** showed signals at δ 58.6 ppm (2x OCH_3), signals at δ 66.2, 69.3, and 70.1 ppm of the methylene groups (8x CH_2), and signals at δ 123.2 (–*C*H– arom.), 129.3 (–*C*H– arom.), and 129.6 (arom.). The CF_3 group resonated as a quartet at δ 129.5 ppm with J = 124 Hz, with another aromatic carbon coupled to the F at δ 133.9 ppm. In the IR spectrum, the aliphatic (ν_{max} 2877 cm^{-1}) C-H stretching vibrations, aromatic C-H bending pattern (ν_{max} 707 cm^{-1}), the asymmetric B-O stretching band at ν_{max} 1345 cm^{-1} and the symmetric B-O stretch at ν_{max} 1071 cm^{-1} were prominent. The mass spectrum displays the molecular ion signal at *m/z* 516.09 for the 2,4,6-tris-(3-(trifluoromethyl)phenyl)boroxine (Appendix C).

Likewise, the ^{1}H-NMR spectrum of bis-(2-(2-methoxyethoxy)ethyl) 3,5-bis(trifluoromethyl) phenylboronate **15** is characterized by a singlet at δ 3.45 ppm corresponding to the methoxy groups (2x OCH_3), multiplets at δ 3.55 ppm and 3.63 ppm corresponding to methylene hydrogens (6 x CH_2), a multiplet at δ 4.22 ppm corresponding to hydrogens of the methylene groups (2x CH_2) adjacent to the B-O bond, and a multiplet in the region δ 7.86-8.18 ppm (3H) corresponding to aromatic hydrogens (3x CH) in the benzene ring. The ^{13}C-NMR spectrum of compound **15** showed signals at δ 58.6 ppm for the methoxy groups, δ 66.3, 70.1, and 71.8 ppm (for the –*C*H_2– groups), and also signals at δ 123.5 and 127.5 ppm (aromatic –*C*H–). The CF_3 groups appeared as a 130 Hz quartet at δ 130.2 ppm, with two more aromatic carbons coupled to the F at δ 132.0 and 134.0 ppm. In the IR spectrum, the aliphatic (ν_{max} 2878 cm^{-1}) C-H stretching vibrations, aromatic C-H bending pattern (ν_{max} 843 and 681 cm^{-1}), the two asymmetric B-O stretching bands at ν_{max} 1456 and 1354 cm^{-1}, and the symmetric B-O stretch at ν_{max} 1108 cm^{-1} could be discerned. Unfortunately, the MS sweep width did not extend to the expected molecular ion signal at *m/z* 720.05 for the 2,4,6-tris-(3,5-bis-(trifluoromethyl)phenyl)boroxine (Appendix C).

Spectroscopic data of bis-(bis(2-(2-methoxyethoxy)ethyl)methylsilyl) phenylboronate **16** could not be assigned unambiguously, because of persistent impurities. The ^{1}H-NMR spectrum shows singlets at δ 0.23 ppm for the Si-Me and δ 3.19 ppm corresponding to hydrogens of the methoxy groups (2x OCH_3), multiplets in the region δ 3.30 ppm - 3.60 ppm corresponding to the hydrogens of methylene groups (8x CH_2), and multiplets in the region of δ 7.14 – 7.27 ppm (3H) and δ 7.37 – 7.49 ppm (2H) for the aromatic protons. In the IR spectrum, the aromatic (ν_{max} 3030 cm^{-1}) and aliphatic (ν_{max} 2878 cm^{-1}) C-H stretching vibrations, aromatic C=C stretch (ν_{max} 1593 cm^{-1}) and C-H bending pattern (ν_{max} 967 cm^{-1}), and the asymmetric B-O stretching band at ν_{max} 1354 cm^{-1} and symmetric B-O stretch at ν_{max} 1083 cm^{-1} were evident.

2.6 CV and EIS of boronates

2.6.1 Cyclic voltammetry

Cyclic voltammetry (CV) has become a favourite tool for studying the redox behaviour of compounds and probe coupled chemical reactions, in particular to determine mechanisms and rates of oxidation/reduction reactions. CV is a several-sweep technique in which the potential difference *V* is increased and decreased cyclically between two limits at different scan rates while the electrode current *i* is recorded. The potential of the working electrode where the reaction of interest occurs is controlled versus the reference electrode.[108] The voltammogram records the potentials at which different electrochemical processes occur; the current measured during this process can be normalised by dividing it by the electrode surface area and is then called the current density *j*. A peak in the measured current appears at the potential of the electrode reaction that takes place, which may be either reduction or oxidation. The peak width and height for a particular process depends on the sweep rate, the electrolyte concentration and the electrode material, while the difference between the oxidation and reduction peaks is characteristic of the number of electrons transferred.[109,110]

A typical cyclic voltammogram recorded for a reversible single electron transfer reaction is shown in Figure 2.7. In this hypothetical case, the voltage is swept from V_1 to V_2 at a fixed scan rate; when the voltage reaches V_2 the scan is reversed, and the voltage is swept back to V_1. During the reversed scan, the system moves back through the equilibrium positions

found *en route*, gradually converting the electrochemical product back to reactant. The current flow now occurs in the opposite sense to the forward sweep.[108]

In the current series of measurements, performed by collaborators at Fudan University (Shanghai, China) and interpreted by the author, the bare electrolyte showed an oxidation peak in the first cycle at 3.85 V and the corresponding reduction peak at 3.05 V (Figure 2.8); this is attributed to the decomposition of EC and exfoliation of graphite. Figure 2.9 shows the CVs of electrolyte with 2% w/w of each of several additives. The electron transfer energies and ionic conductivities that we were able to determine are listed in Tables 2.4 and 2.5, respectively.

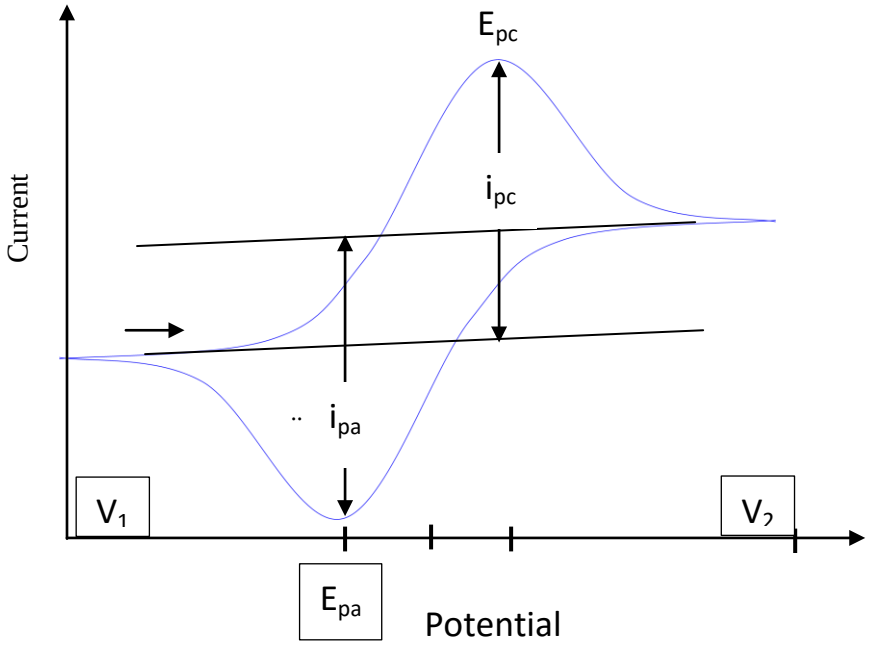

Figure 2.7 CV of a reversible one-electron system. The horizontal arrow shows the direction of the initial scan. The currents i_{pc} and i_{pa} are the peak cathodic (positive electrode) and anodic (negative electrode) currents, respectively. The peak potentials E_{pa} (for oxidation at the negative electrode) and E_{pc} (for reduction at the positive electrode), are separated by 0.057 V for the transfer of one electron. The reduction potential is the mean of E_{pa} and E_{pc}.

Figure 2.9(a) shows the cyclic voltammogram with the graphite negative electrode in 1.0 M $LiPF_6$ solution in EC/DMC/DEC (ethylene carbonate/dimethyl carbonate/ethyl methyl carbonate) 1/1/1 (v/v/v) with 2% (v/v) of **11** added. The CV of electrolyte with **11** demonstrates a small difference in the reduction peak at 3.15 V, which can be attributed to

the decomposition of **11** on the electrode. This result suggests the minimal impact of the methoxyethoxy chain attached to the phenylboronate on the reduction potential.

In Figure 2.9(b) the CV for electrolyte with 2% (v/v) of **12** added, is shown. The oxidation peak was observed near 4.0 V and the reduction peak was observed near 2.76 V, which is less than the reduction peak of the electrolyte without the additive. This result suggests that the reduction would take place before the additive can react; this may be due to the attachment of the electron-withdrawing CF_3 group on the aromatic ring. Fluorine is the most electronegative element and hence would have a significant inductive stabilization effect on anions, decreasing the stability of the anion against oxidation but increasing the stability of the anion against reduction.

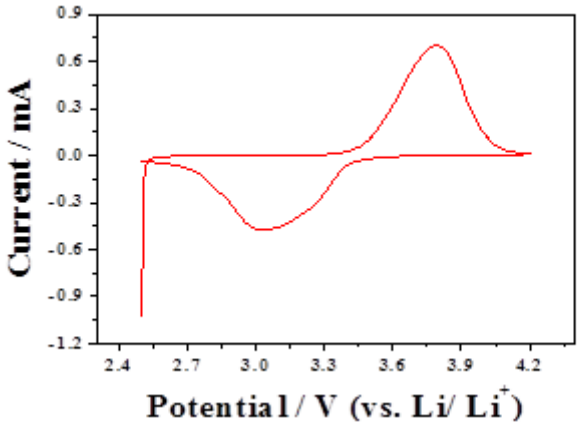

Figure 2.8 Cyclic voltammogram of 1 M $LiPF_6$ solution in EC/DMC/DEC (ethylene carbonate/dimethyl carbonate/ethyl methyl carbonate), 1/1/1 (v/v/v).

When 2% (v/v) of **13** was added to the electrolyte, the oxidation peak was observed near 3.80 V and the reduction peak appeared at 3.24 V (Figure 2.9(c)). There is a slight difference in the reduction peak at 3.15 V, which can be attributed to the decomposition of **13**, and there is also a slightly higher reduction potential, suggesting a small impact of the (methoxyethoxy)ethyl attachment on the performance of the electrolyte.

Figure 2.9(d) shows the cyclic voltammogram when 2% (v/v) of **14** was added to the electrolyte. The oxidation peak was observed near 3.80 V and reduction peak was observed near 2.95 V, which is lower than the reduction peak of the electrolyte without the additive. The reduction therefore takes place before the additive can react, suggesting that the electron-withdrawing groups would not improve the performance of the electrolyte.

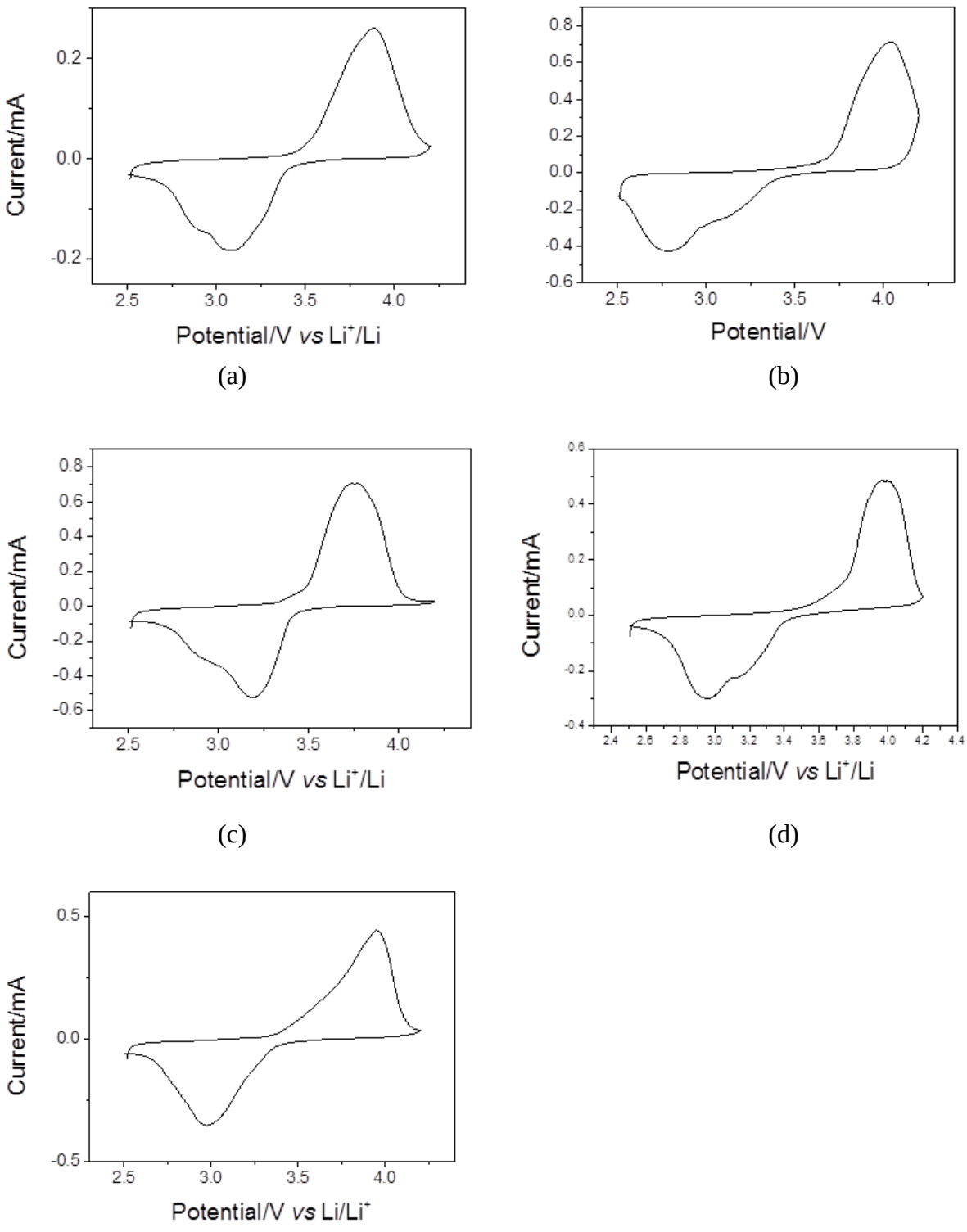

Figure 2.9 Cyclic voltammograms (5th cycle) of 1 M $LiPF_6$ solution in EC/DMC/DEC (ethylene carbonate/dimethyl carbonate/ethyl methyl carbonate), 1/1/1, v/v/v, containing 2% (a) **11** (b) **12**, (c) **13**, (d) **14**, (e) **16** (impure).

Compound **15** did not provide useful data, presumably due to deterioration during transport. When 2% (v/v) of the impure compound **16** was added to the electrolyte (Figure 2.9(e)), the oxidation peak was observed near 3.80 V and the reduction peak was observed near 2.9 V, which is lower than the reduction peak of the electrolyte without the additive. This result suggests that reduction would take place before the additive can react.

2.6.2 Electrochemical impedance spectroscopy (EIS)

EIS (recorded at Fudan University and interpreted by the author) was used for further study of the additive behaviour. Figure 2.10 displays the Nyquist (or *complex plane*) plots in the potential window between 2.4 V and 4.2 V *vs* Li/Li^+; these are plots of the imaginary (Z'') *vs* the real (Z') components of $Z(\omega)$, the electrochemical impedance. In Fig. 2.11 high-frequency plots at different temperatures are shown for several of the boronates, from which the activation energies of the charge-transfer reaction for compounds **11** and **13** (Table 2.4) and the interfacial conductivities (Table 2.5) were calculated according to the Arrhenius equation:

$$1 / R_{ct} = A \exp(-E_a/RT).$$

Table 2.4 Electron-transfer activation energies (E_a) at 25°C of electrolyte (1 M $LiPF_6$ solution in EC/DMC/DEC, 1/1/1, v/v/v) with 2% additive.

Additive	**E_a, kJ mol^{-1}**
11	8.2
13	3.6

Table 2.5 Ionic conductivities at 25°C of electrolyte (1 M $LiPF_6$ solution in EC/DMC/DEC, 1/1/1, v/v/v) with 2% additive.

Additive	**Ionic conductivity, mS cm^{-1}**
Bare electrolyte	0.21
11	0.26
12	0.18
13	0.24
15	0.14
16	0.17

The very low activation energies apparently reflect the energies for desolvation of the lithium ion and imply a very fast process.[111] The influence of solvents on the geometries and electrochemical properties of these additives therefore deserves further study.

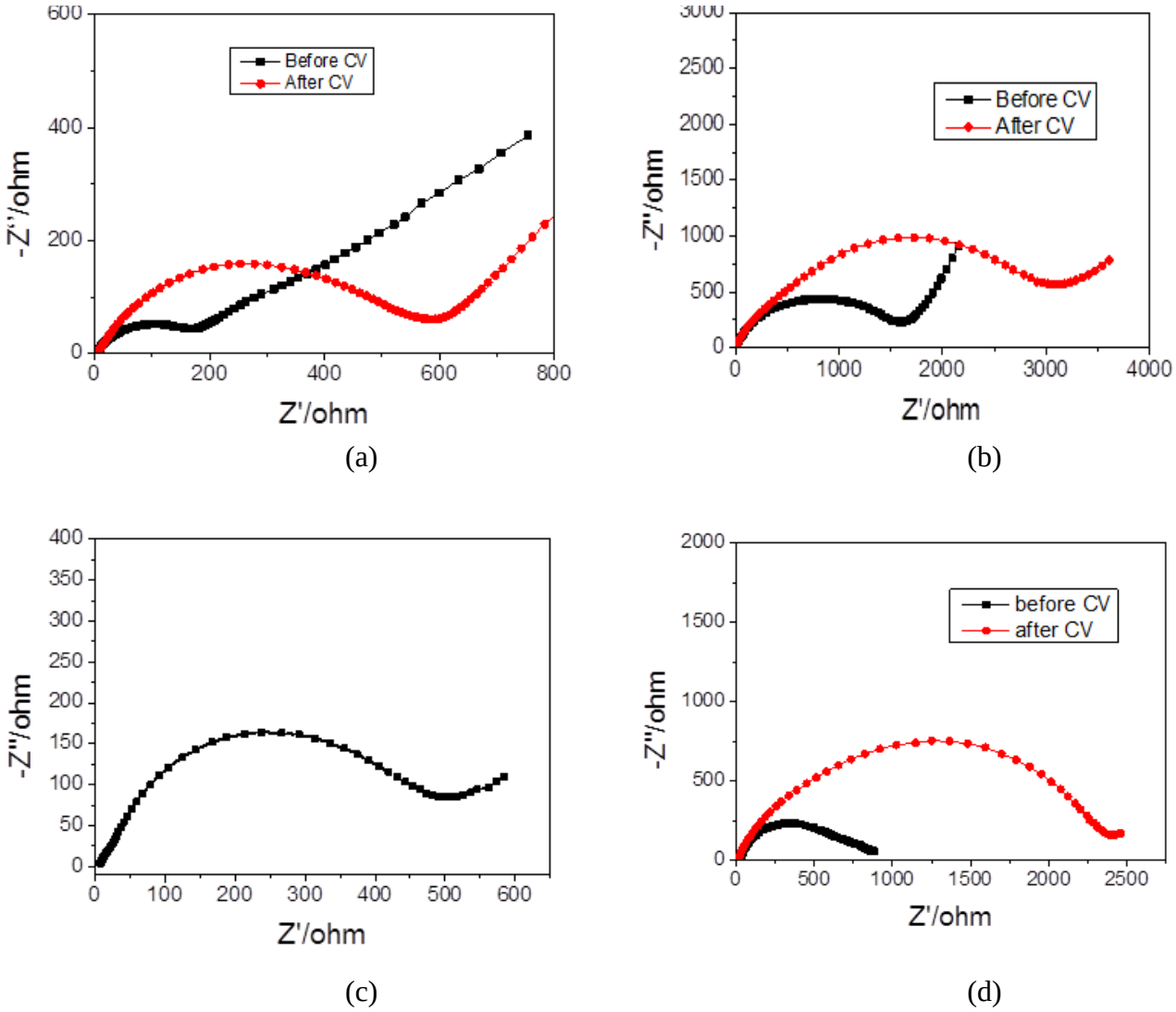

Figure 2.10 EIS spectra of 1 M $LiPF_6$ solution in EC/DMC/DEC (ethylene carbonate/dimethyl carbonate/ethyl methyl carbonate), 1/1/1, v/v/v, containing 2% (a) **11**, (b) **12**, (c) **13**, (d) **14**.

The impedance spectrum in every case is composed of a slightly flattened semicircle in the high-frequency region, which is caused by SEI film and contact resistance (R_{ct}) in parallel with the double-layer capacitance C_{dl}. The R_{ct} values, which are related to the radii of the semicircles, suggest the efficient formation of SEI, as they are related to interfacial transfer of ions and the Li^+ charge-transfer impedance on the electrode/electrolyte interface. The straight line in the low-frequency Warburg region corresponds to the lithium diffusion processes within the electrodes.

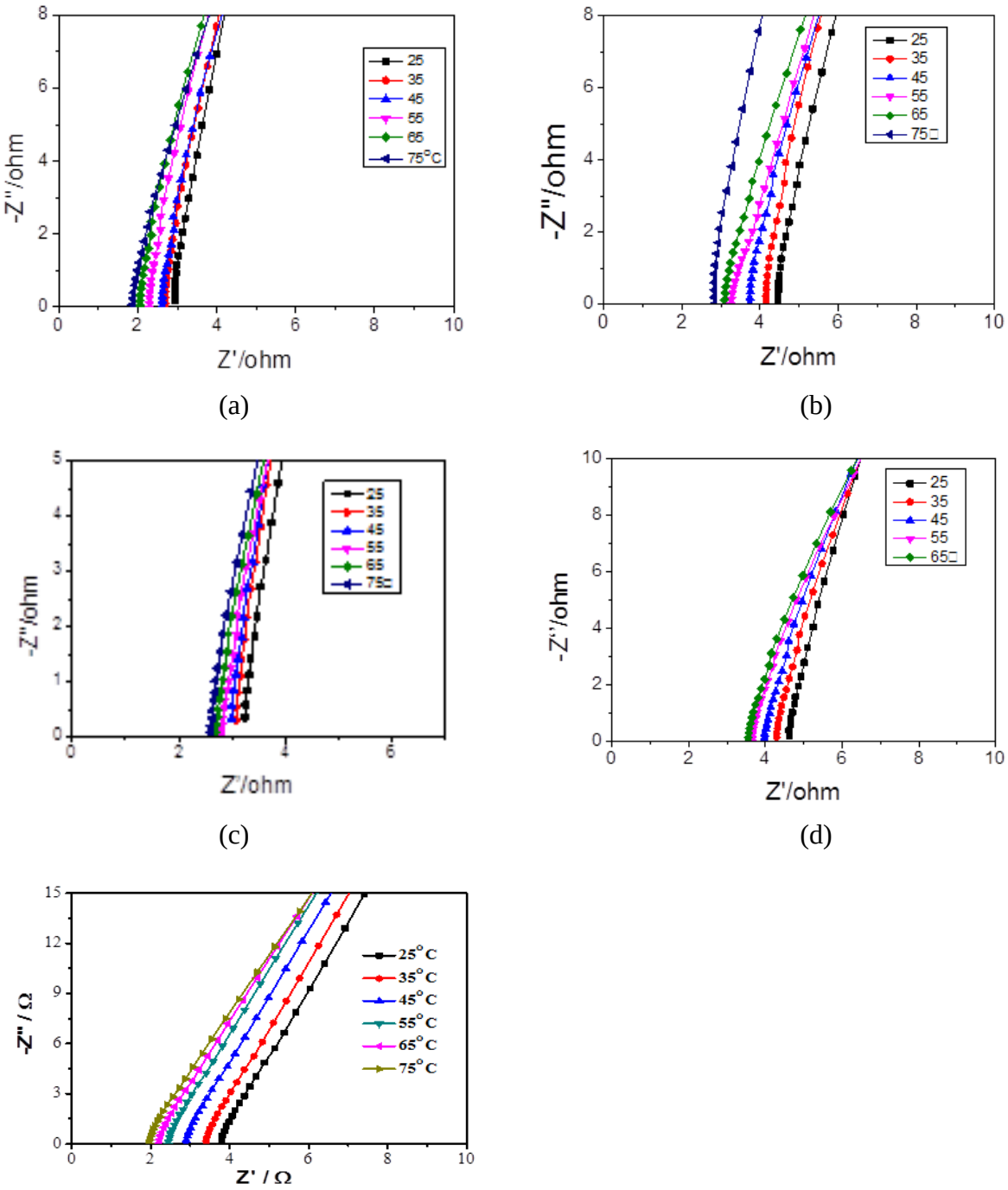

Figure 2.11 High frequency complex plane plots of 1 M $LiPF_6$ solution in EC/DMC/DEC (ethylene carbonate/dimethyl carbonate/ethyl methyl carbonate), 1/1/1, v/v/v, containing 2% (a) **11**, (b) **12**, (c) **13**, (d) **15**, (e) no additive.

The radii of the graphs increase after CV, indicating the occurrence of irreversible reactions (such as solvent decomposition and SEI formation), and that consequently the additives increase the interfacial impedance. This increase is least for compounds **11** and

13. Excess additive can influence the ion migration process by increasing the interfacial impedance; therefore, only 2% was added in this series of experiments.

From the above discussion, it follows that Compounds **11** and **13** could be useful additives; addition of these compounds to the electrolyte also results in increased ionic conductivity of the electrolyte (Table 2.5), favouring their use as electrolyte additives.

Chapter 3
Conclusions

To produce safe rechargeable lithium-ion batteries, non-flammable electrolytes or a flame retardant additive(s) are required.[112] Additives that inhibit electrode exfoliation, for example by developing a SEI layer, are also needed. Boronic esters promise to develop into bi-functional additives that are not only fire-retardant, but can also contribute to stabilization of electrode materials.[113-115] The boronate esters described in this study are expected to form a stable SEI film on the surfaces of electrodes, as shown by the calculations and preliminary electrochemistry results. Addition of 2% boronate should suppress the decomposition and the co-intercalation of solvent and have little effect on cycling behaviour.

The results also show that the compounds synthesized so far, especially **11** and **13**, can be expected to perform well as redox shuttles. The HOMO-LUMO energy differences indicate higher reactivity of the boronates, which would presumably contribute to efficient SEI formation. Except for compound **7**, an electron-withdrawing group such as $-CF_3$ on the aromatic ring apparently is not beneficial.

The influence of solvents on the geometries and electrochemical properties of these additives deserves further study. In planned future work, therefore, molecular modelling would have to account for solvent effects, since solvation of the additives would be expected to affect the boronate reaction centre strongly. This becomes clear when inspecting the solvent accessibility of a compound such as **14** (Fig. 3.1). Another avenue to be explored would be the solvation of lithium ions and its effect on the coordination of lithium with the crown ether-like EO groups attached to the boronate (*e.g.*, Fig. 3.2). Finally, it is envisaged that the additives will be tested in full cycling cells in collaboration with the Fudan University and South China University of Technology (SCUT) groups.

The combination of flame retardancy with SEI functionality is an attractive development for high-capacity lithium-ion battery applications in EVs. These functionalities can potentially be varied using a range of substituents and EO chain lengths.

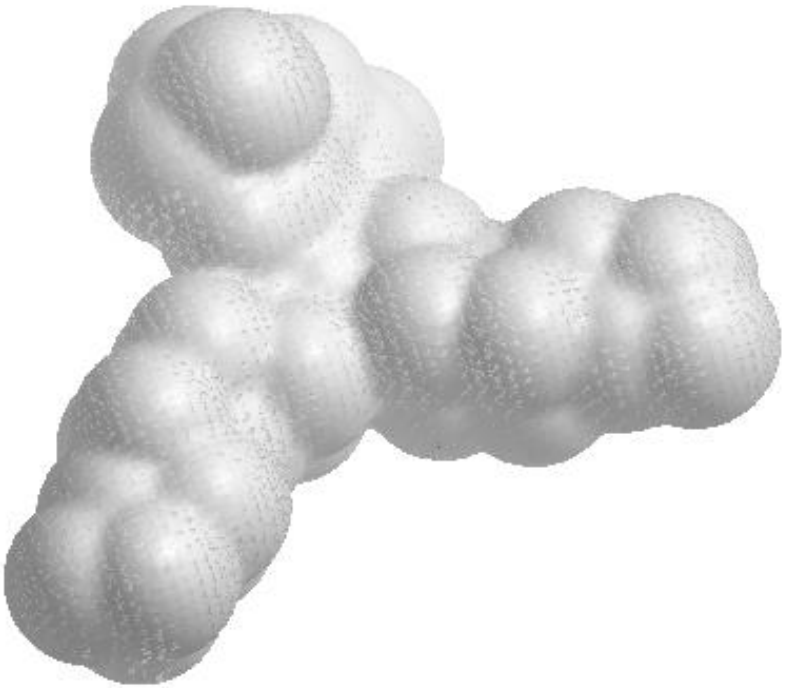

Figure 3.1 Solvent-accessible view of Compound **14**.

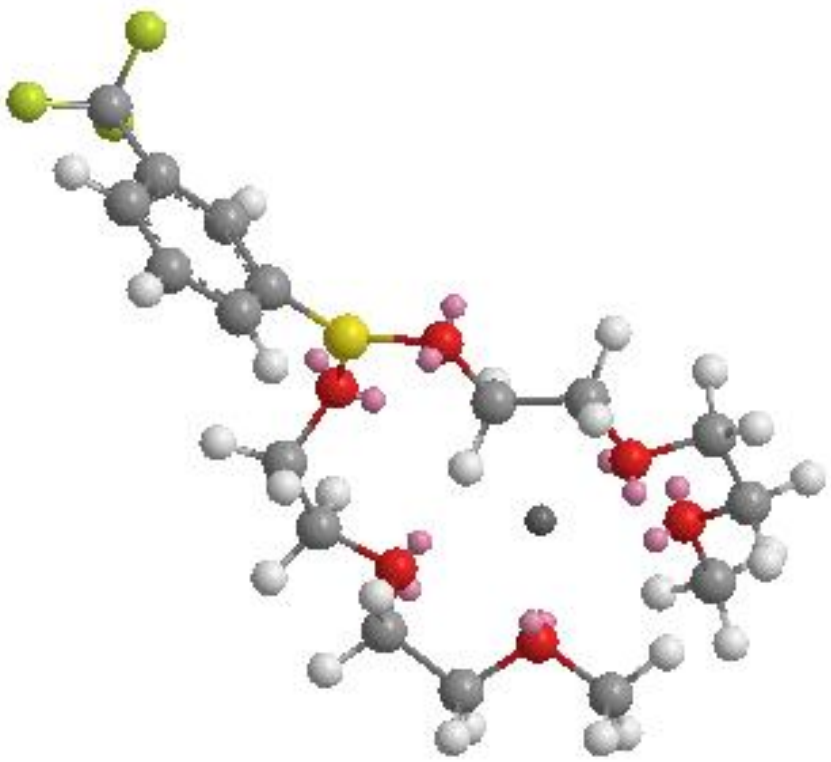

Figure 3.2 A lithium ion complexed with the EO sidechains of Compound **14**.

Chapter 4
Experimental

4.1 General conditions

All reagents used were commercially sourced from Aldrich and solvents were dried and distilled before use. The syntheses were done in oven-dried glassware under an argon atmosphere. All reactions were monitored by thin-layer chromatography on precoated TLC plates (silica gel with UV indicator added). NMR spectra were recorded on a Bruker Avance III 400 at the following frequencies: 400 MHz (^{1}H) and 100 MHz (^{13}C). Chemical shifts of ^{1}H and ^{13}C NMR spectra are reported in ppm using residual non-deuterated solvent as an internal standard. Infrared spectra were recorded neat on a Bruker Alpha FTIR spectrometer. Analysis by GC–MS was performed on an Agilent 7890A – 5975C GC-MSD combination using the following conditions: HP-5MS column (5% diphenyl–95% dimethylpolysiloxane, 30 m x 250 μm x 0.25 μm), 1 μL splitless injection at 280 °C. Carrier gas was He (head pressure 67.467 kPa, flow rate 1.2 mL/min, linear velocity 39.92 cm/s); transfer line temp. 280 °C; initial column temp. 50 °C held for 2 min, then raised to 120 °C at 20 °C/min, then raised to 200 °C at 30 °C/min, raised to 300 °C at 45 °C/min and finally held at 300 °C for 30 min.

4.2 Computational methods

In this study, the conformations and redox properties of various boronates were investigated through computational study with Gaussian 03 software[104] using density functional theory (DFT) and the Becke's three-parameter hybrid method utilizing the Lee-Young-Parr correlation functional (B3LYP). After initial energy optimization using Møller-Plesset perturbation theory (MP2), the conformational preferences and energetics were investigated using DFT calculations and the 6-31G(d,p) basis set *in vacuo*. The dihedral scans of Compound **6** were performed at the restricted Hartree-Fock (RHF) level due to time restrictions. IR frequency calculations confirmed in every case that minimum energy conformers were found. Visualization was by means of Gaussview 4.1.[116] The compounds that have lower LUMO energies than the carbonates are presumably better

electron acceptors[102] and would be expected to decompose on the negative electrode before the solvent does. The energy gap between each molecule's HOMO and LUMO was calculated as

$$\Delta E = |E_{HOMO} - E_{LUMO}|$$

4.3 Synthesis of boron derivatives

The arylboronates were prepared by reaction of the respective arylboronic acid with anhydrous diethylene or triethylene glycol monomethyl ether as follows: Arylboronic acid (10 mmol) was dissolved in 100 mL anhydrous benzene, and heated under reflux under Dean-Stark conditions. The solution was cooled down to about 70 ºC and 20.5 mmol diethylene or triethylene glycol monomethyl ether (EO) was added. The solution was heated under reflux until consumption of arylboronic acid (TLC monitoring) indicated completion of the reaction. Reaction times are shown below for the different compounds. Because of the high boiling points and viscosities of the products, the solvent and excess diethylene or triethylene glycol monomethyl ether were removed by vacuum distillation (240 °C at 1 mmHg) to yield the product quantitatively as colourless oil. Further purification by chromatography was impossible due to the high viscosities of the products.

Bis(2-(2-(2-methoxyethoxy)ethoxy)ethyl) phenylboronate 11

Yield: 4.10 g (99%) colourless oil after heating for 16 h.

IR (neat): 3450, 3030 (arom. C-H), 2878, 1593 (arom. C=C), 1456 (asym. B-O), 1354 (asym. B-O), 1199, 1108, 1083 (sym. B-O), 967 (monosub. phenyl C-H) cm^{-1}.

^{1}H-NMR ($CDCl_3$): δ_H 3.19 (6H, s, O–*Me*), 3.3–3.6 (16H, m, 8× –CH_2-), 7.20 (3H, m, arom.), 7.47 (2H, m, arom.).

^{13}C-NMR ($CDCl_3$): δ_C 58.7 (2× -O*Me*), 61.4, 64.7, 70.4, 72.1 (–OCH_2–), 127.4 (–*C*H– arom.), 131.9 (–*C*H– arom.), 133.9 (arom.).

Bis(2-(2-(2-methoxyethoxy)ethoxy)ethyl) 3,5-bis-(trifluoromethyl)phenylboronate 12

Yield: 5.31 g (96%) colourless oil after heating for 23 h.

IR (neat): 2869, 1277, 1124 (sym. B-O), 710, 681 (1,3,5-trisub. phenyl C-H) cm^{-1}.

^{1}H-NMR ($CDCl_3$): δ_H 3.24 (6H, s, 2× -O*Me*), 3.3–3.5 (20H, m, 10× –CH_2–), 3.94 (4H, 2× –CH_2–), 7.62 (2H, s, arom.), 8.07 (1H, s, arom.).

^{13}C-NMR ($CDCl_3$): δ_C 61.0 (2× -O*Me*), 66.2, 69.3, 70.1 (–*C*H_2–), 123.2 (–*C*H– arom.), 127.6 (–*C*H– arom.), 130.1 (quart, $^1J_{CF}$ = 130 Hz, -*C*F_3), 134.0 (quint), 137.0.

Bis(2-(2-methoxyethoxy)ethyl) phenylboronate 13

Yield: 3.08 g (94%) colourless oil after heating for 10 h.

IR (neat): 3054 (arom. C-H), 2878, 1573 (arom. C=C), 1440 (asym. B-O), 1341 (asym. B-O), 1098, 1065 (sym. B-O), 1021, 702, 648 (monosub. phenyl C-H) cm^{-1}.

^{1}H-NMR ($CDCl_3$): δ_H 3.26 (6H, s, 2× -O*Me*), 3.4–3.6 (12H, m, 6× –C*H*$_2$–), 4.09 (4H, s, 2× –C*H*$_2$–), 7.24 (3H, m, arom.), 7.70 (2H, m, arom.).

^{13}C-NMR ($CDCl_3$): δ_C 58.7 (2× -O*Me*), 61.4, 63.8, 70.4, 71.7 (–*C*H_2–), 127.5 (–*C*H– arom.), 127.4 (arom.), 130.2 (–*C*H– arom.), 133.9 (arom.).

MS: 312 (100%), 235 (6%), 208 (9%), 164 (30%), 137 (6%), 104 (35%). Boroxine $C_{18}H_{15}B_3O_3$ requires 312.13004, found 312.12.

Bis(2-(2-methoxyethoxy)ethyl) 3-trifluoromethylphenylboronate 14

Yield: 2.97 g (75%) colourless oil after heating for 18h.

IR (neat): 2877, 1345 (asym. B-O), 1102, 1071 (sym. B-O), 707(1,3-disub. phenyl C-H) cm^{-1}.

^{1}H-NMR ($CDCl_3$): δ_H 3.25 (6H, s, 2× O–*Me*), 3.4–3.6 (12H, m, 6× –C*H*$_2$–), 4.07 (4H, m, 2× –C*H*$_2$–), 7.43 (3H, m, arom.), 7.80 (1H, m, arom.).

^{13}C-NMR ($CDCl_3$): δ_C 58.6 (2× -O*Me*), 66.2, 69.3, 70.1 (–*C*H_2–), 123.2 (–*C*H– arom.), 129.5 (Q, $^1J_{CF}$ = 124 Hz, -*C*F_3), 129.6 (arom.), 133.9 (b).

MS: 516 (100%), 448 (15%), 403 (10%), 306 (10%), 231 (11%), 199 (23%), 171 (11%), 126 (60%). Boroxine $C_{21}H_{12}B_3F_9O_3$ requires 516.09219, found 516.10.

Bis(2-(2-methoxyethoxy)ethyl) 3,5-bis(trifluoromethyl)phenylboronate 15

Yield: 4.12 g (89%) colourless oil after heating for 44 h.

IR (neat): 2878, 1278, 1171, 1108 (sym. B-O), 843, 710, 681 (1,3,5-trisub. phenyl C-H) cm^{-1}.

^{1}H-NMR ($CDCl_3$): δ_H 3.46 (6H, s, 2× O–*Me*), 3.5–3.6 (12H, m, 6× –C*H*$_2$–), 4.22 (4H, m, 2× –C*H*$_2$–), 7.86-8.18 (3H, m, arom.).

^{13}C-NMR ($CDCl_3$): δ_C 58.6 (2× -O*Me*), 66.3, 70.1, 71.8 (–*C*H_2–), 123.5 (–*C*H– arom.), 127.5 (–*C*H– arom.), 130.2 (quart, $^1J_{CF}$ = 130 Hz, -*C*F_3), 132 (quart), 134.0.

Bis-(bis(2-(2-methoxyethoxy)ethyl)methylsilyl) phenylboronate 16

Yield: 6.92 g (100%) brownish oil after heating for 32 h.

IR (neat): 3450, 3030 (arom. C-H), 2878, 1593 (arom. C=C), 1456 (asym. B-O), 1354, 1199, 1108, 1083 (sym. B-O), 967 (monosub. phenyl C-H) cm^{-1}.

^{1}H-NMR ($CDCl_3$): δ_H 0.23 (3H, *s*, Si–Me), 3.19 (6H, s, OMe), 3.3–3.6 (16H, m, 8×–CH_2–), 7.14 – 7.27 (3H, m, arom.), 7.37 – 7.49 (2H, m, arom.).

4.4 Electrochemistry

The electrolyte solution was 1M $LiPF_6$ dissolved in ethylene carbonate (EC): diethyl carbonate (DEC): ethyl methyl carbonate (EMC) at a 1:1:1 volume ratio. The bare electrolyte was supplied by Guotai Huarong Co. Ltd., China, and used as the electrolyte without further treatment except addition of 2% test additive. The additive was added to the bare electrolyte in an argon-filled glove box (water content less than 10 ppm). The bare EC-based electrolyte, 1.0 M $LiPF_6$ in EC/EMC/DMC (1:1:1, v/v/v), was used as control. The anode consisted of 85 wt.% CMS with 10 wt.% polyvinylidene difluoride (PVDF) and 5 wt.% carbon black.[117] Electrochemical performance of the electrode was determined with coin-type cells with lithium foil as the counter and reference electrode, and Celgard 2400 as the separator.

The cyclic voltammetry and electrochemical impedance spectroscopy measurements were performed at 25°C on a CHI660C electrochemical workstation (Chenhua, China). The scan rate was 1.0 mV/s in the potential range 2.4 – 4.2 V.

References

1. Dunn, B.; Kamath, H.; Tarascon, J-M. Electrical Energy Storage for the Grid: A Battery of Choices. *Science* **2011**, *334*, 928 – 935.

2. Etacheri, V.; Marom, R.; Elazari, R.; Salitra, G.; Aurbach, D. Challenges in the development of advanced Li-ion batteries: a review. *Energy Environ. Sci.* **2011,** *4*, 3243 – 3262.

3. Jeong, G.; Kim, Y.U.; Kim, H.; Kim, Y.J.; Sohn, H.G. Prospective materials and applications for Li secondary batteries. *Energy Environ. Sci.* **2011**, *4*, 1986–2002.

4. Reddy, T.B.; Hossain, S. Rechargeable lithium batteries (ambient temperature). In: *Handbook of Batteries;* Toolenaar, F.; Reddy, T.B., Eds; McGraw-Hill: New York, 2002.

5. Pancaldi, G. *Volta: Science and culture in the age of enlightenment*. Princeton University Press: Ewing (NJ), 2003.

6. Von Handorf, D.E.; Crotty, D.E. The Baghdad battery - myth or reality? *Plating and Surface Finishing* **2002**, *89*, 84–87.

7. Wu, Y.P.; Yuan, X.Y.; Zhao, S.Y.; van Ree, T. *Chapter 1: Introduction;* In: *Lithium-Ion Batteries: Fundamentals and Applications;* Wu, Y.P., Ed; CRC Press Taylor&Francis: Boca Raton, *2015, pp 1 – 17.*

8. Matsuki, K.; Ozawa, K. *General concepts*; In: *Lithium Ion Rechargeable Batteries;* Ozawa, K., Ed; WILEY-Verlag Chemie: Weinheim, 2009.

9. van Schalkwijk, W.A.; Scrosati, B. *Introduction*; In: *Advances in Lithium-Ion Batterie;* van Schalkwijk, W.A.; Scrosati, B., Eds; Springer: New York, 2002.

10. Xia, Y. Capacity Fading on Cycling of 4 V Li/$LiMn_2O_4$ Cells. *J. Electrochem. Soc.* **1997**, *144*, 2593 – 2600.

11. Waldmann, T.; Wilka, M.; Kasper, M.; Fleischhammer, M.; Wohlfahrt-Mehrens, M. Temperature dependent ageing mechanisms in Lithium-ion batteries – A Post-Mortem study. *J. Power Sources* **2014**, *262*, 129-135.

12. Biensan, P.; Simon, B.; Peres, J.P.; de Guibert, A.; Broussely, M.; Bodet, J.M.; Perton, F. On safety of lithium-ion cells. *J. Power Sources* **1999**, *81-82*, 906-912.

13. Chen, Z.H.; Amine, K. Bifunctional electrolyte additive for lithium-ion batteries. *Electrochem. Commun.* **2007**, ***9***, 703-707.

14. Dahn, J.R.; Fuller, E.W.; Obrovac, M.; von Sacken, U. Thermal stability of Li_xCoO_2, Li_xNiO_2 and λ-MnO_2 and consequences for the safety of Li-ion cells. *Solid State Ionics* **1994**, *69*, 265-270.

15. Kumai, K.; Miyashiro, H.; Kobayashi, Y.; Takei, K.; Ishikawa, R. Gas generation mechanism due to electrolyte decomposition in commercial lithium-ion cell. *J. Power Sources* **1999**, *81-82*, 715-719.

16. MacNeil, D.D.; Dahn, J.R. The Reactions of $Li_{0.5}CoO_2$ with Nonaqueous Solvents at Elevated Temperatures. *J. Electrochem. Soc.* **2002**, *149*, A912-A919.

17. Moshuchak, L.M.; Bulinski, M.; Lamanna, W.M.; Wang, R.L.; Dahn, J.R. Direct comparison of 2,5-di-*tert*-butyl-1,4-dimethoybenzene and 4-*tert*-butyl-1,2-dimethoxybenzene as redox shuttles in $LiFePO_4$-based Li-ion cells. *Electrochem. Commun.* **2007**, *9*, 1497-1501.

18. Xiao, L.F.; Ai, X.P.; Cao, Y.L.; Wang, Y.D.; Yang, H.X. A composite polymer membrane with reversible overcharge protection mechanism for lithium ion batteries. *Electrochem. Commun.* **2005,** *7*, 589-592.

19. Zhang, S.S. A review on electrolyte additives for lithium-ion batteries. J. Power Sources ***2006****, 162, 1379-1394.*

20. Wang, Q.; Sun, J.; Chu, G. 2005. Lithium Ion Battery Fire and Explosion. *Fire Safety Science – Proceedings of the Eighth International Symposium*, pp 375-382.

21. Brissot, C.; Rosso, M.; Chazalviel, J.N.; Lascaud, S. Dendritic growth mechanisms in lithium/polymer cells. *J. Power Sources* **1999**, *81*, 925–929.

22. Wang, B.; Yuan, X.Y.; Zhao, S.Y.; Wu, Y.P.; van Ree, T. *Chapter 9: Liquid Electrolytes;* In: *Lithium-Ion Batteries: Fundamentals and Applications;* Wu, Y.P., Ed; CRC Press Taylor & Francis: Boca Raton, *2015, pp 273 – 339.*

23. Balbuena, P.B.; Wang, Y., Eds; *Lithium-Ion Batteries: Solid-Electrolyte Interphase*; Imperial College Press: London, 2004.

24. Chen, R.; Wu, F.; Li, L.; Guan, Y.B.; Qiu, X.P.; Chen, S.; Li, Y.J.; Wu, S.X. Butylene sulfite as a film-forming additive to propylene carbonate-based electrolytes for lithium ion batteries. *J. Power Sources* **2007**, *172*, 395-403.

25. Korepp, C.; Santner, H.J.; Fujii, T.; Ue, M.; Besenhard, J.O.; Möller, K-C.; Winter, M. 2-Cyanofuran - A novel vinylene electrolyte additive for PC-based electrolytes in lithium-ion batteries. *J. Power Sources* **2006**, *158*, 578-582.

26. Schroeder, G.; Gierczyk, B.; Waszak, D.; Walkowiak, M. Impact of ethyl tris-2-methoxyethoxy silane on the passivation of graphite electrode in Li-ion cells with PC-based electrolyte. *Electrochem. Commun.* **2006**, *8*, 1583-1587.

27. Walkowiak, M.; Waszak, D.; Schroeder, G.; Gierczyk, B. Polyether-functionalized disiloxanes as new film-forming electrolyte additive for Li-ion cells with graphitic anodes. *Electrochem. Commun.* **2008**, *10*, 1676-1679.

28. MacNeil, D.D.; Dahn, J.R. Test of Reaction Kinetics Using Both Differential Scanning and Accelerating Rate Calorimetries As Applied to the Reaction of Li_xCoO_2 in Non-aqueous Electrolyte. *J. Phys. Chem. A* **2001**, *105*, 4430-4439.

29. Gnanaraj, J.S.; Levi, M.D.; Gofer, Y.; Aurbach, D. $LiPF_3(CF_2CF_3)_3$: A Salt for Rechargeable Lithium Ion Batteries. *J. Electrochem. Soc.* **2003**, *150*, A445-A454.

30. Xu, K.; Zhang, S.S.; Jow, T.R.; Xu, W.; Angell, C.A. LiBOB as Salt for Lithium-Ion Batteries: A Possible Solution for High Temperature Operation. *Electrochem. Solid-State Lett.* **2002**, *5*, A26-A29.

31. Gao, J.; Fu, L.J.; Zhang, H.P.; Zhang, T.; Wu, Y.P.; Wu, H.Q. Suppression of PC decomposition at the surface of graphitic carbon by Cu coating. *Electrochem. Commun.* **2006**, *8*, 1726-1730.

32. Gao, J.; Fu, L.J.; Zhang, H.P.; Yang, L.C.; Wu, Y.P. Improving electrochemical performance of graphitic carbon in PC-based electrolyte by nano-TiO_2 coating. *Electrochim. Acta* **2008**, *53*, 2376-2379.

33. Kazuyasu, F. High temperature cycle; anodes, cathodes and nonaqueous electrolytes; intercalation; nonaqueous solvent containing an alkylaromatic hydrocarbon. US Patent 20060166102, 2006.

34. Kim, J.H. Electrolyte for Lithium Rechargeable Battery and Lithium Rechargeable Battery Comprising the Same. US Patent 20060160000, 2006.

35. Xiao, L.F.; Ai, X.P.; Cao, Y.L.; Yang, H.X. Electrochemical behavior of biphenyl as polymerizable additive for overcharge protection of lithium ion batteries. *Electrochim. Acta* **2004**, *49*, 4189-4196.

36. Mao, H.; Wainwright, D.S. Improvement comprises a monomer additive mixed in nonaqueous electrolyte which polymerizes to form electroconductive polymer at battery voltages greater than maximum operating charging voltage and creates an internal short circuiting. US Patent 6,074,776, 1998.

37. Reimers, J.N.; Way, B.M. Additives selected from the group consisting of phenyl-aliphatic hydrocarbon-phenyl compounds, fluorine substituted biphenyl compounds, and 3-thiopheneacetonitrile can provide better cycling performances; fireproofing. US Patent 6,074,777, 2000.

38. Wang, L.; Huang, Y.; Jia, D. Triethyl orthoformate as a new film-forming electrolytes solvent for lithium-ion batteries with graphite anodes. *Electrochim. Acta* **2006**, *51*, 4950-4955.

39. Xu, K. Nonaqueous Liquid Electrolytes for Lithium-Based Rechargeable Batteries. *Chem. Rev.* **2004**, *104*, 4303-4418.

40. Fu, L.J.; Liu, H.; Zhang, H.P.; Li, C.; Zhang, T.; Wu, Y.P.; Holze, R.; Wu, H.Q. Synthesis and electrochemical performance of novel core/shell structured nanocomposites. *Electrochem. Commun.* **2006**, *8*, 1-4.

41. Zhao, N.H.; Fu, L.J.; Yang, L.C.; Zhang, T.; Wang, G.J.; Deng, Y.H.; Wu, Y.P.; van Ree, T. Nanostructured anode materials for lithium-ion batteries. *Pure Appl. Chem*. **2008**, *80*, 2283-2295.

42. Zhang, T.; Gao, J.; Zhang, H.P.; Yang, L.C.; Wu, Y.P.; Wu, H.Q. Preparation and electrochemical properties of core-shell Si/SiO nanocomposite as anode material for lithium ion batteries. *Electrochem. Commun.* **2007**, *9*, 886-890.

43. Zhao, N.H.; Wang, G.J.; Huang, Y.; Wang, B.; Yao, B.D.; Wu, Y.P. Preparation of Nanowire Arrays of Amorphous Carbon Nanotube-Coated Single Crystal SnO_2. *Chem. Mater.* **2008**, *20*, 2612-2614.

44. Yang, L.C.; Gao, Q.S.; Zhang, Y.H.; Tang, Y.; Wu, Y.P. Tremella-like molybdenum dioxide consisting of nanosheets as an anode material for lithium ion battery. *Electrochem. Commun.* **2008**, *10*, 118-122.

45. Sethuraman, V.A.; Hardwick, L.J.; Srinivasan, V.; Kostecki, R. Surface structural disordering in graphite upon lithium intercalation/deintercalation. *J. Power Sources* **2010**, *195*, 3655-3660.

46. Agubra, V.; Fergus, J. Lithium Ion Battery Anode Aging Mechanisms. *Materials* **2013**, 1310 – 1325.

47. Xia, Q.; Wang, B.; Wu, Y.P.; Luo, H.J.; Zhao, S.Y.; van Ree, T. Phenyl tris-2-methoxydiethoxysilane as an additive to PC-based electrolytes for lithium-ion batteries. *J. Power Sources* **2008**, *180*, 602-606.

48. Wang, B.; Qu, Q.T.; Xia, Q.; Wu, Y.P.; Li, X.; Gan, C.L.; van Ree, T. Effects of 3,5-bis(trifluoromethyl)benzeneboronic acid as an additive on electrochemical performance of propylene carbonate-based electrolytes for lithium ion batteries. *Electrochim. Acta* **2008**, *54*, 816-820.

49. Amine, K.; Wang, Q.Z.; Vissers, D.R.; Zhang, Z.C.; Rossi, N.; West, R. Novel silane compounds as electrolyte solvents for Li-ion batteries. *Electrochem. Commun.* **2006**, *8*, 429-433.

50. Korepp, C.; Kern, W.; Lanzer, E.A.; Raimann, P.R.; Besenhard, J.O.; Yang, M.; Möller, K.C.; Shieh, D.T.; Winter, M. Ethyl isocyanate - An electrolyte additive from the large family of isocyanates for PC-based electrolytes in lithium-ion batteries. *J. Power Sources* **2007**, *174*, 628-631.

51. Lu, M.; Cheng, H.; Yang, Y. A comparison of solid electrolyte interphase (SEI) on the artificial graphite anode of the aged and cycled commercial lithium ion cells. *Electrochim. Acta* **2008**, *53*, 3539-3546.

52. Schroeder, G.; Gierczyk, B.; Waszak, D.; Kopczyk, M.; Walkowiak, M. Vinyl tris-2-methoxyethoxy silane – A new class of film-forming electrolyte components for Li-ion cells with graphite anodes. *Electrochem. Commun.* **2006**, *8*, 523-527.

53. Walkowiak, M.; Schroeder, G.; Gierczyk, B.; Waszak, D.; Osinska, M. New lithium ion conducting polymer electrolytes based on polysiloxane grafted with Si-tripodand centers. *Electrochem. Commun.* **2007**, *9*, 1558-1562.

54. Lee, J.T.; Lin, Y.W.; Jan, Y.S. Allyl ethyl carbonate as an additive for lithium-ion battery electrolytes. *J. Power Sources* **2004**, *132*, 244-248.

55. Santner, H.J.; Möller, K-C.; Ivančo, J.; Ramsey, M.G.; Netzer, F.P.; Yamaguchi, S.; Besenhard, J.O.; Winter, M. Acrylic acid nitrile, a film-forming electrolyte component for lithium-ion batteries, which belongs to the family of additives containing vinyl groups. *J. Power Sources* **2003**, *119–121*, 368-372.

56. Hu, Y.S.; Kong, W.H.; Wang, Z.X.; Huang, X.J.; Chen, L.Q. Tetrachloroethylene as new film-forming additive to propylene carbonate-based electrolytes for lithium ion batteries with graphitic anode. *Solid State Ionics* **2005**, *176*, 53-56.

57. Wrodnigg, G.H.; Besenhard, J.O.; Winter, M. Ethylene Sulfite as Electrolyte Additive for Lithium-Ion Cells with Graphitic Anodes. *J. Electrochem. Soc.* **1999**, *146*, 470.

58. Wrodnigg, G.H.; Wrodnigg, T.M.; Besenhard, J.O.; Winter, M. Propylene sulfite as film-forming electrolyte additive in lithium ion batteries. *Electrochem. Commun.* **1999**, *1*, 148.

59. Oesten, R.; Heider, U.; Schmidt, M. Advanced electrolytes. *Solid State Ionics* **2002**, *148*, 391-397.

60. Shu, Z.X.; McMillan, R.S.; Murray, J.J. Use of Chloroethylene Carbonate as an Electrolyte Solvent for a Lithium Ion Battery Containing a Graphitic Anode. *J. Electrochem. Soc.* **1995**, *142*, L161-L162.

61. Trofimov, B.A.; Myachina, G.F.; Oparina, L.A.; Korzhova, S.A.; Gusarova, N.K.; Doo, S.G.; Cho, M.D.; Kim, H. Triethyl 2-(1,3-oxazolidin-3-yl)ethyl orthosilicate as a new type electrolyte additive for lithium-ion batteries with graphite anodes. *J. Power Sources* **2005**, *147*, 260-263.

62. Wang, B.; Qu, Q.T.; Yang, L.C.; Xia, Q.; Wu, Y.P.; Zhou, D.L.; Gu, X.J.; van Ree, T. 2-Phenylimidazole as an additive to prevent the co-intercalation of propylene carbonate in organic electrolyte for lithium-ion batteries. *J. Power Sources* **2009**, *189*, 757-760.

63. Wang, B.; Xia, Q.; Zhang, P.; Li, G.C.; Wu, Y.P.; Luo, H.J.; Zhao, S.Y.; van Ree, T. *N*-Phenylmaleimide as a new polymerizable additive for overcharge protection of lithium-ion batteries, *Electrochem. Commun.* **2008**, *10*, 727-730.

64. Gokel, G.W.; Murillo, O.M. Podands. *Compreh. Supramolec. Chem.* **1996**, 1-34.

65. Atwood, J.L.; Steed, J.W. *Encyclopedia of Supramolecular Chemistry*; Marcel Dekker Inc.: New York, 2004.

66. Steed, J.W.; Atwood, J.L. *Supramolecular Chemistry*; Wiley: NewYork: 2000.

67. Danil de Namor, A.F.; Ng, J.C.Y.; Llosa Tanco, M.A.; Salomon, M. Thermodynamics of Lithium−Crown Ether (12-crown-4 and 1-Benzyl-1-aza-12-crown-4) Interactions in Acetonitrile and Propylene Carbonate. The Anion Effect on the Coordination Process. *J. Phys. Chem.* **1996**, *100*, 14485-14491.

68. Sporzyński, A.; Miśkiewicz, A.; Gierczyk, B.; Pankiewicz, R.; Schroeder, G.; Brzezinski, B. Polyoxaalkyl esters of phenylboronic acids as new podands. *J. Mol. Struc.* **2006**, *791*, 111-116.

69. Gao, M.; Wang, Y.; Yi, Q.; Su, Y.; Sun, P.; Wang, X.; Zhao, J.; Zou, G. A novel solid-state electrolyte based on a crown ether lithium salt complex. *J. Mater. Chem. A* **2015**, *3*, 20541-20546.

70. Whittingham, M.S. Lithium batteries and cathode materials. *Chem. Rev*. **2004**, *104*, 4271-4301.

71. Fergus, J.W. Recent developments in cathode materials for lithium ion batteries. *J. Power Sources* **2010**, *195*, 939–954.

72. Antolini, E. $LiCoO_2$: Formation, structure, lithium and oxygen nonstoichiometry, electrochemical behavior and transport properties. *Solid State Ionics* **2004**, *170*, 159–171.

73. Belov, D.; Yang, M.H. Failure mechanism of Li-ion battery at overcharge conditions. *J. Solid State Electrochem.* **2008**, *12*, 885–894.

74. Shi, X.; Wang, C.; Ma, X.; Sun, J. Synthesis and electrochemical properties of $LiNi_{0.9}Co_{0.1}O_2$ cathode material for lithium secondary battery. *Mater. Chem. Phys.* **2009**, *113*, 780–783.

75. Wang, L.; Li, J.; He, X.; Pu, W.; Wan, C.; Jiang, C. Recent advances in layered $LiNi_xCo_yMn_{1-x-y}O_2$ cathode materials for lithium ion batteries. *J. Solid State Electrochem.* **2009**, *13*, 1157–1164.

76. Tang, W.; Wang, X.J.; Hou, Y.Y.; Li, L.L.; Sun, H.; Zhu, Y.S.; Bai, Y.; Wu, Y.P.; Zhu, K.; van Ree, T. Nano $LiMn_2O_4$ as cathode material of high rate capability for lithium ion batteries. *J. Power Sources* **2012**, *198*, 308-311.

77. Jansen, A.N.; Kahaian, A.J.; Kepler, K.D.; Nelson, P.A.; Amine, K.; Dees, D.W.; Vissers, D.R.; Thackeray, M.M. Development of a high-power lithium-ion battery. *J. Power Sources* **1999**, *81–82*, 902–905.

78. Mai, L.Q.; Gao, Y.; Guan, J.G.; Hu, B.; Xu, L.; Jin, W. Formation and Lithiation of Ferroselite Nanoflowers as High-energy Li-ion Battery Electrodes. *Int. J. Electrochem. Sci.* **2009**, *4*, 755-761.

79. Xu, K. Whether EC and PC Differ in Interphasial Chemistry on Graphitic Anode and How. *J. Electrochem. Soc.* **2009**, *156*, A751-A755.

80. Wu, Y.P.; Jiang, C.; Wan, C.; Holze, R. Modified natural graphite as anode material for lithium ion batteries. *J. Power Sources* **2002**, *111*, 329-334.

81. Matsuta, S.; Asada, T.; Kitaura, K. Vibrational Assignments of Lithium Alkyl Carbonate and Lithium Alkoxide in the Infrared Spectra: An *Ab Initio* MO Study. *J. Electrochem. Soc.* **2000**, *147*, 1695-1702.

82. Verma, P.; Maire, P.; Novák, P. A review of the features and analyses of the solid electrolyte interphase in Li-ion batteries. *Electrochim. Acta* **2010**, *55*, 6332-6341.

83. Tasaki, K.; Goldberg, A.; Lian, J-J.; Walker, M.; Timmons, A.; Harris, S.J. Solubility of Lithium Salts Formed on the Lithium-Ion Battery Negative Electrode Surface in Organic Solvents. *J. Electrochem. Soc.* **2009**, *156*, A1019-A1027**.**

84. Li, L.L.; Li, L.; Wang, B.; Liu, L.L.; Wu, Y.P.; van Ree, T.; Thavhiwa, K.A. Methyl phenyl bis-methoxydiethoxysilane as bi-functional additive to propylene carbonate-based electrolyte for lithium ion batteries. *Electrochim. Acta* **2011,** *56*, 4858-4864.

85. Wang, Q.; Zakeeruddin, S.M.; Exnar, I.; Grätzel, M. A new strategy of molecular overcharge protection shuttles for lithium ion batteries. *Electrochem. Commun*. **2008**, *10*, 651–654.

86. Wang, R.L.; Buhrmester, C.; Dahn, J.R. Calculations of Oxidation Potentials of Redox Shuttle Additives for Li-Ion Cells. *J. Electrochem. Soc.* **2006**, *153*, A445-A449.

87. Zhang, H.P.; Xia, Q.; Wang, B.; Yang, L.C.; Wu, Y.P.; Sun, D.L.; Gan, C.L.; Luo, H.J.; Bebeda, A.W.; van Ree, T. Vinyl-tris-(methoxydiethoxy)silane as an effective and ecofriendly flame retardant for electrolytes in lithium ion batteries. *Electrochem. Commun.* **2009**, *11*, 526-529.

88. Acevedo-Peña, P.; Haro, M.; Rincón, M.E.; Bisquert, J.; Garcia-Belmonte, G. Facile kinetics of Li-ion intake causes superior rate capability in multiwalled carbon nanotube@TiO_2 nanocomposite battery anodes. *J. Power Sources* **2014**, *268*, 397-403.

89. Ota, H.; Shima, K.; Ue, M.; Yamaki, J.. Effect of vinylene carbonate as additive to electrolyte for lithium metal anode. *Electrochim. Acta* **2004**, *49*, 565-572.

90. Pasgreta, E.; Puchta, R.; Zahl, A.; van Eldik, R. Ligand Exchange Processes on Solvated Lithium Cations Part V – Complexation by Cryptands in Acetone as Solvent. *Eur. J. Inorg. Chem.* **2007**, 3067-3076.

91. Allinger, N.L. Calculation of molecular structure and energy by force-field methods. *Advan. Phys. Org. Chem.* **1976**, *13*, 1-82.

92. Hoffmann, R. An Extended Hückel Theory. I. Hydrocarbons. *J. Chem. Phys.* **1963**, *39*, 1397-1412.

93. Čársky, P.; Urban, M. *Ab Initio Calculations: Methods and Applications in Chemistry*. Springer: Berlin, 1980.

94. Hohenberg, P.; Kohn, W. Inhomogeneous Electron Gas. *Phys. Rev.* **1964**, *136*, B864–871.

95. Dewar, M.J.S.; Zoebisch, E.G.; Healy, E.F.; Stewart, J.J.P. Development and use of quantum molecular models. 75. Comparative tests of theoretical procedures for studying chemical reactions. *J. Amer. Chem. Soc.* **1985**, *107*, 3902–3909.

96. Dewar, M.J.S.; Thiel, W. Ground states of molecules. 38. The MNDO method. Approximations and parameters. *J. Amer. Chem. Soc.* **1977**, *99*, 4899-4907.

97. Stewart, J.J.P. Optimization of parameters for semiempirical methods: I. Method. *J. Computat. Chem.* **1989**, *10*, 209–220.

98. Becke, A.D. Density-functional exchange-energy approximation with correct asymptotic behavior. *Phys. Rev. A* **1988**, *38*, 3098-3100.

99. Lee, C.; Yang, W.; Parr, R.G. Development of the Colle-Savetti correlation-energy formula into a functional of the electron density. *Phys. Rev. B* **1988**, *37*, 785-789.

100. Becke, A.D. A new mixing of Hartree-Fock and local density-functional theories. *J. Chem. Phys.* **1993**, *98*, 1372–1377.

101. Magalhães, A.L. Gaussian-Type Orbitals versus Slater-Type Orbitals: A Comparison, *J. Chem. Educ.* **2014**, *91*, 2124–2127.

102. Maccoll, A. Reduction Potentials of Conjugated Systems. *Nature* **1949**, *163*, 178–179.

103. Abe, K.; Ushigoe, Y.; Yoshitake, H.; Yoshio, M. Functional electrolytes: Novel type additives for cathode materials, providing high cycleability performance. *J. Power Sources* **2006**, *153*, 328-335.

104. *Gaussian 03, Revision D.01;* Frisch, M.J.; Trucks, G.W.; Schlegel, H.B. *et al.*; Gaussian, Inc.: Wallingford (CT), 2004.

105. Sporzyński, A. Hydrogen bonds in boronic acids and their complexes *Pol. J. Chem.* **2007**, *81*, 757-766.

106. Lee, H.S.; Sun, X.; Yang, X.Q.; McBreen, J. Synthesis and Study of New Cyclic Boronate Additives for Lithium Battery Electrolytes. *J. Electrochem. Soc.* **2002**, *149*, A1460-A1465.

107. Peak, D.; Luther, G.W.; Sparks, D.L. ATR-FTIR spectroscopic studies of boric acid adsorption on hydrous ferric oxide. *Geochim. Cosmochim. Acta* **2003**, *67*, 2551–2560.

108. Kissinger, P.T.; Heineman, W.R. Cyclic Voltammetry. *J. Chem. Educ*. **1983**, *60*, 702-706.

109. Mabbott, G.A. An Introduction to Cyclic Voltammetry. *J. Chem. Educ.* **1983**, *60*, 697-702.

110. Van Benschoten, J.J.; Lewis, J.Y.; Heineman, W.R.; Roston, D.A.; Kissinger, P.T. Cyclic Voltammetry Experiment. *J. Chem. Educ*. **1983**, *60*, 772-776.

111. Yamada, Y.; Iriyama, Y.; Abe, T.; Ogumi, Z. Kinetics of Electrochemical Insertion and Extraction of Lithium Ion at SiO. *J. Electrochem. Soc.* **2010**, *157*, A26-A30.

112. Goodenough, J.B.; Kim, Y. Challenges for Rechargeable Li Batteries. *Chem. Mater*. **2010**, *22*, 587-603.

113. Bebeda, A.W.; van Ree, T. *Designing new electrolyte additives for better lithium-ion battery performance and overcharge protection*, 10th International IUPAC Symposium on Novel Materials and their Synthesis (NMS-X), Zhengzhou, 10-16 October, 2014.

114. Bebeda, A.W.; van Ree, T. *Conformational Preferences and Electrochemical Performance of Some Substituted Phenylboronates*, 10th International IUPAC Symposium on Novel Materials and their Synthesis (NMS-X), Zhengzhou, 10-16 October, 2014.

115. Bebeda, A.W.; van Ree, T. Conformational Preferences and Electrochemical Performance of Ethyleneoxy Phenylboronate Electrolyte Additives. *Arab. J. Sci. Eng.* **2015**, *40*, 2841 – 2851.

116. *GaussView, Version 4.1;* Dennington, R.; Keith, T.; Millam, J. *Semichem Inc.*: Shawnee Mission (KS), 2006.

117. Wang, B.; Zhang, H.P.; Yang, L.C.; Qu, Q.T.; Wu, Y.P.; Gan, C.L.; Zhou, D.L. Improving electrochemical performance of graphitic carbon in PC-based electrolytes by using *N*-vinyl-2-pyrrolidone as an additive. *Electrochem. Commun.* **2008**, *10*, 1571-1574.

118. Longstaff, C.; Rose, M.E. Derivatization and mass spectrometric investigations of substituted benzeneboronic acids. The use of linked scanning during gas chromatography mass spectrometry. *Org. Mass Spec.* ***1982***, *17*, 508–518.

119. Hall, D.G. Chapter 1: Structure, Properties, and Preparation Of Boronic Acid Derivatives. Overview of Their Reactions and Applications. In: *Boronic Acids - Preparation, Applications in Organic Synthesis and Medicine;* Hall, D.G. Ed; Wiley-VCH: Weinheim (Germany), 2005.

Appendix A

Typical Gaussian output (partial)

```
Entering Link 1 = C:\G03W\l1.exe PID=      2564.

 Copyright (c) 1988,1990,1992,1993,1995,1998,2003,2004, Gaussian, Inc.
                    All Rights Reserved.

 This is the Gaussian(R) 03 program.  It is based on the
 the Gaussian(R) 98 system (copyright 1998, Gaussian, Inc.),
 the Gaussian(R) 94 system (copyright 1995, Gaussian, Inc.),
 the Gaussian 92(TM) system (copyright 1992, Gaussian, Inc.),
 the Gaussian 90(TM) system (copyright 1990, Gaussian, Inc.),
 the Gaussian 88(TM) system (copyright 1988, Gaussian, Inc.),
 the Gaussian 86(TM) system (copyright 1986, Carnegie Mellon
 University), and the Gaussian 82(TM) system (copyright 1983,
 Carnegie Mellon University). Gaussian is a federally registered
 trademark of Gaussian, Inc.

 This software contains proprietary and confidential information,
 including trade secrets, belonging to Gaussian, Inc.

 This software is provided under written license and may be
 used, copied, transmitted, or stored only in accord with that
 written license.

 The following legend is applicable only to US Government
 contracts under FAR:

                       RESTRICTED RIGHTS LEGEND

 Use, reproduction and disclosure by the US Government is
 subject to restrictions as set forth in subparagraphs (a)
 and (c) of the Commercial Computer Software - Restricted
 Rights clause in FAR 52.227-19.

 Gaussian, Inc.
 340 Quinnipiac St., Bldg. 40, Wallingford CT 06492


 ----------------------------------------------------------------
 Warning -- This program may not be used in any manner that
 competes with the business of Gaussian, Inc. or will provide
 assistance to any competitor of Gaussian, Inc.  The licensee
 of this program is prohibited from giving any competitor of
 Gaussian, Inc. access to this program.  By using this program,
 the user acknowledges that Gaussian, Inc. is engaged in the
 business of creating and licensing software in the field of
 computational chemistry and represents and warrants to the
 licensee that it is not a competitor of Gaussian, Inc. and that
 it will not use this program in any manner prohibited above.
 ----------------------------------------------------------------


 Cite this work as:
 Gaussian 03, Revision D.01,
 M. J. Frisch, G. W. Trucks, H. B. Schlegel, G. E. Scuseria,
```

```
M. A. Robb, J. R. Cheeseman, J. A. Montgomery, Jr., T. Vreven,
K. N. Kudin, J. C. Burant, J. M. Millam, S. S. Iyengar, J. Tomasi,
V. Barone, B. Mennucci, M. Cossi, G. Scalmani, N. Rega,
G. A. Petersson, H. Nakatsuji, M. Hada, M. Ehara, K. Toyota,
R. Fukuda, J. Hasegawa, M. Ishida, T. Nakajima, Y. Honda, O. Kitao,
H. Nakai, M. Klene, X. Li, J. E. Knox, H. P. Hratchian, J. B. Cross,
V. Bakken, C. Adamo, J. Jaramillo, R. Gomperts, R. E. Stratmann,
O. Yazyev, A. J. Austin, R. Cammi, C. Pomelli, J. W. Ochterski,
P. Y. Ayala, K. Morokuma, G. A. Voth, P. Salvador, J. J. Dannenberg,
V. G. Zakrzewski, S. Dapprich, A. D. Daniels, M. C. Strain,
O. Farkas, D. K. Malick, A. D. Rabuck, K. Raghavachari,
J. B. Foresman, J. V. Ortiz, Q. Cui, A. G. Baboul, S. Clifford,
J. Cioslowski, B. B. Stefanov, G. Liu, A. Liashenko, P. Piskorz,
I. Komaromi, R. L. Martin, D. J. Fox, T. Keith, M. A. Al-Laham,
C. Y. Peng, A. Nanayakkara, M. Challacombe, P. M. W. Gill,
B. Johnson, W. Chen, M. W. Wong, C. Gonzalez, and J. A. Pople,
Gaussian, Inc., Wallingford CT, 2004.

******************************************
Gaussian 03:  IA32W-G03RevD.01 13-Oct-2005
               07-Jun-2014
******************************************
-------------------------------------
#T RB3LYP/6-31G(d,p) Opt Pop=Reg Test
-------------------------------------
----------
Untitled-4
----------
Symbolic Z-matrix:
Charge =  0 Multiplicity = 1
C                     0    -0.4435   -0.16379  -2.27248
C                     0     0.81343   0.22195  -1.80898
C                     0    -1.38243  -0.65955  -1.36671
C                     0     1.1228    0.11682  -0.45168
C                     0     0.19191  -0.377     0.47266
C                     0    -1.06677  -0.76758  -0.01245
B                     0     0.51755  -0.51343   2.00757
O                     0     0.96278  -1.72269   2.45316
O                     0     0.37534   0.5023    2.91547
C                     0     1.82169   0.80084  -2.7666
C                     0    -2.7603   -1.03102  -1.85149
F                     0     1.72089   2.14833  -2.8382
F                     0     1.65768   0.32523  -4.01866
F                     0     3.08861   0.52264  -2.3848
F                     0    -3.60136   0.02759  -1.80562
F                     0    -3.31068  -2.00618  -1.09824
F                     0    -2.74078  -1.46307  -3.1315
H                     0    -0.68147  -0.09602  -3.32744
H                     0     2.12096   0.40476  -0.13216
H                     0    -1.79874  -1.17015   0.679
H                     0     1.11333  -1.71892   3.40741
H                     0    -0.00559   1.31029   2.55594


GradGradGradGradGradGradGradGradGradGradGradGradGradGradGradGradGradGrad
Initialization pass.
                          ----------------------------
                          !    Initial Parameters    !
                          ! (Angstroms and Degrees)  !
```

Name	Definition	Value	Derivative Info.
R1	R(1,2)	1.3941	estimate D2E/DX2
R2	R(1,3)	1.3956	estimate D2E/DX2
R3	R(1,18)	1.0836	estimate D2E/DX2
R4	R(2,4)	1.3961	estimate D2E/DX2
R5	R(2,10)	1.5062	estimate D2E/DX2
R6	R(3,6)	1.3948	estimate D2E/DX2
R7	R(3,11)	1.5072	estimate D2E/DX2
R8	R(4,5)	1.4017	estimate D2E/DX2
R9	R(4,19)	1.0869	estimate D2E/DX2
R10	R(5,6)	1.4043	estimate D2E/DX2
R11	R(5,7)	1.575	estimate D2E/DX2
R12	R(6,20)	1.0844	estimate D2E/DX2
R13	R(7,8)	1.3635	estimate D2E/DX2
R14	R(7,9)	1.3697	estimate D2E/DX2
R15	R(8,21)	0.9661	estimate D2E/DX2
R16	R(9,22)	0.9629	estimate D2E/DX2
R17	R(10,12)	1.3531	estimate D2E/DX2
R18	R(10,13)	1.3494	estimate D2E/DX2
R19	R(10,14)	1.3521	estimate D2E/DX2
R20	R(11,15)	1.3528	estimate D2E/DX2
R21	R(11,16)	1.3495	estimate D2E/DX2
R22	R(11,17)	1.3511	estimate D2E/DX2
A1	A(2,1,3)	119.2806	estimate D2E/DX2
A2	A(2,1,18)	120.2913	estimate D2E/DX2
A3	A(3,1,18)	120.4187	estimate D2E/DX2
A4	A(1,2,4)	120.1457	estimate D2E/DX2

```
 !  A5       A(1,2,10)                  119.9001              estimate
D2E/DX2                !
 !  A6       A(4,2,10)                  119.9155              estimate
D2E/DX2                !
 !  A7       A(1,3,6)                   120.3587              estimate
D2E/DX2                !
 !  A8       A(1,3,11)                  119.5947              estimate
D2E/DX2                !
 !  A9       A(6,3,11)                  120.0081              estimate
D2E/DX2                !
 !  A10      A(2,4,5)                   121.3641              estimate
D2E/DX2                !
 !  A11      A(2,4,19)                  117.9937              estimate
D2E/DX2                !
 !  A12      A(5,4,19)                  120.6217              estimate
D2E/DX2                !
 !  A13      A(4,5,6)                   117.7375              estimate
D2E/DX2                !
 !  A14      A(4,5,7)                   122.4019              estimate
D2E/DX2                !
 !  A15      A(6,5,7)                   119.8588              estimate
D2E/DX2                !
 !  A16      A(3,6,5)                   121.1118              estimate
D2E/DX2                !
 !  A17      A(3,6,20)                  119.677               estimate
D2E/DX2                !
 !  A18      A(5,6,20)                  119.2074              estimate
D2E/DX2                !
 !  A19      A(5,7,8)                   117.5693              estimate
D2E/DX2                !
 !  A20      A(5,7,9)                   124.0733              estimate
D2E/DX2                !
 !  A21      A(8,7,9)                   118.3568              estimate
D2E/DX2                !
 !  A22      A(7,8,21)                  111.7299              estimate
D2E/DX2                !
 !  A23      A(7,9,22)                  114.5713              estimate
D2E/DX2                !
 !  A24      A(2,10,12)                 111.4996              estimate
D2E/DX2                !
 !  A25      A(2,10,13)                 111.9074              estimate
D2E/DX2                !
 !  A26      A(2,10,14)                 111.6295              estimate
D2E/DX2                !
 !  A27      A(12,10,13)                107.0289              estimate
D2E/DX2                !
 !  A28      A(12,10,14)                106.8355              estimate
D2E/DX2                !
 !  A29      A(13,10,14)                107.6603              estimate
D2E/DX2                !
 !  A30      A(3,11,15)                 111.383               estimate
D2E/DX2                !
 !  A31      A(3,11,16)                 111.8031              estimate
D2E/DX2                !
 !  A32      A(3,11,17)                 111.7362              estimate
D2E/DX2                !
 !  A33      A(15,11,16)                107.0353              estimate
D2E/DX2                !
```

```
 !  A34      A(15,11,17)                  106.9377                 estimate
D2E/DX2                !
 !  A35      A(16,11,17)                  107.6746                 estimate
D2E/DX2                !
 !  D1       D(3,1,2,4)                     -0.2672                estimate
D2E/DX2                !
 !  D2       D(3,1,2,10)                 -178.0051                 estimate
D2E/DX2                !
 !  D3       D(18,1,2,4)                 -179.1551                 estimate
D2E/DX2                !
 !  D4       D(18,1,2,10)                   3.107                  estimate
D2E/DX2                !
 !  D5       D(2,1,3,6)                     0.0157                 estimate
D2E/DX2                !
 !  D6       D(2,1,3,11)                  177.7595                 estimate
D2E/DX2                !
 !  D7       D(18,1,3,6)                  178.9021                 estimate
D2E/DX2                !
 !  D8       D(18,1,3,11)                  -3.3541                 estimate
D2E/DX2                !
 !  D9       D(1,2,4,5)                     0.1838                 estimate
D2E/DX2                !
 !  D10      D(1,2,4,19)                  178.5472                 estimate
D2E/DX2                !
 !  D11      D(10,2,4,5)                  177.9213                 estimate
D2E/DX2                !
 !  D12      D(10,2,4,19)                  -3.7153                 estimate
D2E/DX2                !
 !  D13      D(1,2,10,12)                  90.5748                 estimate
D2E/DX2                !
 !  D14      D(1,2,10,13)                 -29.2705                 estimate
D2E/DX2                !
 !  D15      D(1,2,10,14)                -150.0152                 estimate
D2E/DX2                !
 !  D16      D(4,2,10,12)                 -87.1683                 estimate
D2E/DX2                !
 !  D17      D(4,2,10,13)                 152.9864                 estimate
D2E/DX2                !
 !  D18      D(4,2,10,14)                  32.2416                 estimate
D2E/DX2                !
 !  D19      D(1,3,6,5)                     0.3274                 estimate
D2E/DX2                !
 !  D20      D(1,3,6,20)                 -178.9555                 estimate
D2E/DX2                !
 !  D21      D(11,3,6,5)                 -177.4071                 estimate
D2E/DX2                !
 !  D22      D(11,3,6,20)                   3.31                   estimate
D2E/DX2                !
 !  D23      D(1,3,11,15)                 -88.7432                 estimate
D2E/DX2                !
 !  D24      D(1,3,11,16)                 151.5546                 estimate
D2E/DX2                !
 !  D25      D(1,3,11,17)                  30.7896                 estimate
D2E/DX2                !
 !  D26      D(6,3,11,15)                  89.0086                 estimate
D2E/DX2                !
 !  D27      D(6,3,11,16)                 -30.6936                 estimate
D2E/DX2                !
```

```
 !  D28      D(6,3,11,17)                  -151.4586                  estimate
D2E/DX2               !
 !  D29      D(2,4,5,6)                     0.1501                  estimate
D2E/DX2               !
 !  D30      D(2,4,5,7)                   179.6572                  estimate
D2E/DX2               !
 !  D31      D(19,4,5,6)                  -178.1706                 estimate
D2E/DX2               !
 !  D32      D(19,4,5,7)                    1.3364                  estimate
D2E/DX2               !
 !  D33      D(4,5,6,3)                    -0.4044                  estimate
D2E/DX2               !
 !  D34      D(4,5,6,20)                  178.8818                  estimate
D2E/DX2               !
 !  D35      D(7,5,6,3)                   -179.9245                 estimate
D2E/DX2               !
 !  D36      D(7,5,6,20)                   -0.6383                  estimate
D2E/DX2               !
 !  D37      D(4,5,7,8)                   -94.8351                  estimate
D2E/DX2               !
 !  D38      D(4,5,7,9)                    85.4544                  estimate
D2E/DX2               !
 !  D39      D(6,5,7,8)                    84.6618                  estimate
D2E/DX2               !
 !  D40      D(6,5,7,9)                   -95.0487                  estimate
D2E/DX2               !
 !  D41      D(5,7,8,21)                  -178.4737                 estimate
D2E/DX2               !
 !  D42      D(9,7,8,21)                    1.2537                  estimate
D2E/DX2               !
 !  D43      D(5,7,9,22)                    4.173                   estimate
D2E/DX2               !
 !  D44      D(8,7,9,22)                  -175.5354                 estimate
D2E/DX2               !
 ---------------------------------------------------------------------------
--
 Number of steps in this run= 111 maximum allowed number of steps= 132.
 GradGradGradGradGradGradGradGradGradGradGradGradGradGradGradGradGradGrad
```

Distance matrix (angstroms):

		1	2	3	4	5
1	C	0.000000				
2	C	1.394094	0.000000			
3	C	1.395628	2.407166	0.000000		
4	C	2.418130	1.396076	2.777812	0.000000	
5	C	2.825766	2.439441	2.437553	1.401716	0.000000
6	C	2.420898	2.782415	1.394754	2.401940	1.404336
7	B	4.400526	3.897991	3.875184	2.609870	1.574994
8	O	5.171014	4.687184	4.606703	3.442011	2.515452
9	O	5.294233	4.752985	4.772495	3.470582	2.602718
10	C	2.511120	1.506233	3.789299	2.513008	3.812647
11	C	2.509363	3.787256	1.507156	4.284332	3.813781
12	F	3.217217	2.365100	4.436216	3.190645	4.435855
13	F	2.775474	2.367729	4.152698	3.612882	4.776352
14	F	3.599940	2.366097	4.735425	2.786761	4.167163
15	F	3.197922	4.419073	2.363991	4.915168	4.443327
16	F	3.604720	4.741103	2.367206	4.957921	4.170143
17	F	2.775535	4.149800	2.367541	4.960326	4.771812
18	H	1.083591	2.154432	2.157160	3.401577	3.909279

19	H	3.388308	2.134188	3.864012	1.086880	2.167523
20	H	3.400096	3.866704	2.149180	3.386756	2.152752
21	H	6.091243	5.573831	5.490295	4.273472	3.355970
22	H	5.067372	4.572497	4.600343	3.426859	2.688124

		6	7	8	9	10
6	C	0.000000				
7	B	2.579756	0.000000			
8	O	3.333249	1.363485	0.000000		
9	O	3.502138	1.369750	2.347213	0.000000	
10	C	4.288179	5.120623	5.861040	5.870856	0.000000
11	C	2.513859	5.089645	5.733210	5.908226	5.018740
12	F	4.925281	5.658128	6.599841	6.133884	1.353149
13	F	4.966548	6.190209	6.823580	7.053927	1.349355
14	F	4.955792	5.193906	5.741639	5.954413	1.352132
15	F	3.204979	5.639018	6.483214	6.190972	5.561554
16	F	2.783560	5.150698	5.563747	5.999087	6.083095
17	F	3.607561	6.158618	6.706131	7.080869	5.106329
18	H	3.404200	5.483992	6.226145	6.359929	2.717482
19	H	3.398574	2.827083	3.542769	3.513503	2.680812
20	H	1.084409	2.749828	3.328502	3.539135	5.372564
21	H	4.165733	1.941061	0.966063	2.391750	6.705922
22	H	3.469909	1.974922	3.185472	0.962911	5.650478

		11	12	13	14	15
11	C	0.000000				
12	F	5.582374	0.000000			
13	F	5.104374	2.172833	0.000000		
14	F	6.075197	2.172347	2.180833	0.000000	
15	F	1.352829	5.821522	5.713469	6.733220	0.000000
16	F	1.349534	6.753082	6.216833	7.000080	2.172808
17	F	1.351106	5.747588	4.830279	6.203423	2.172702
18	H	2.715543	3.323825	2.475257	3.935077	3.294993
19	H	5.370680	3.243881	3.914827	2.454513	5.973916
20	H	2.710594	5.980864	6.020882	6.011534	3.295052
21	H	6.567661	7.371047	7.721488	6.517360	7.242531
22	H	5.700489	5.725357	6.852895	5.882625	5.796389

		16	17	18	19	20
16	F	0.000000				
17	F	2.180347	0.000000			
18	H	3.940912	2.479512	0.000000		
19	H	6.020684	6.010105	4.279511	0.000000	
20	H	2.478608	3.936136	4.295762	4.301430	0.000000
21	H	6.321016	7.594536	7.156345	4.248980	4.028087
22	H	5.939329	6.893461	6.086761	3.545140	3.590385

		21	22
21	H	0.000000	
22	H	3.339618	0.000000

Framework group C1[X(C8H5BF6O2)]
Deg. of freedom 60

Standard orientation:

Center Number	Atomic Number	Atomic Type	Coordinates (Angstroms) X	Y	Z
1	6	0	-0.106581	-1.187834	-0.048971
2	6	0	-1.247460	-0.386659	-0.045827
3	6	0	1.151596	-0.583959	-0.038729
4	6	0	-1.127461	1.004122	-0.026930
5	6	0	0.127705	1.627992	-0.014608
6	6	0	1.266294	0.806005	-0.025161

```
     7          5           0        0.291516    3.194387   -0.001191
     8          8           0        0.465536    3.820968   -1.199609
     9          8           0        0.275269    3.957966    1.135866
    10          6           0       -2.612031   -1.023442   -0.011312
    11          6           0        2.389107   -1.442907    0.009190
    12          9           0       -3.046146   -1.197392    1.258452
    13          9           0       -2.616082   -2.237539   -0.600134
    14          9           0       -3.534388   -0.259862   -0.639376
    15          9           0        2.752360   -1.713917    1.283845
    16          9           0        3.441436   -0.839270   -0.581970
    17          9           0        2.198200   -2.630267   -0.606617
    18          1           0       -0.196831   -2.267286   -0.077418
    19          1           0       -2.039291    1.595197   -0.049393
    20          1           0        2.249322    1.263729   -0.034468
    21          1           0        0.580338    4.774079   -1.091545
    22          1           0        0.216994    3.455181    1.955016
 ---------------------------------------------------------------------
 Rotational constants (GHZ):      0.4161668      0.3667723      0.2182316
   280  basis  functions,     511  primitive  gaussians,     280  cartesian  basis
functions
    64 alpha electrons       64 beta electrons
       nuclear repulsion energy      1250.9927073680 Hartrees.
 NAtoms=    22 NActive=    22 NUniq=    22 SFac= 7.50D-01 NAtFMM=    80 NAOKFM=F
Big=F
 Harris functional with IExCor=  402 diagonalized for initial guess.
 ExpMin= 1.27D-01 ExpMax= 7.00D+03 ExpMxC= 1.05D+03 IAcc=1 IRadAn=           1
AccDes= 1.00D-06
 HarFok:  IExCor= 402 AccDes= 1.00D-06 IRadAn=         1 IDoV=1
 ScaDFX=  1.000000  1.000000  1.000000  1.000000
 Initial guess orbital symmetries:
       Occupied  (A) (A) (A) (A) (A) (A) (A) (A) (A) (A) (A) (A)
                 (A) (A) (A) (A) (A) (A) (A) (A) (A) (A) (A) (A)
                 (A) (A) (A) (A) (A) (A) (A) (A) (A) (A) (A) (A)
                 (A) (A) (A) (A) (A) (A) (A) (A) (A) (A) (A) (A)
                 (A) (A) (A) (A) (A) (A) (A) (A) (A) (A) (A) (A)
                 (A) (A) (A) (A)
       Virtual   (A) (A) (A) (A) (A) (A) (A) (A) (A) (A) (A) (A)
                 (A) (A) (A) (A) (A) (A) (A) (A) (A) (A) (A) (A)
                 (A) (A) (A) (A) (A) (A) (A) (A) (A) (A) (A) (A)
                 (A) (A) (A) (A) (A) (A) (A) (A) (A) (A) (A) (A)
                 (A) (A) (A) (A) (A) (A) (A) (A) (A) (A) (A) (A)
                 (A) (A) (A) (A) (A) (A) (A) (A) (A) (A) (A) (A)
                 (A) (A) (A) (A) (A) (A) (A) (A) (A) (A) (A) (A)
                 (A) (A) (A) (A) (A) (A) (A) (A) (A) (A) (A) (A)
                 (A) (A) (A) (A) (A) (A) (A) (A) (A) (A) (A) (A)
                 (A) (A) (A) (A) (A) (A) (A) (A) (A) (A) (A) (A)
                 (A) (A) (A) (A) (A) (A) (A) (A) (A) (A) (A) (A)
                 (A) (A) (A) (A) (A) (A) (A) (A) (A) (A) (A) (A)
                 (A) (A) (A) (A) (A) (A) (A) (A) (A) (A) (A) (A)
                 (A) (A) (A) (A) (A) (A) (A) (A) (A) (A) (A) (A)
                 (A) (A) (A) (A) (A) (A) (A) (A) (A) (A) (A) (A)
                 (A) (A) (A) (A) (A) (A) (A) (A) (A) (A) (A) (A)
                 (A) (A) (A) (A) (A) (A) (A) (A) (A) (A) (A) (A)
                 (A) (A) (A) (A) (A) (A) (A) (A) (A) (A) (A) (A)
 The electronic state of the initial guess is 1-A.
 Integral accuracy reduced to 1.0D-05 until final iterations.
 Initial convergence to 1.0D-05 achieved.  Increase integral accuracy.
 SCF Done:  E(RB+HF-LYP) =  -1082.34691971     A.U. after   14 cycles
             Convg  =    0.3931D-08             -V/T =  2.0077
```

```
          S**2   =   0.0000

 ******************************************************************

          Population analysis using the SCF density.

 ******************************************************************

 Orbital symmetries:
       Occupied  (A) (A) (A) (A) (A) (A) (A) (A) (A) (A) (A) (A)
                 (A) (A) (A) (A) (A) (A) (A) (A) (A) (A) (A) (A)
                 (A) (A) (A) (A) (A) (A) (A) (A) (A) (A) (A) (A)
                 (A) (A) (A) (A) (A) (A) (A) (A) (A) (A) (A) (A)
                 (A) (A) (A) (A) (A) (A) (A) (A) (A) (A) (A) (A)
                 (A) (A) (A) (A)
       Virtual   (A) (A) (A) (A) (A) (A) (A) (A) (A) (A) (A) (A)
                 (A) (A) (A) (A) (A) (A) (A) (A) (A) (A) (A) (A)
                 (A) (A) (A) (A) (A) (A) (A) (A) (A) (A) (A) (A)
                 (A) (A) (A) (A) (A) (A) (A) (A) (A) (A) (A) (A)
                 (A) (A) (A) (A) (A) (A) (A) (A) (A) (A) (A) (A)
                 (A) (A) (A) (A) (A) (A) (A) (A) (A) (A) (A) (A)
                 (A) (A) (A) (A) (A) (A) (A) (A) (A) (A) (A) (A)
                 (A) (A) (A) (A) (A) (A) (A) (A) (A) (A) (A) (A)
                 (A) (A) (A) (A) (A) (A) (A) (A) (A) (A) (A) (A)
                 (A) (A) (A) (A) (A) (A) (A) (A) (A) (A) (A) (A)
                 (A) (A) (A) (A) (A) (A) (A) (A) (A) (A) (A) (A)
                 (A) (A) (A) (A) (A) (A) (A) (A) (A) (A) (A) (A)
                 (A) (A) (A) (A) (A) (A) (A) (A) (A) (A) (A) (A)
                 (A) (A) (A) (A) (A) (A) (A) (A) (A) (A) (A) (A)
                 (A) (A) (A) (A) (A) (A) (A) (A) (A) (A) (A) (A)
                 (A) (A) (A) (A) (A) (A) (A) (A) (A) (A) (A) (A)
                 (A) (A) (A) (A) (A) (A) (A) (A) (A) (A) (A) (A)
                 (A) (A) (A) (A) (A) (A) (A) (A) (A) (A) (A) (A)
 The electronic state is 1-A.
 Alpha  occ. eigenvalues --  -24.73177 -24.73132 -24.73061 -24.73059 -24.72560
 Alpha  occ. eigenvalues --  -24.72542 -19.17981 -19.17083 -10.44021 -10.43986
 Alpha  occ. eigenvalues --  -10.23087 -10.23064 -10.22645 -10.22413 -10.22402
 Alpha  occ. eigenvalues --  -10.20450  -6.80594  -1.30705  -1.30697  -1.22173
 Alpha  occ. eigenvalues --   -1.22157  -1.21690  -1.21689  -1.05210  -1.01834
 Alpha  occ. eigenvalues --   -0.89313  -0.81082  -0.78715  -0.71203  -0.70404
 Alpha  occ. eigenvalues --   -0.64273  -0.63793  -0.60206  -0.58843  -0.58531
 Alpha  occ. eigenvalues --   -0.58474  -0.58228  -0.57133  -0.54581  -0.53188
 Alpha  occ. eigenvalues --   -0.51796  -0.48690  -0.46395  -0.46226  -0.46091
 Alpha  occ. eigenvalues --   -0.45782  -0.45504  -0.42936  -0.42496  -0.42461
 Alpha  occ. eigenvalues --   -0.42140  -0.41180  -0.40802  -0.40329  -0.40235
 Alpha  occ. eigenvalues --   -0.40060  -0.39625  -0.38697  -0.37840  -0.36438
 Alpha  occ. eigenvalues --   -0.33759  -0.33220  -0.28433  -0.28024
 Alpha virt. eigenvalues --   -0.04519  -0.04040   0.03271   0.05705   0.08036
 Alpha virt. eigenvalues --    0.09841   0.10770   0.12893   0.14623   0.15025
 Alpha virt. eigenvalues --    0.15338   0.19740   0.20084   0.20872   0.21523
 Alpha virt. eigenvalues --    0.22004   0.24457   0.26971   0.28544   0.29375
 Alpha virt. eigenvalues --    0.30501   0.33984   0.34342   0.39297   0.39924
 Alpha virt. eigenvalues --    0.46288   0.46641   0.47012   0.48499   0.49622
 Alpha virt. eigenvalues --    0.50166   0.51475   0.52669   0.53283   0.55462
 Alpha virt. eigenvalues --    0.55630   0.56592   0.57206   0.60292   0.61809
 Alpha virt. eigenvalues --    0.61964   0.63505   0.64674   0.70937   0.72040
 Alpha virt. eigenvalues --    0.73061   0.73556   0.74433   0.76495   0.76999
 Alpha virt. eigenvalues --    0.79131   0.79585   0.81058   0.87259   0.87472
 Alpha virt. eigenvalues --    0.88551   0.90851   0.94151   0.94908   0.95593
```

```
 Alpha virt. eigenvalues --    0.98979   1.01769   1.02811   1.06043   1.06552
 Alpha virt. eigenvalues --    1.08202   1.08821   1.09072   1.09995   1.10789
 Alpha virt. eigenvalues --    1.13583   1.14140   1.14401   1.14985   1.18734
 Alpha virt. eigenvalues --    1.19440   1.22581   1.23099   1.24530   1.29504
 Alpha virt. eigenvalues --    1.30918   1.32537   1.32981   1.33148   1.34345
 Alpha virt. eigenvalues --    1.34388   1.36405   1.37109   1.37408   1.37658
 Alpha virt. eigenvalues --    1.37805   1.38032   1.40647   1.41108   1.41161
 Alpha virt. eigenvalues --    1.44565   1.44790   1.45782   1.48868   1.53773
 Alpha virt. eigenvalues --    1.54263   1.57584   1.58545   1.60314   1.61153
 Alpha virt. eigenvalues --    1.61584   1.63501   1.64384   1.65444   1.66696
 Alpha virt. eigenvalues --    1.68052   1.70124   1.70310   1.71846   1.74481
 Alpha virt. eigenvalues --    1.76550   1.77103   1.82899   1.83949   1.84323
 Alpha virt. eigenvalues --    1.84991   1.87326   1.87971   1.89664   1.91355
 Alpha virt. eigenvalues --    1.94832   1.95144   1.96524   1.96610   1.97021
 Alpha virt. eigenvalues --    1.98504   1.99040   2.00100   2.00646   2.01025
 Alpha virt. eigenvalues --    2.04175   2.06073   2.06136   2.06471   2.06797
 Alpha virt. eigenvalues --    2.07854   2.09061   2.11332   2.11558   2.12208
 Alpha virt. eigenvalues --    2.13387   2.16033   2.20385   2.21587   2.22500
 Alpha virt. eigenvalues --    2.26859   2.28575   2.32048   2.32970   2.36583
 Alpha virt. eigenvalues --    2.38691   2.38956   2.39503   2.39710   2.43832
 Alpha virt. eigenvalues --    2.49383   2.49645   2.51613   2.52506   2.59382
 Alpha virt. eigenvalues --    2.61107   2.61669   2.62783   2.63017   2.65559
 Alpha virt. eigenvalues --    2.67014   2.67660   2.68303   2.71249   2.72132
 Alpha virt. eigenvalues --    2.75970   2.77253   2.78177   2.79156   2.83574
 Alpha virt. eigenvalues --    2.85888   2.88678   2.90361   2.97659   3.01737
 Alpha virt. eigenvalues --    3.02660   3.02876   3.04422   3.06274   3.08419
 Alpha virt. eigenvalues --    3.09998   3.10302   3.18460   3.27890   3.31954
 Alpha virt. eigenvalues --    3.37915   3.38724   3.46939   3.66930   3.74353
 Alpha virt. eigenvalues --    4.00676   4.08212   4.09023   4.14931   4.21862
 Alpha virt. eigenvalues --    4.25700   4.28026   4.40427   4.48292   4.49957
 Alpha virt. eigenvalues --    4.53572   4.54804   4.75999   4.85207   5.43940
 Alpha virt. eigenvalues --    5.53755
     Molecular Orbital Coefficients
                           60        61        62        63        64
                         (A)--O    (A)--O    (A)--O    (A)--O    (A)--O
     EIGENVALUES --    -0.36438  -0.33759  -0.33220  -0.28433  -0.28024
   1 1   C  1S           0.00007   0.00065   0.00012  -0.00002  -0.00056
   2        2S          -0.00048  -0.00821   0.00055   0.00006   0.00237
   3        2PX         -0.20818   0.00114   0.00096  -0.00829   0.00107
   4        2PY          0.01303  -0.07858   0.01129   0.00096   0.00545
   5        2PZ          0.00007   0.01934  -0.00567   0.00786  -0.32795
   6        3S           0.00343   0.03638  -0.00034  -0.00081   0.00087
   7        3PX         -0.11839   0.00633   0.00689  -0.01392   0.00234

.....
......

.....
.........

.....
.........
Condensed to atoms (all electrons):
 Mulliken atomic charges:
              1
     1  C   -0.115973
     2  C   -0.040399
     3  C   -0.043335
     4  C   -0.151055
```

```
     5  C    0.031706
     6  C   -0.136612
     7  B    0.411568
     8  O   -0.472354
     9  O   -0.481077
    10  C    0.793377
    11  C    0.796401
    12  F   -0.258411
    13  F   -0.265581
    14  F   -0.270005
    15  F   -0.258382
    16  F   -0.265557
    17  F   -0.268221
    18  H    0.132389
    19  H    0.087497
    20  H    0.132991
    21  H    0.321104
    22  H    0.319929
Sum of Mulliken charges=   0.00000
Atomic charges with hydrogens summed into heavy atoms:
             1
     1  C    0.016417
     2  C   -0.040399
     3  C   -0.043335
     4  C   -0.063559
     5  C    0.031706
     6  C   -0.003621
     7  B    0.411568
     8  O   -0.151250
     9  O   -0.161148
    10  C    0.793377
    11  C    0.796401
    12  F   -0.258411
    13  F   -0.265581
    14  F   -0.270005
    15  F   -0.258382
    16  F   -0.265557
    17  F   -0.268221
    18  H    0.000000
    19  H    0.000000
    20  H    0.000000
    21  H    0.000000
    22  H    0.000000
Sum of Mulliken charges=   0.00000
Electronic spatial extent (au):  <R**2>=  4539.4912
Charge=     0.0000 electrons
Dipole moment (field-independent basis, Debye):
   X=    -1.0071    Y=     2.5860    Z=     0.2770  Tot=     2.7889
Orbital energies and kinetic energies (alpha):
                          1         2
     60  (A)--O       -0.36534   2.25262
     61  (A)--O       -0.34062   1.94185
     62  (A)--O       -0.33150   2.34831
     63  (A)--O       -0.28625   1.33002
     64  (A)--O       -0.28323   1.26851
     65  (A)--V       -0.05548   1.43848
     66  (A)--V       -0.04667   1.56545
     67  (A)--V        0.04351   1.28066
     68  (A)--V        0.05208   1.79292
```

```
     69  (A)--V        0.08134   1.31541
 Total kinetic energy from orbitals= 1.074116305562D+03

 Test job not archived.
 1|1|UNPC-UNK|FOpt|RB3LYP|6-31G(d,p)|C8H5B1F6O2|PCUSER|08-Jun-2014|0||#
 T RB3LYP/6-31G(d,p) Opt Pop=Reg Test||Untitled-4||0,1|C,-0.4726933895,
 -0.1560651125,-2.2657123932|C,0.7338473367,0.3430811945,-1.777233463|C
 ,-1.3665003308,-0.7651973661,-1.3837318915|C,1.0376863642,0.2373365485
 ,-0.4186895266|C,0.151516125,-0.3695339943,0.4820030335|C,-1.056056962
 8,-0.8731690455,-0.0282324993|B,0.472725777,-0.5089608911,2.0175629128
 |O,-0.3132277452,-1.3457242463,2.7532254759|O,1.4842826704,0.160442506
 4,2.6538089569|C,1.6885126419,1.0432017242,-2.7084636986|C,-2.69457356
 57,-1.2616781165,-1.8948145897|F,1.4509812398,2.3745922555,-2.75312344
 3|F,1.5885485973,0.5813724044,-3.9723855868|F,2.9727956933,0.887471169
 3,-2.3152216828|F,-3.6381415617,-0.2938801206,-1.8377196612|F,-3.15276
 08525,-2.3038891943,-1.1701627647|F,-2.6173291488,-1.6605190809,-3.183
 4251253|H,-0.704963307,-0.0875184348,-3.3218848021|H,1.9981551216,0.61
 66731361,-0.0797512021|H,-1.7510303537,-1.3636384409,0.6443278978|H,-0
 .0578601164,-1.3492558039,3.6849145231|H,1.9614177668,0.7862159088,2.0
 9892453||Version=IA32W-G03RevD.01|State=1-A|HF=-1082.3528502|RMSD=3.27
 8e-009|RMSF=3.431e-006|Thermal=0.|Dipole=0.5560324,0.214204,0.9213676|
 PG=C01 [X(C8H5B1F6O2)]||@


 OUR LITTLE SYSTEMS HAVE THEIR DAY,
   THEY HAVE THEIR DAY AND CEASE TO BE.
   THEY ARE BUT BROKEN LIGHTS OF THEE,
 AND THOU, OH LORD, ART MORE THAN THEY.
          --------------------
 LET KNOWLEDGE GROW FROM MORE TO MORE,
   BUT MORE OF REVERENCE IN US DWELL.
   THAT MIND AND SOUL, ACCORDING WELL,
 MAY MAKE ONE MUSIC AS BEFORE.....
          --------------------
                    LORD TENNYSON
 Job cpu time:  0 days  2 hours 50 minutes 38.0 seconds.
 File lengths (MBytes):  RWF=     60 Int=      0 D2E=      0 Chk=      9 Scr=
1
 Normal termination of Gaussian 03 at Sun Jun 08 00:40:35 2014.
```

Appendix B

Calculated and measured IR spectra

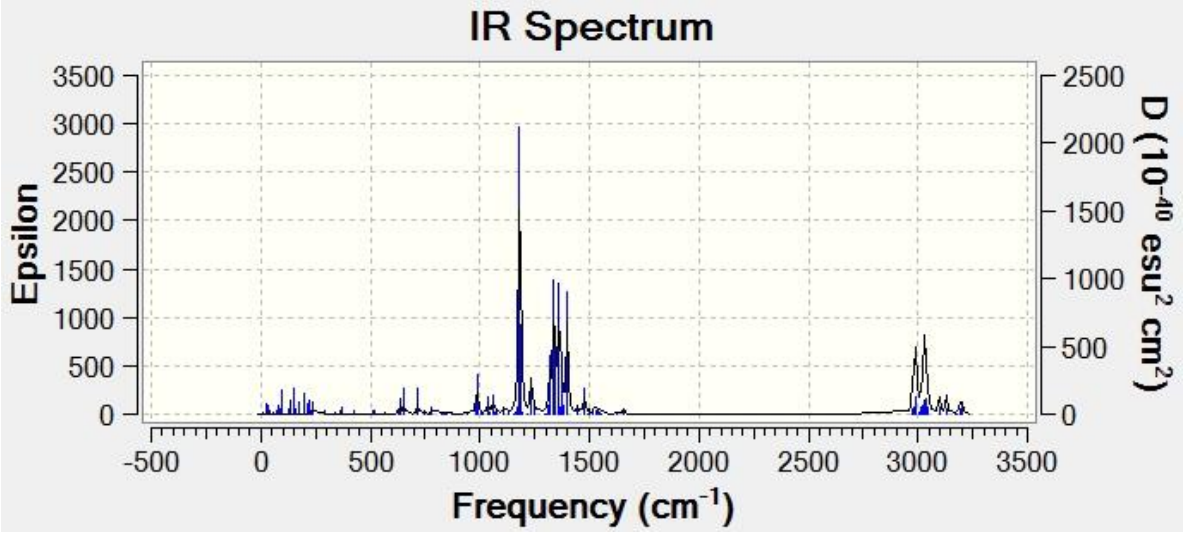

Compound **13** Calculated IR spectrum

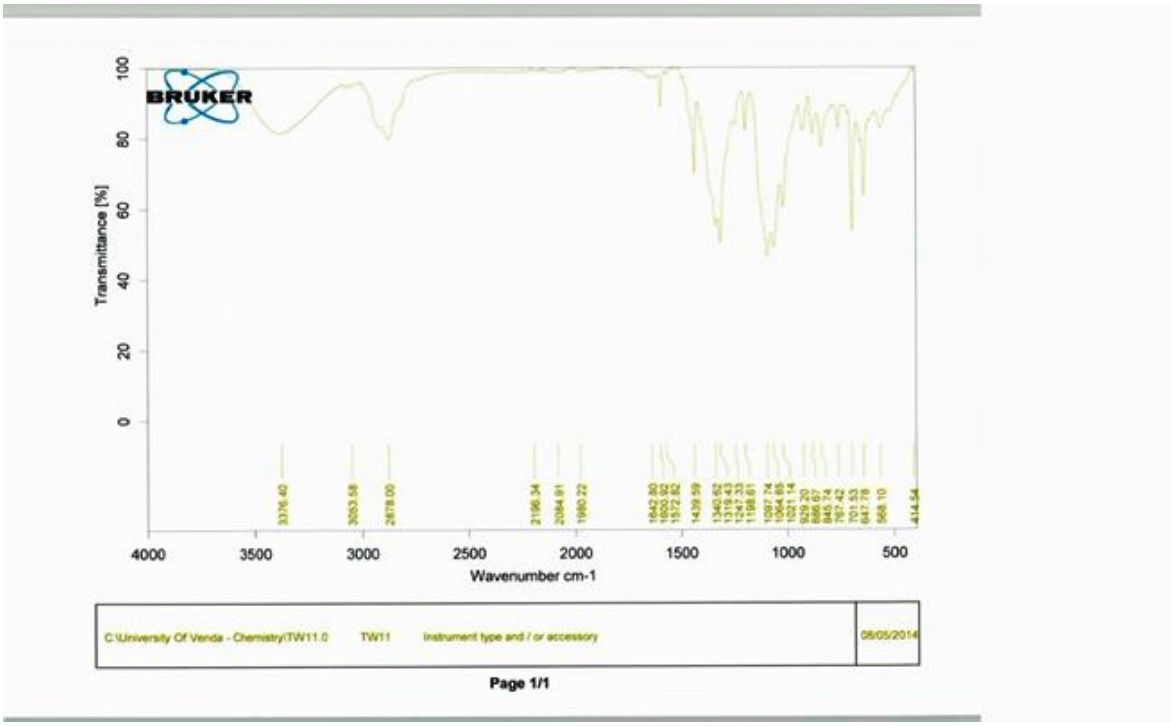

Compound **13** Recorded IR spectrum.

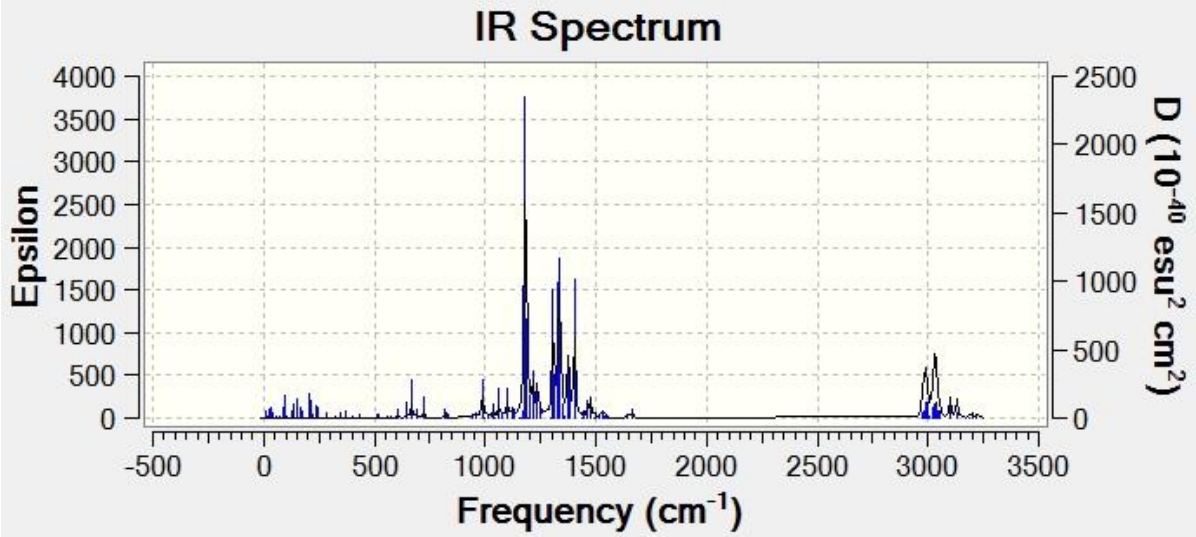

Compound **14** Calculated IR spectrum.

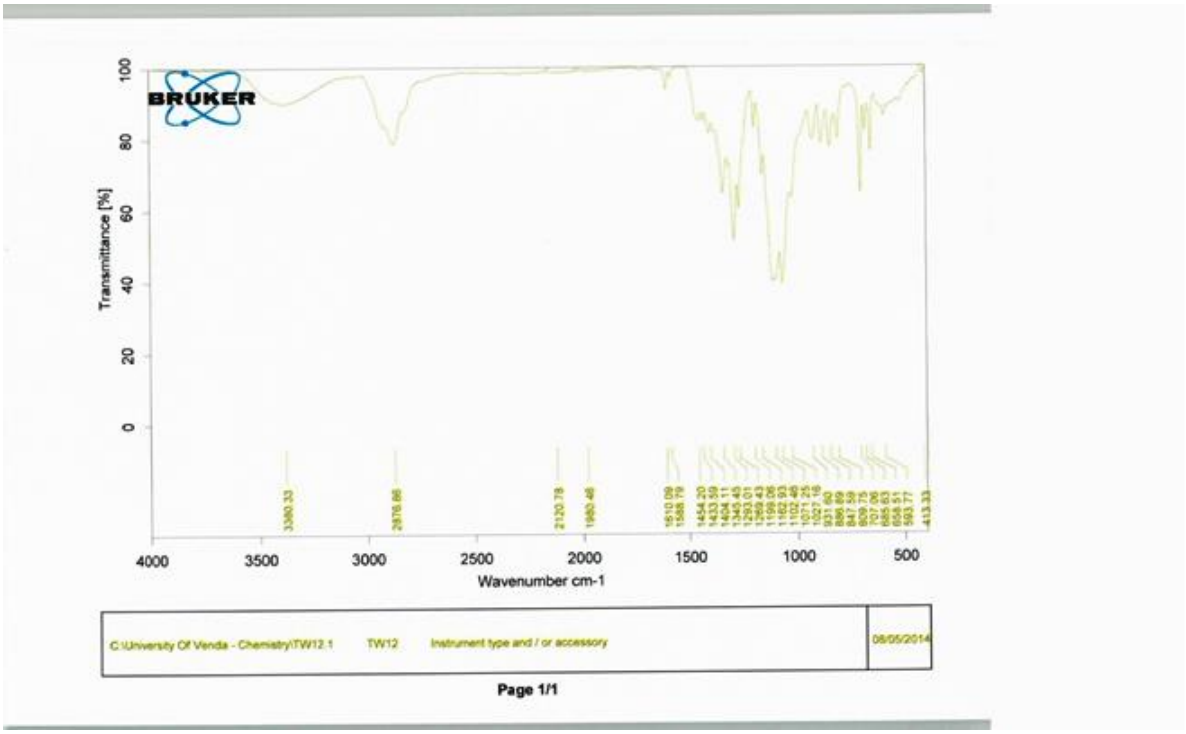

Compound **14** Recorded IR spectrum.

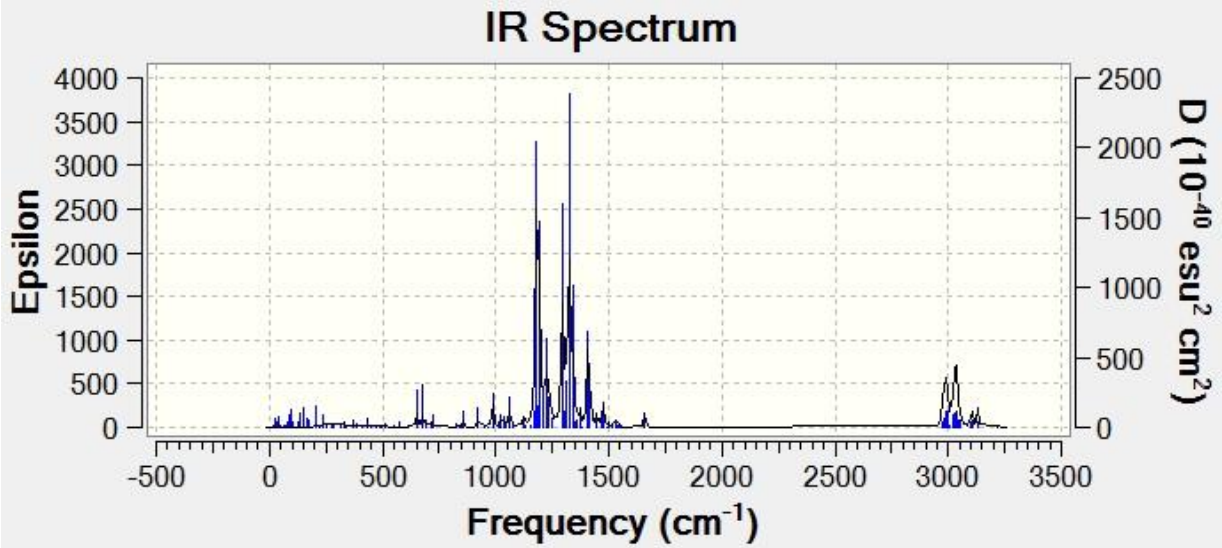

Compd **15** Calculated IR spectrum.

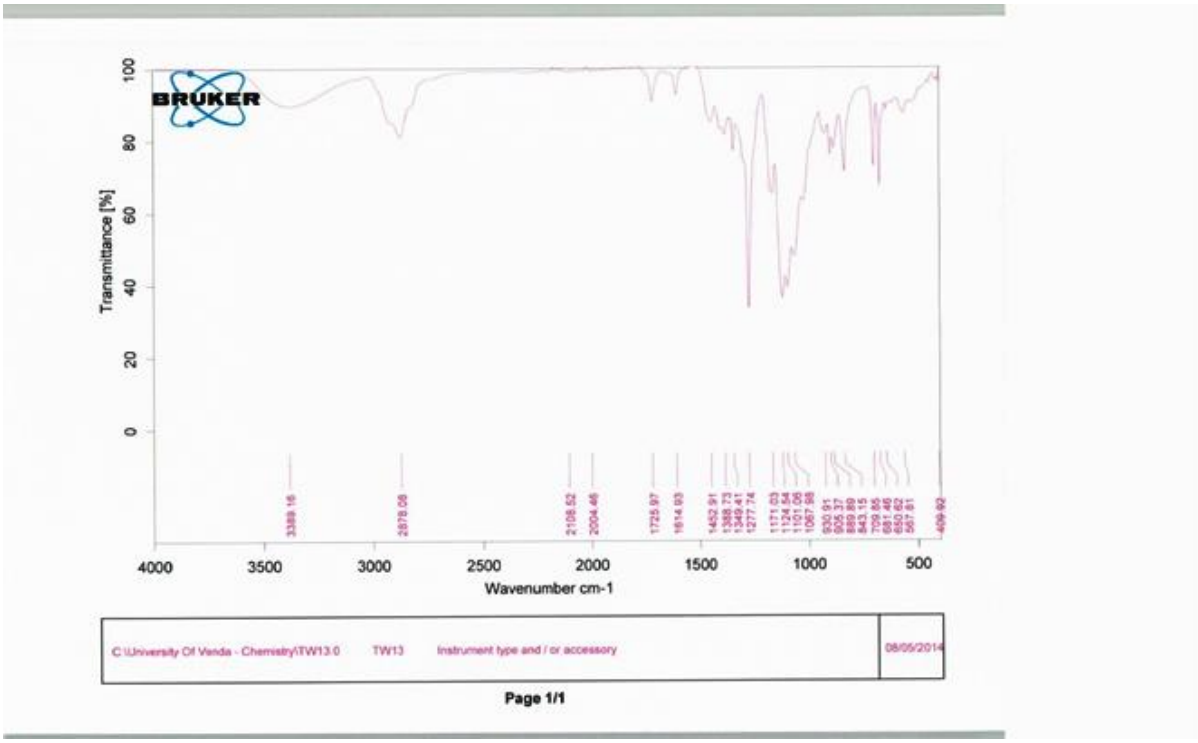

Compound **15** Recorded IR spectrum.

Appendix C

NMR Spectra of Compound 14

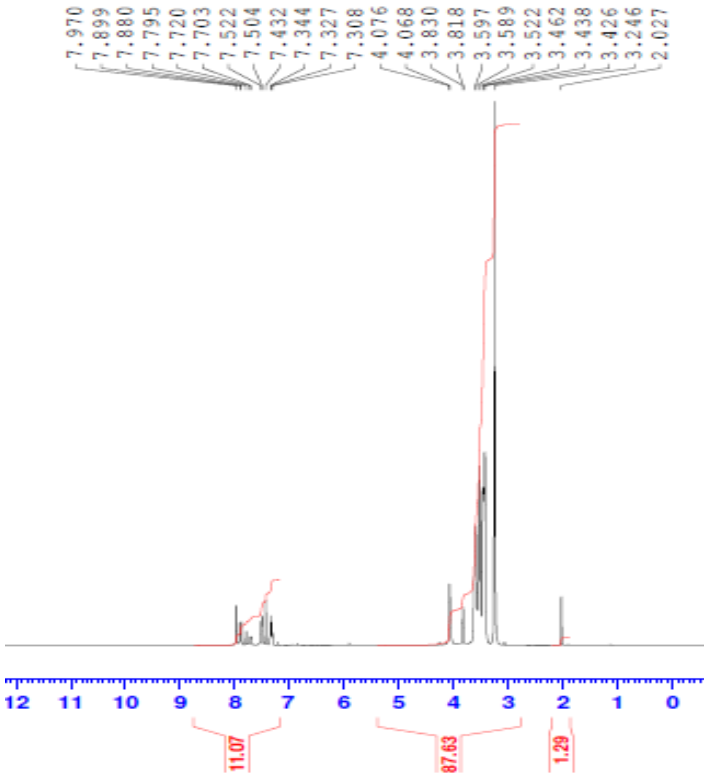

^{1}H-NMR spectrum.

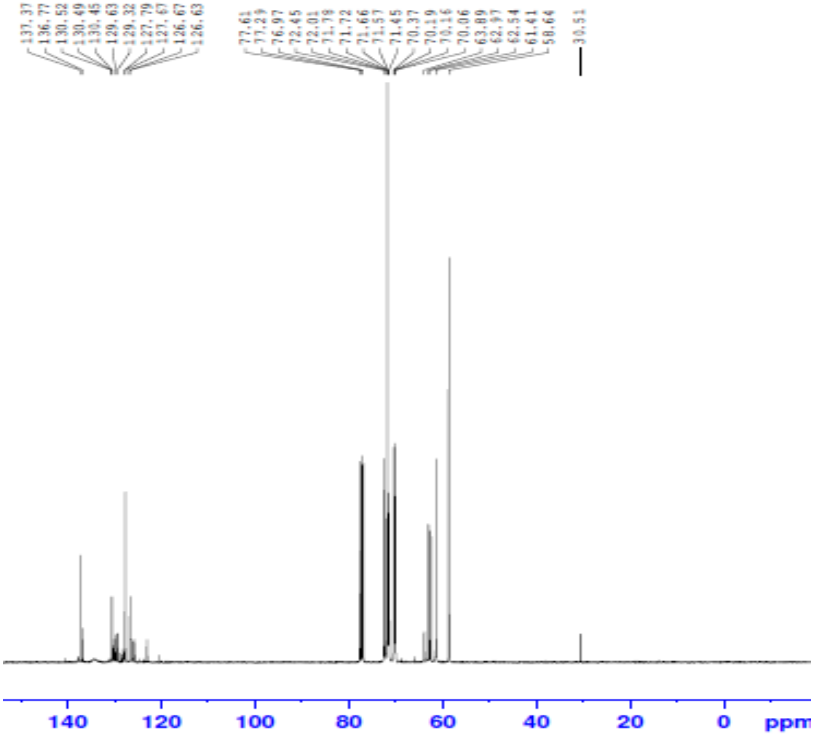

^{13}C-NMR spectrum.

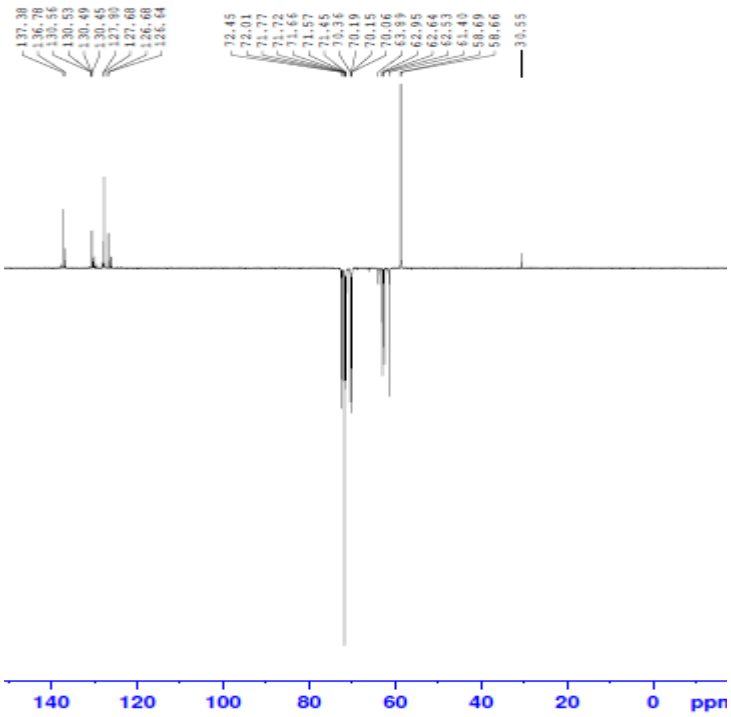

DEPT135 spectrum.

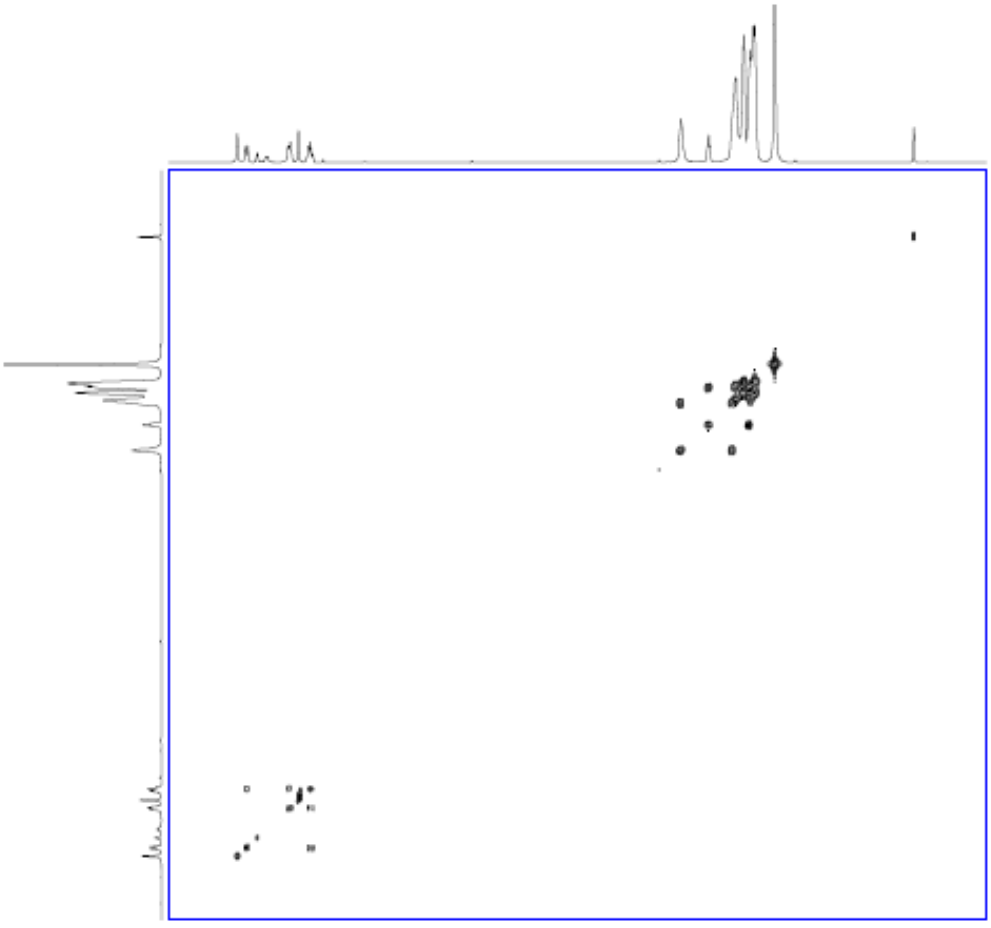

COSY spectrum.

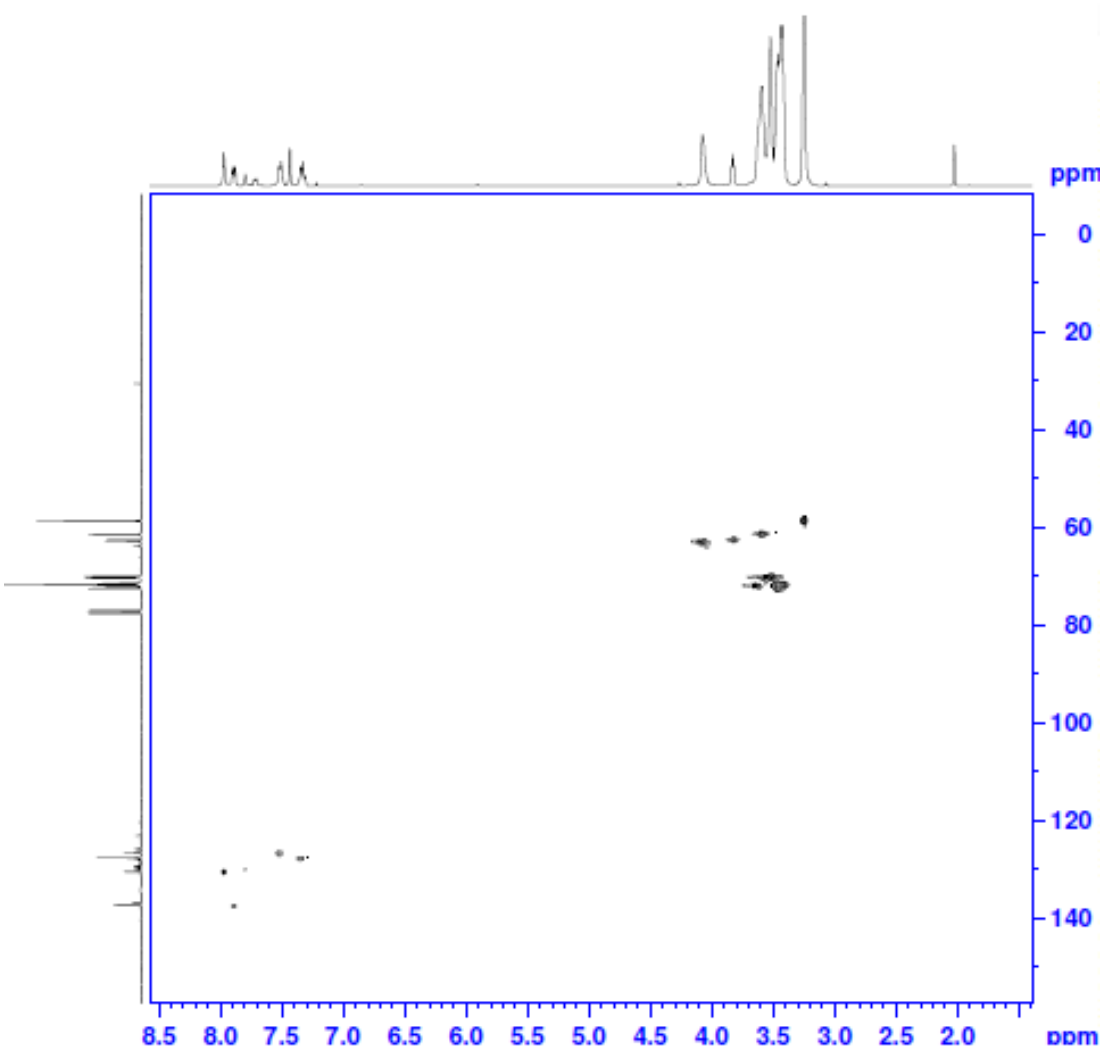

HSQC spectrum.

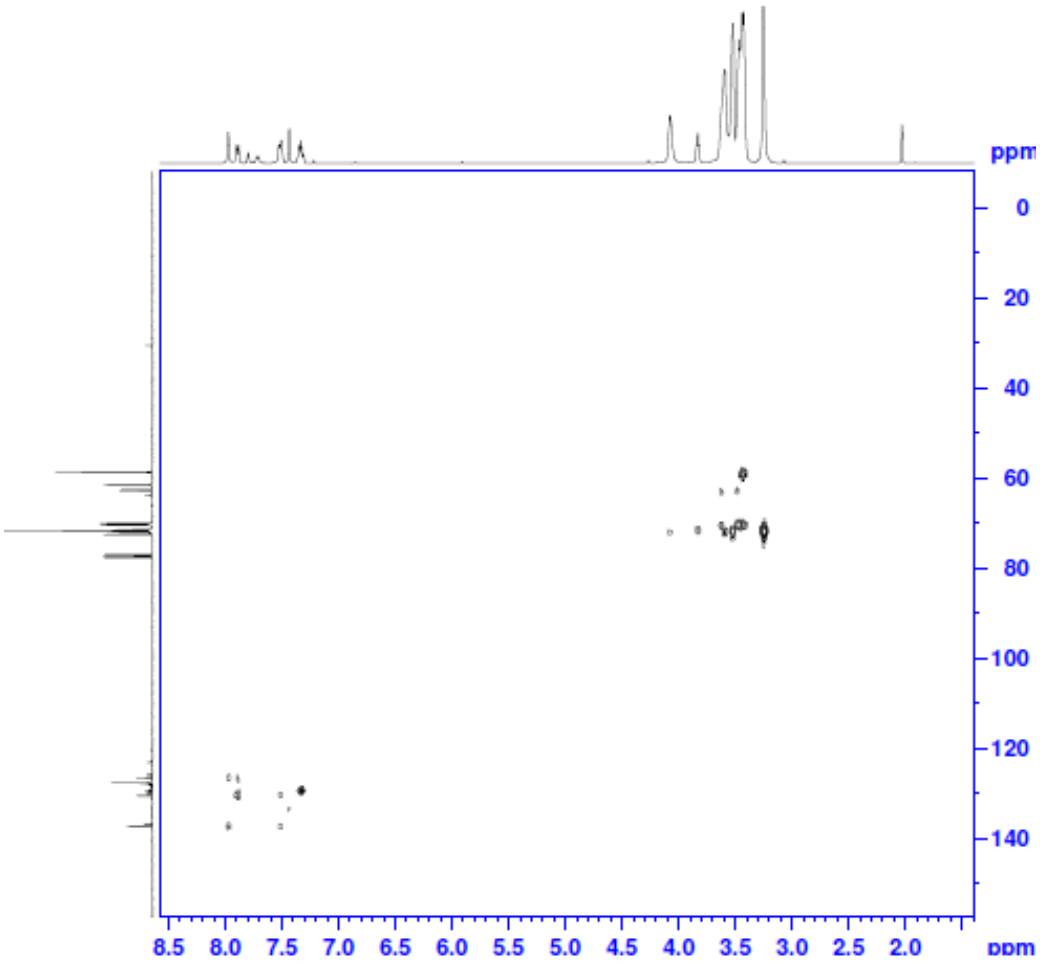

HMBC spectrum.

Appendix D

Mass Spectra

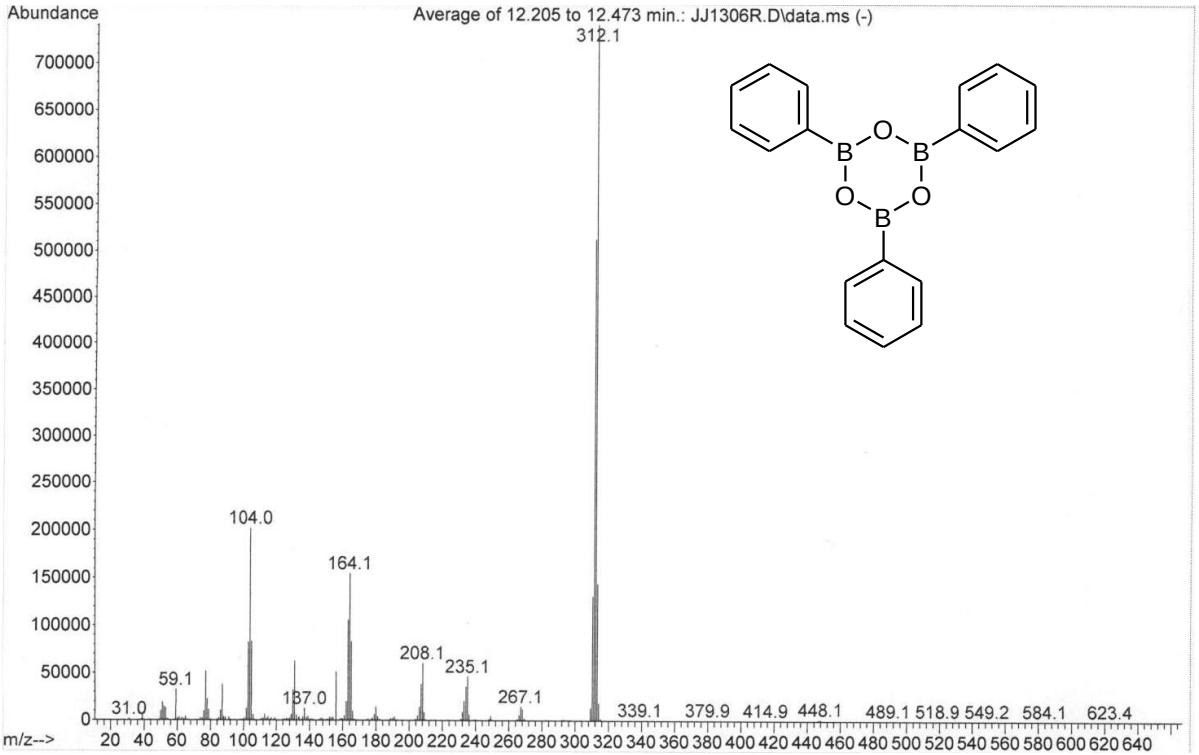

Compound **13** MS with molecular ion at *m/z* 312.12

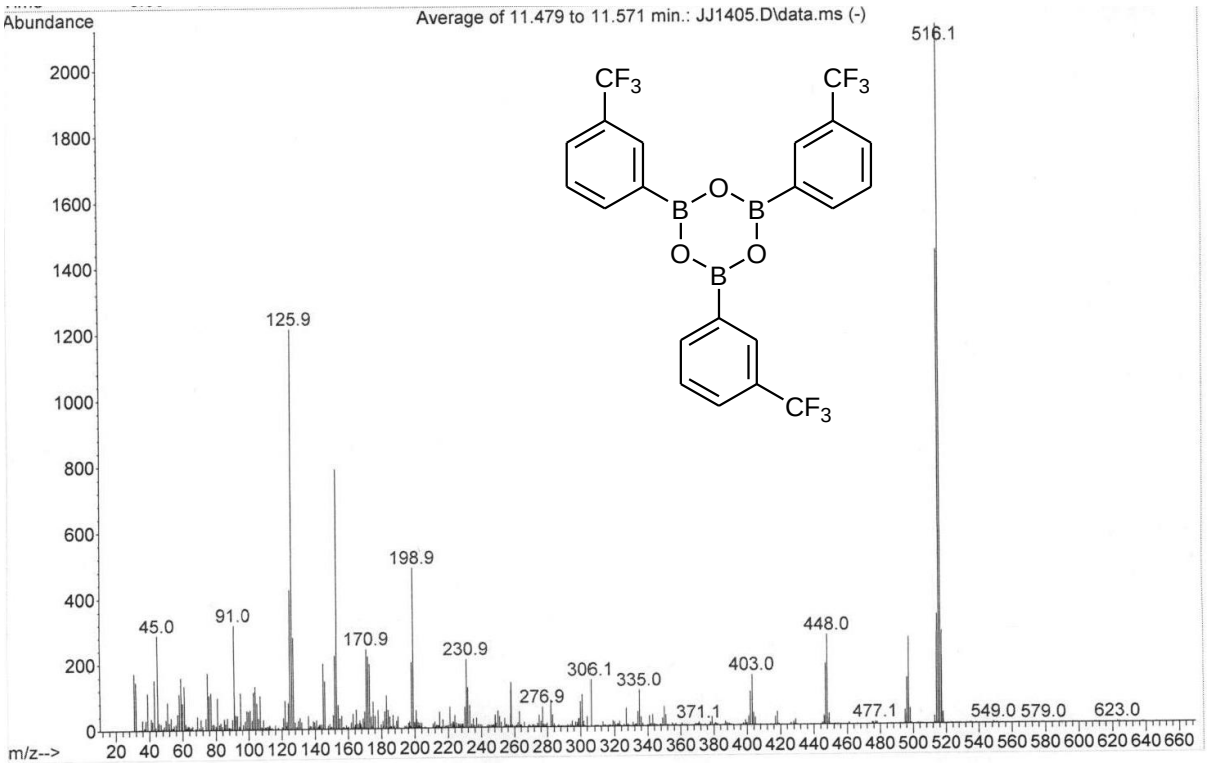

Compound **14** MS with molecular ion at *m/z* 516.10

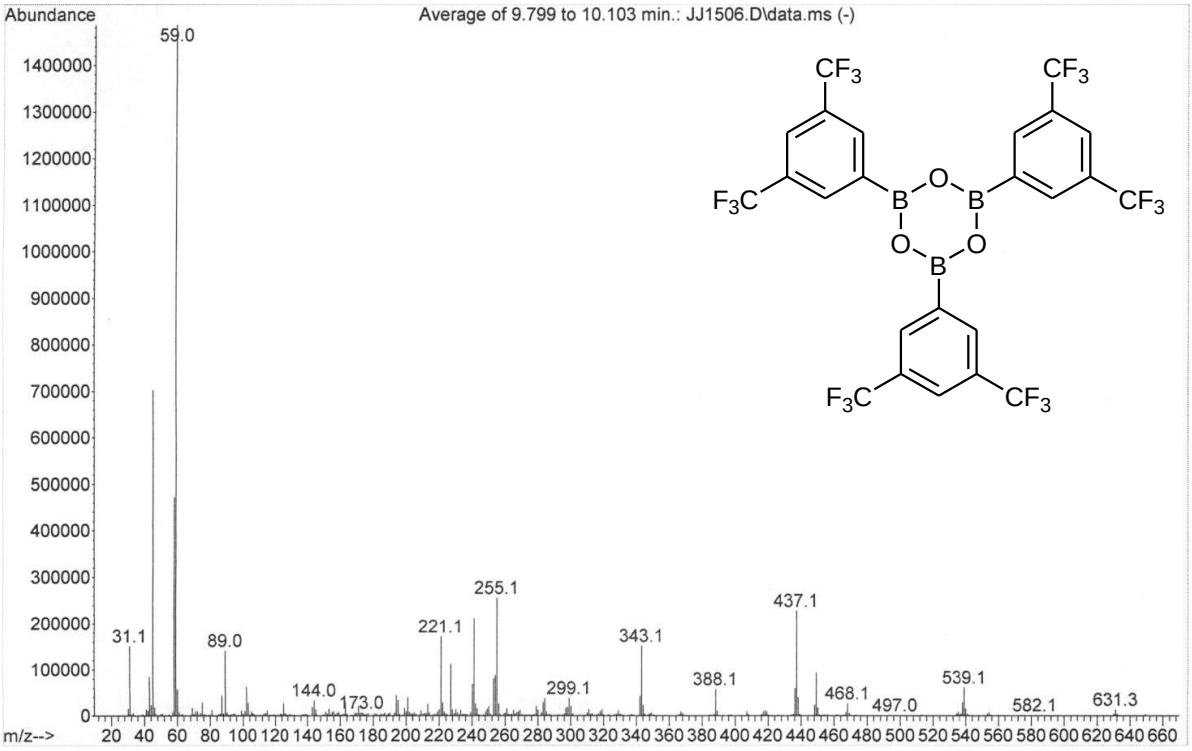

Compound **15** MS. The molecular ion is outside the sweep width at *m/z* 720.12